Mitigation of silver pollution by biochar adsorption

MPhil Thesis

Md Anwarul Islam (MSc)

in April 2022

For the degree of Master of Philosophy

in the College of Science and Engineering

James Cook University

Townsville

Advisors: Dr. Elsa Antunes, Prof. Mohan Jacob

DECLARATION

I declare that this thesis is my own work and has not been submitted elsewhere in whole or in part to obtain other degree awards. The content of this thesis is the result of my work, and the contribution of others has been acknowledged in the statement of contribution.

_____

Md Anwarul Islam

April 2022

STATEMENT OF ACCESS TO THIS THESIS

I, the undersigned, the author of this research work, understand that James Cook University will make this thesis available for use within the University Library and via the Australian Digital Thesis Network, for use elsewhere.

I understand that an unpublished work, a thesis has significant protection under the Copyright Act. I do not wish to place any restriction on access to this thesis, but any use of its content must be acknowledged.

_____

Md Anwarul Islam

April 2022

STATEMENT ON THE CONTRIBUTIONS OF OTHERS

Nature of assistance	Type of Contribution	Description of Contribution
Intellectual support	Editorial Assistance	I would like to thank my advisory panel (Dr. Elsa Antunes and Prof Mohan Jacob) for helping me with the editing of my thesis and publications. I would also like to thank Dr Liz Tynan and Kellie Johns for their proof reading support.
Financial Support	Fee offset	Graduate Research School, James Cook University to waive my tuition fee.
	Research Costs	My primary advisor, Dr. Elsa Antunes to support the outsourced analyses cost.

ACKNOWLEDGEMENTS

I would like to acknowledge the extensive support from my advisory panel for my project thesis. I would like to thank Dr. Elsa Antunes and Prof. Mohan Jacob for trusting me and giving me the freedom to develop my research idea, providing me with the necessary resources to successfully develop my research work. I want to thank both my advisors for being both a supporter and critics and for steering me through my research project and for helping me to improve my writing skill.

I would like to express my heartfelt gratitude to my primary advisor, Dr. Elsa Antunes, for her extra ordinary support and guidance that was the key to my mental well-being during the pandemic. Every meeting with her motivated me to achieve my goals on time, and more often, the end of the meeting with "*sounds good*" was quite a stress buster.

I would thank Dr. Dana Roberts from James Cook University for allowing me to use their laboratory for determining the surface functional groups on the biochar.

I would specially thank my best friend, Tewodros Dada (PhD student at James Cook University), for helping me to use several laboratory equipment and software to analyse my preliminary results.

I thank all my research group mates and friends for their support in my MPhil journey.

I would like to acknowledge the Advanced Analytical Centre at James Cook University for the access to scanning electron microscopy, X-ray diffraction and inductively coupled plasma.

I am grateful for the tuition fee waived by the Graduate Research School, James Cook University. I acknowledge the extra financial support of my primary advisor, Dr. Elsa Antunes, for this research, which was fundamental for all the outsourced analyses.

Last but not least, I would like to thank my beloved family members and friends for their incredible support, encouragement, and motivation in my MPhil journey. Especially my wife Irin, my daughter Saba, and my son Aryan, are great inspirations every day in my life.

ABSTRACT

Mitigation of silver and other potentially toxic heavy metals from wastewater has gained substantial focus in the scientific research community in recent years. These heavy metals can destabilise the natural environment and cause severe threats to the natural ecosystem and human health. For instance, monovalent silver (Ag^{+}) and silver nanoparticles (Ag NPs) at very low concentrations can bioaccumulated in living organisms, which impact cell metabolisms. Most research in this field mainly highlights the pollution control technologies for specific heavy metals, such as chromium, lead, copper, and mercury. However, mitigation of silver and, most especially, silver nanoparticles (Ag NPs) are not well studied. Many technologies, ion-exchange, reverse osmosis, and activated sludge processes can eliminate silver species, but none of them is suitable due to their cost-effectiveness and non-eco-friendly nature. Finding a cost-effective and sustainable solution to mitigate silver pollution from aquatic sources such as wastewater is still a challenging topic. Silver adsorption onto biochar is considered a sustainable and cost-effective approach to remove silver ions or nanoparticles from wastewater.

This research studied the impact of biomass wastes and the pyrolysis conditions to produce optimum biochar for silver adsorption. Characterisation of biomass and the respective biochar revealed the physical and chemical properties. This preliminary characterisation data assisted in understanding how these properties influence silver adsorption. This investigation also allowed to select the best biomass from the pre-selected biomasses, algae, waste coffee grounds (SCGs), sawdust, and the optimum pyrolysis conditions to produce desired biochar. Pyrolysis kinetics and the composition of pyrolysis vapour established the possibility of utilising the pyrolysis by-products to offset the pyrolysis cost. Detailed studies of silver removal in batch mode and pilot-scale continuous process demonstrated the feasibility for scaling up this process. Biochar samples were produced from different biomass feedstocks to investigate the impact of different types of biomass wastes, such as SCGs, sawdust, and algae on biochar properties and their implication on silver adsorption. A detailed thermogravimetric analysis of biomass, specific surface area, surface functional groups, and pyrolysis kinetic study revealed that the SCGs were the most suitable biomass waste to produce biochar at 500^{o}C and a heating rate of 10°C/min for 2 h retention time. Although sawdust produced the biochar with a higher surface area of 345.7 m^2/g, the biochar provided low silver

adsorption capacity. On the contrary, SCGs biochar produced at 500°C had a low surface area of 40.1 m^2/g, but SCGs biochar showed the highest adsorption capacity of 49.0 mg/g. The FTIR analysis confirmed the presence of remaining surface functional groups, such as -OH, -CO-, and carboxylic acids groups in SCGs derived biochar. These groups might be responsible for the high silver adsorption of SCGs derived biochar. According to the Pyrolysis-gas chromatography-mass spectrometry (Py-GCMS) results, SCGs biomass decomposed to produce a significant amount of fatty acids 49.6%, and algae produced 56.0% of ketones and aldehydes, while sawdust generated 28.7% of phenols. Collection of condensable pyrolysis gas as bio-oil or recovery of chemicals from the pyrolysis vapour can offset the pyrolysis cost by up to 50%.

To optimise the pyrolysis temperature, SCGs biomass was pyrolysed again at temperatures between 500 and 1000°C to produce biochar and investigate their silver removal performances. Results demonstrated that the biochar produced at 500°C (yield of 23.48%) showed a maximum surface area of 40.1 m^2/g and the highest silver adsorption capacity of 49.0 mg/g with 99.9% silver removal efficiency. However, biochar derived at higher temperatures gradually showed a noticeable decrease in surface area, surface functional groups, and silver adsorption capacity. The characteristics of adsorbed silver on biochar were studied by using Scanning electron microscopy and dispersive X-ray spectrometry (SEM-EDS), X-ray diffraction (XRD), and X-ray photoelectron spectroscopy (XPS). Results confirmed an even distribution of silver on the biochar surface, and part of the silver ions was transformed into metallic silver (Ag^0)/Ag NPs during adsorption. The kinetics and isothermal evaluation showed that silver adsorption by biochar complied with the pseudo-second-order model and Langmuir isotherm. This could also be interpreted that silver adsorption is mainly dominated by chemisorption and monolayer silver deposited on a homogeneous biochar surface.

Finally, a dynamic performance study was conducted on a fixed-bed adsorption column packed with SCGs biochar to remove silver ions (Ag^+) and Ag NPs from wastewater. A series of experiments under different column operating conditions revealed that adsorption capacities were remarkably impacted by the initial concentration of silver, biochar quantity, and forms of silver (Ag^+ and Ag NPs). Further validation by using Thomas and Yoon-Nelson models showed a good agreement with both these models, where the simulated values of column parameters were similar to the experimental values.

SEM-EDS and XRD analyses of silver-loaded biochar confirmed the morphology of deposited silver, crystal structure, and changes in the ionic state of silver. XPS data showed that both forms of silver (Ag^+ and Ag NPs) underwent a chemical transformation during the adsorption. After each adsorption cycle, the saturated column was regenerated by using 0.05 M HNO_3 as eluent, which allowed the biochar column to be used at least 3 times with a total of 14.4% capacity loss compared to the performance of the first cycle of adsorption. This demonstrated the feasibility and the effectiveness of using biochar for silver adsorption. Overall, this study concludes that silver adsorption by SCGs biochar is an economically feasible and sustainable solution to mitigate silver pollution from wastewater as well as an alternative solution to reduce greenhouse gas (GHG) emissions from the landfilling of biomass waste.

In a nutshell, this thesis suggests that biochar production from renewable biomass sources could be a sustainable and economical approach for silver removal from aqueous solutions. Thus, this approach could be considered when structuring effective strategies for silver mitigation from wastewater.

TABLE OF CONTENTS

LIST OF FIGURES

LIST OF TABLES

LIST OF PUBLICATONS

Journal Publications

- Islam, M. A., M. V. Jacob, and E. Antunes (2021). "*A critical review on silver nanoparticles: From synthesis and applications to its mitigation through low-cost adsorption by biochar*" Journal of Environmental Management, 2021, 281: 111918.

- Islam, M. A., Dada, T. K., Parvin, M. I., Duan, A. X., Sarmah, A. K., Antunes, E., "*A thermogravimetric and kinetic study of biomass feedstocks for the production of value-added chemicals and biochar for silver removal from wastewater*", Journal of Environmental Chemical Engineering (to be submitted).

- Islam, M. A., Dada, T. K., Parvin, M. I., A. K., Kumar, R., Antunes, E., "*Optimisation of pyrolysis temperature to produce spent coffee grounds (SCGs) derived biochar for silver adsorption and its validation by kinetic and isothermal modelling*", Environmental Research (submitted).

- Islam, M. A., Dada, T. K., Parvin, M. I., Vuppaladadiyam, A. K., Kumar, R., Antunes, E. (2022), "*Silver ions and silver nanoparticles removal by coffee derived biochar using continuous fixed-bed adsorption column*", Journal of Water Process Engineering, 48, 102935.

1 INTRODUCTION

1.1 Problem statement

Human technophilia increased the application of silver over the past 50 years as silver is used for numerous applications, such as mirrors, photographic plates, solar panels, radiography, jewellery, and high-value tableware. Silver has some unique properties, such as high electrical and thermal conductivity, excellent corrosion and oxidation resistance among metals [1]. In addition, special optical, physicochemical, and powerful antimicrobial properties make silver nanoparticles (Ag NPs) suitable for various products, such as medical and health care products, textiles, electronics, food packaging, catalysts, paints, and coatings. Worldwide, the total estimated production of Ag NPs is about 500 tonnes per year, with an increase every year [2-5].

The widespread application of silver species causes their release into the aquatic system and poses a severe threat to the aquatic ecosystem and a potential risk to human health [6, 7]. Silver is more toxic to fish than copper or mercury [8]. High exposure to silver compounds may cause several toxic health effects, such as argyria, liver, kidney, and respiratory disorders [9]. Ag NPs show toxicity to cell-based in vitro systems, bacterial growth, algae, fishes [10, 11], water plants, and human health [12]. Therefore, silver in the water body is classified as a hazardous material by the World Health Organisation (WHO), Australia, the U.S. Environmental Protection Agency (USEPA), and Germany [13-15]. Silver can be present in wastewater as a mixture of Ag NPs, aggregated nanoparticles, silver ions, and silver sulphide [16]. Over time, chemical transformations often occur through oxidation, reduction, dissolution, and/or sulfidation [17, 18].

Silver ions interrupt the electron-transport system and DNA reproduction in the cell. They can also directly interact with DNA [1] and denature DNA and RNA [2]. However, the dissolution of Ag NPs into Ag^{+} ions can produce reactive oxygen species (ROS) that deactivate microorganisms [3]. Therefore, Ag NPs are likely to be more toxic than silver ions in the same environmental conditions. The transformation of silver in the natural environment depends on several factors, such as pH, coexisting pollutants, humic acids, dissolved oxygen (DO), natural

organic matter (NOM), and so on. It is vital to remove both forms of silver from wastewater before discharging it into the natural environment [19, 20].

Many techniques are available to treat silver from wastewater, for example, chemical precipitation, activated sludge, ion exchange, and reverse osmosis. None of these technologies is cost-effective or eco-friendly due to their limitations in being able to deal with low concentrations (ng/L to μg/L) of silver in the influent, which may result in the production of toxic sludge [21]. Therefore, developing an economically and environmentally feasible technology to mitigate silver pollution is crucial. Adsorption can be a promising sustainable alternative to remove low concentration silver from wastewater.

Several studies have demonstrated the application of different adsorbents for silver removal, such as activated carbons, zeolites, clays, biowaste materials, graphene, cellulosic materials, and biochar [22, 23]. Biochar has additional advantages compared to other adsorbents. Biochar can be produced from renewable sources using thermochemical conversion processes such as pyrolysis, which requires relatively less energy and chemicals. Producing biochar from waste biomass is an effective way to sequester carbon, which would produce greenhouse gas (GHG) through conventional disposals, such as landfill [24]. Overall, biochar has a lower environmental footprint compared to other adsorbents.

Biomass wastes are biodegradable and produced from different agro-industries, seaweeds, food processing, wood processing, municipal wastes, and wastewater treatment plants [25]. Biomass consists of mainly cellulose, hemicellulose, lignin, and some micro and macronutrients [26]. Approximately 140 gigatonnes of biomass wastes are generated annually, with a significant increase each year [27]. Most of the waste biomass ends up in landfill, which is a major source of greenhouse gas (GHG) emissions. However, biomass waste can be converted into high value-added chemicals, renewable energy, biochar, and building materials [28]. Any proportion of biomass waste conversion into value-added products can significantly decrease GHG emissions and reduce environmental risks. Thermochemical conversion of biomass waste into valuable products is considered as a promising alternative to step forward to a circular economy approach.

1.2 Research objectives

The primary objective of this research is to understand the impact of preselected biomass wastes and pyrolysis conditions on biochar properties to achieve maximum silver adsorption. Secondary adsorption is to reveal pyrolysis kinetics and pyrolysis vapour composition to assess the possibility to utilise the by-products to offset pyrolysis cost, a batch study of silver adsorption, and the transformation of silver species during the adsorption. The last part of this research was to develop a fixed-bed adsorption column to scale up the batch process to a continuous mode for both silver ions and silver nanoparticles.

The specific research objectives of this thesis are as follows:

- Study the impact of different types of biomass waste, such as spent coffee grounds (SCGs), sawdust, and algae on biochar properties and their implication on silver adsorption, pyrolysis kinetics and pyrolysis vapour composition
- Examine the impact of pyrolysis conditions on biochar yield and their physicochemical properties, and how these properties influence silver adsorption and validation of silver adsorption mechanism by kinetics and isothermal modelling
- A comprehensive pilot-scale study by designing a fixed-bed biochar adsorption column to remove both silver ions and silver nanoparticles in a continuous mode.

1.3 Thesis organisation

This thesis is comprised of four chapters. Each chapter is either published in a peer-reviewed journal or submitted as a manuscript for publication. Since this thesis is a combination of several separate chapters, each chapter contains its materials and methods section to cover the individual knowledge gap and scope of work.

Chapter 1 – Introduction: This section includes the motivation for this research work and the potential outcomes. This also includes the outline of the research objectives as well as the orientation of thesis chapters.

Chapter 2 – Literature Review: A critical review that collates the development of Ag NPs from synthesis and applications to its mitigation through low-cost adsorption by biochar. This chapter explains the synthesis, application, chemical transformation of Ag NPs, silver toxicity, and low-cost mitigation of silver pollution. The low-cost mitigation section also includes the advantages and disadvantages of different adsorbents.

This chapter has been published as Islam, M. A., M. V. Jacob, and E. Antunes (2021). "A critical review on silver nanoparticles: From synthesis and applications to its mitigation through low-cost adsorption by biochar." Journal of Environmental Management, 2021, 281: 111918.

Chapter 3 – Impact of biomass feedstocks and pyrolysis kinetics on biochar properties and vapour compositions: This chapter consists of four separate steps. In the first step, biomass feedstock was preselected based on the literature review and availability in QLD, Australia. Secondly, a pyrolysis kinetics study and pyrolysis GCMS analyses were carried out to predict the optimum pyrolysis condition and the pyrolysis vapour compositions, respectively. Thirdly, biochar was produced at different temperatures and characterised. Finally, preliminary silver removal performance from the aqueous solution was assessed for all the biochars derived from different biomass feedstocks. It was demonstrated that a collection of bio-oil from the pyrolysis process could offset the cost of pyrolysis to a great extent.

This chapter will be submitted as Islam, M. A., Dada, T. K., Parvin, M. I., Duan, A. X., Sarmah, A. K., Antunes, E., "A thermogravimetric and kinetic study of biomass feedstocks for the production of value-added chemicals and biochar for silver removal from wastewater."

Chapter 4 – Investigating the impact of pyrolysis conditions and mechanisms of silver adsorption by biochar: In this chapter, SCGs biochars were produced by pyrolysing at a range of temperatures from 500 to 1000°C. The optimum pyrolysis temperature was determined based on the silver adsorption efficiency of the biochars. Biochar produced at 500°C provided the maximum adsorption of silver. The kinetic and isothermal studies of silver adsorption were carried out to understand the adsorption mechanisms. Further characterisation of the silver-loaded biochar established the silver adsorption kinetics. XPS analysis of silver-loaded biochar reconfirmed the chemical transformation of silver ions during adsorption.

This chapter has been submitted as Islam, M. A., Dada, T. K., Parvin, M. I., A. K., Kumar, R., Antunes, E., "Optimisation of pyrolysis temperature to produce spent coffee grounds (SCGs) derived biochar for silver adsorption and its validation by kinetic and isothermal modelling."

Chapter 5 – Silver removal performance in a fixed-bed adsorption column: This chapter provides an insight into scaling up the batch adsorption process to continuous mode. After the successful application of SCGs biochar to remove silver ions from aqueous media, a fixed-bed biochar column was designed and packed with SCGs biochar along with quartz sand. A dynamic study of silver ions and Ag NPs adsorption by the biochar column was evaluated. Finally, the regenerating and reusing potential of the fixed-bed adsorption column was assessed to understand the economic feasibility of scaling up the whole process and the reusability of biochar.

This chapter has been published as Islam, M. A., Dada, T. K., Parvin, M. I., Vuppaladadiyam, A. K., Kumar, R., Antunes, E., "Silver ions and silver nanoparticles removal by coffee derived biochar using a continuous fixed-bed adsorption column."

Chapter 6 – Conclusion and recommendation: This chapter summarises the overall outcome of this research and provides recommendations for future research.

2 LITERATURE REVIEW

Abstract

Silver nanoparticles are one of the most beneficial forms of heavy metals in nanotechnology. Due to its exceptional antimicrobial properties, low electrical and thermal resistance, and surface plasmon resonance, silver nanoparticles are used in a wide variety of products, including consumer goods, healthcare, catalysts, electronics, and analytical equipment. As the production and applications of silver nanoparticles containing products increase daily, the environmental pollution due to silver nanoparticles release is increasing and affecting especially the aqueous ecosystem. Silver nanoparticles can kill useful bacteria in soil and water, bioaccumulate in living organisms and even at low concentrations from 10^{-2} to 10 µg/mL silver can show antibacterial effects. On the other hand, the maximum silver discharge limit into freshwater is 0.1 µg/L and 3.2 µg/L for Australia and the USA, respectively. To reduce its toxic consequences and meet the regulatory guidelines, it is crucial to remove silver nanoparticles from wastewater before it is discharged into other water streams. Several technologies are available to remove silver nanoparticles, but the adsorption process using low-cost adsorbents is a promising alternative to mitigate silver nanoparticle pollution in the bulk stage. As one of the low-cost adsorbents, biochar produced from biomass waste could be a suitable adsorbent. This review focuses on collating the latest evidence on silver nanoparticle production, applications, environmental consequences, and cost-effective technological approaches for silver removal from wastewater.

Keywords: adsorption; biochar; environmental pollution; nano silver; nanoparticles

2.1 Introduction

Silver nanoparticle (Ag NP) is an important innovation in nanotechnology. Unique physicochemical and strong antimicrobial properties make silver nanoparticles suitable for numerous applications [12, 29, 30]. Particularly biomedicines, medical devices, functional textiles, cosmetics, food packaging, food supplements, odour-resistant items, electronics, household appliances, dental amalgams, water disinfectants, paints, and room spray [10, 31]. Therefore, increasing demand has led to a rise in silver nanoparticles production. Worldwide, the total estimated production of silver nanoparticles was about 500 tonnes per year in 2009, while expecting an increase of approximately 900 tonnes by 2025 [2-5, 32].

Silver ion and metallic silver nanoparticles are both hazardous to living organisms and aquatic ecosystems [33]. Ingestion of silver may cause health risks by metabolising and depositing in subcutaneous fat [13, 14]. Silver ion in the water system is classified as a hazardous material by the World Health Organization (WHO), the U.S. Environmental Protection Agency (USEPA), Australia, and Germany [13-15]. Further, wastewater generating from manufacturing processes and usage of these products are contaminated with silver nanoparticles and/or silver ions [34-37]. Therefore, it is important to remove either form of silver from the wastewater before discharging the effluent into the natural environment [19, 20].

The concentration of silver nanoparticles or silver compounds in wastewater varies depending on the wastewater generating points. In Malaysia, concentrations of silver nanoparticles found in sewage treatment plant (STP) vary between 0.13 and 20.02 mg /L [5], in Canada up to 1.9 µg/L [38], and in Germany between 0.32 and 3.05 µg/L [39]. A wastewater treatment plant (WWTP) with primary treatment processes, such as screening, precipitation, coagulation, and followed by biological treatment can remove most of the silver nanoparticles and silver compounds [20, 39, 40]. However, wastewater treatment facilities, which have no preliminary or primary treatment process, can be impacted by silver toxicity and may lead to a discharge of contaminated effluents [41, 42] as silver ions have a negative influence on bacteria dominant aerobic treatment processes [2, 43-45]. Even low concentrations of silver (ng/L) are toxic and still represent a real threat to the environment for the long run [21, 46].

In terms of economic feasibility, easy operation, and sustainability, adsorption is a promising method to remove low concentrations of heavy metals including silver and other precious metals from wastewater [47-50]. Adsorption is the adhesion of atoms, ions, or molecules to the surface of a substrate by chemical or physical interactions [50]. Silver adsorption study by using a low-cost adsorbent has gained substantial interest in recent years [13, 51]. Several studies have been found on silver removal using different adsorbents, but just a few research has been done so far on the application of biochar to remove silver from an aqueous solution [50, 52]. However, biochar produced from biomass might bring a breakthrough [53].

The present review made an effort to analyse the progress on silver nanoparticles application, consequences, and mitigation of its environmental toxicity by adsorption. To our best knowledge, this is the first review on silver nanoparticles from the synthesis processes to their environmental mitigation.

2.2 Silver nanoparticles synthesis

Metallic silver is a naturally available soft, white, lustrous rare element with high thermal and electrical conductivity [54-56]. Silver nanoparticles are a special form of metallic silver having less than 100 nm size in at least one dimension, which offers silver nanoparticles a high surface area to volume ratio [3, 30]. Silver nanoparticles can be produced by several methods, such as physical and chemical processes as shown in Figure 1 [57]. Each process has some advantages and disadvantages in terms of process complexity, particle size distribution, stability, applications of Ag NPs, and cost.

In the physical process, metallic solid silver is firstly evaporated in a furnace by conventional heating or electrical arc discharge and then condensed as nanoparticles [58]. Uniform particle size, narrow particle size distribution, and uniform shape of Ag NPs can be produced by changing the thermal or ac power, and arc discharge [59]. The common drawbacks of this conventional process are the high energy consumption, heating up the surrounding environment, and a long time to achieve thermal stability [60]. However, laser ablation is one of the most used physical processes where the metal plate absorbs a laser impulse to produce a plasma phase of silver atoms which form different particle sizes of silver nanoparticles by varying silver ions [61]. The cooling liquid medium allows condensation of nano drops of silver, and finally, high purity and desirable silver nanoparticles are produced by this process

[62]. The laser ablation process produces pure Ag NP colloids as there is no use of chemicals in the solution.

Spray pyrolysis (thermal decomposition) is another physical method by which monodisperse Ag NPs in poly (vinylpyrrollidone) matrix can be produced without any reducing agent [63]. In this process, an aqueous solution of $AgNO_3$, and dextran or polyvinylalcohol (PVA) is first injected into an electrically heated horizontal tubular reactor [64], and then the solution is ultrasonically atomised and carried out from the reactor by nitrogen gas which protects the Ag NPs from oxidation [65, 66]. Silver nanoparticles can be also produced from direct silver metal sputtering into a liquid medium (glycerol and water). The silver nanoparticles produced from metal sputtering were spherical with a uniform particle size distribution with an average diameter of approximately 3.5 nm [67]. Another potential production method for silver nanoparticles is the emulsion detonation synthesis using precursors, such as silver salts or metal particles [68]. In summary, the physical processes require high energy and are costly, but produce silver nanoparticles with a narrow particle size distribution and are the most suitable methods to produce a large volume of Ag NPs in the form of powder [60].

Chemical processes are the most common and simple methods to produce Ag NPs. Controlling particle growth in order to produce small spherical Ag NPs with narrow particle size distribution is one of the main challenges of this method. Chemical synthesis methods of silver nanoparticles often use three main components: metal precursor, reducing, and stabilising agents. Silver nanoparticles are mainly produced from the reduction [69] of silver salts such as silver nitrate ($AgNO_3$), silver perchlorate ($AgClO_4$), and silver tetrafluoroborate ($AgBF_4$). Commonly used reducing agents are ethylene glycol ($C_2H_6O_2$), ethanol (C_2H_5OH), glucose ($C_6H_{12}O_6$), sodium borohydride ($NaBH_4$), hydrazine (N_2H_4), and sodium citrate ($C_6H_5Na_3O_7$) [57, 69]. During the chemical synthesis of silver nanoparticles, it is also essential to use some sort of stabilising agents to stabilise the nanoform of silver by avoiding the aggregation of freshly prepared nanoparticles. For instance, polyvinyl pyrrolidone (PVP), polysaccharide, polyvinyl alcohol (PVA), polyethylene glycol (PEG), chitosan, oleylamine, and gluconic acid [57, 70]. The formation of initial nuclei and the subsequent growth of nuclei are the most important processing stages to determine the uniformity of size and shape of Ag NPs, which can be controlled by the reaction conditions, such as pH, reaction time, silver salts, reducing agents, and capping chemicals [71, 72]. A chemical process is more suitable to produce highly monodispersed and shape-specific Ag NPs [73, 74].

Some researchers have successfully used selective plant extract or living organisms as a reducing agent to replace synthetic chemicals. Using plant extract in the chemical reduction process is often termed biological reduction or eco-friendly or green manufacturing process of silver nanoparticles [57, 70, 75]. Recently, this biological pathway has been gaining high interest because of a potential lower environmental impact compared to other chemical processes [76, 77]. The biological method is not only simpler and low-cost, but also has a lower environmental impact due to the elimination of toxicity from the unreacted synthetic chemicals and their disposal [78, 79]. Ag NPs produced from the green synthesis route are less likely to aggregate in the cell biological environment, which helps Ag NPs in their biomedical applications [80].

Silver nanoparticles can also be synthesised by electrochemical cell methods where a silver anode dissolves gradually. Under the electrolysis conditions, produced silver ions are reduced at the platinum cathode, and subsequently, a colloidal suspension of silver nanoparticles is produced [81, 82]. Silver nanoparticles are produced by photochemical methods using electromagnetic radiation. In this process, ultraviolet and visible lights are used. The reduction is carried out by the silver ions which are produced by the irradiation of the solvent molecules [12, 83].

Ag NPs are also produced by mechanical ball milling (mechanical process), which is a top-down physical process. The silver nanoparticles are produced by grinding coarse silver particles (usually microparticles) that are placed in a ball mill and subjected to high-energy collision from ceramic balls. [84]. The final size of Ag NPs depends on the size of the ceramic balls, milling time, and concentration of silver particles in the mill. However, solid powder of silver salts, such as silver nitrate can also be milled with an organic reducing agent (i.e., lignin, plant extracts) by ball mill and produce Ag NPs, and this process is often classified as a mechano-chemical process [85, 86]. Mechanical ball milling is advantageous for its low energy consumption, simplicity, and high potential for mass production of Ag NPs [85]. A representation of the production methods is presented in Figure 1 while Table 1 summarises the main processing conditions, properties, and applications of Ag NPs for the most used production methods.

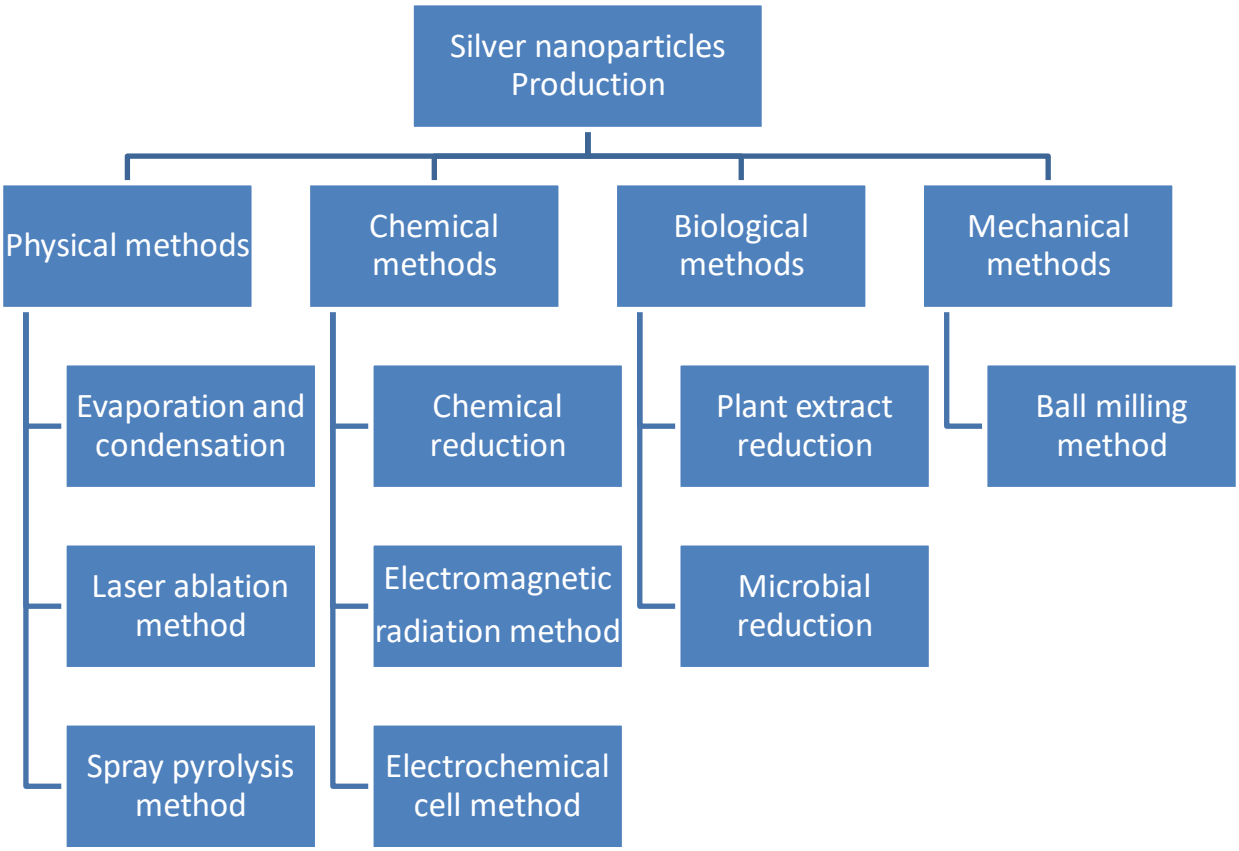

Figure 1: Main silver nanoparticles production methods.

Table 1: Few examples of shape-specific Ag NPs synthesis methods, properties, and their applications.

Method	Process	Reagents and Conditions	Properties of Ag NPs	Application of Ag NPs	Reference
Physical Methods	Laser ablation	Precursor = Silver 99.99% Laser ablation at 355, 532 and 1064 nm light and laser power 12 mJ/pulse for 30 min	Size: 10 - 30 nm Shape: Spherical	Electronic devices, catalyst	[87]
		Precursor = Silver 99.99% Laser ablation at 532 nm light and laser power 0.34 J/pulse for 5 min	Size: 2 - 5 nm Shape: Spherical	Electronic devices, catalyst	[88]
Chemical Methods	Chemical reduction	Precursor = Silver chloride (0.01 M) Reducing agents = hydrazine hydrate (0.1 M) Capping agent = 2% PVA pH 8–9 by ammonia at room temperature	Size: 10 - 60 nm Shape: Spherical or pseudo-spherical	Biomedical science (anti-bacterial)	[71]
		Precursor = Silver nitrate (10 mM) Reducing agents = $NaBH_4$ (8 mM) in NaOH (0.125 M) Capping agent = trisodium citrate (100 mM) silver seeds are instantly irradiated with a 70 W sodium lamp for 2 h	Size: 4 - 5 nm Shape: Triangular / nanoprisms	Plasmonic and sensing, analytical devices, photovoltaics, molecular detection	[89]
		Precursor = Silver nitrate (95 mM) Reducing agents = hydrochloric acid in ethylene glycol (3mM) Capping agent = 2% PVP at 130°C for 10 h	Size: 50 ± 5 nm Shape: Nanocubes	Cysteine sensing, analytical devices	[90]
		Precursor = Silver oxide Reducing agents = Not Applicable as reaction supports oxidation reduction growth at 200 - 300°C	Size: 40 - 55 nm Shape: Nanorods	Plasmonic and sensing, analytical devices	[91]
		Precursor = Silver nitrate (0.1 M) Reducing agents = Trisodium citrate (0.1 M) Capping agent = Formaldehyde (1.5 M) Irradiated by MW (650 W, 2.45 GHz) for 1 min	Size: 24 - 132 nm Shape: Spherical	Anti-bacterial	[92]
		Precursor = Silver nitrate (0.25 mM) Reducing agent = Starch Capping agent = cetyl trimethyl ammonium bromide (0.2 M) at 40°C temperature for 12 h	Size: ~ 60 nm Shape: Hexagonal	Plasmonic and sensing, analytical devices	[93]
		Precursor = Silver nitrate (15 mM) Reducing agent = Starch Capping agent = Cetyl trimethyl ammonium bromide (0.1 M) at 27°C temperature for 20 h	Size: ~ 40 nm Shape: Flower-shaped	Analytical devices (SERS), catalysis	[93]

		Precursor = Silver nitrate Reducing agent = $NaBH_4$ Capping agent = trisodium citrate and ascorbic acid electrochemical cell process at room temperature	Size: 2 - 5 nm diameter and 2 - 4 μm length Shape: Nanorods and nanowires	Plasmonic and sensing, analytical devices	[94]
Biological methods	Biological reduction by plant extracts	Precursor = Silver nitrate (20 mM) Reducing agents = fresh extract of Artichoke (Cynara scolymus L.) flower heads pH 7 at 40°C temperature	Size: 30 - 80 nm Shape: Spherical	Electronic applications	[76]
		Precursor = Silver nitrate (1.0 mM) Reducing agents = turmeric powders at room temperature	Size: 5 - 35 Shape: Spherical and quasi-spherical	Agricultural and food industries	[95]
		Precursor = Silver nitrate (1.0 mM) Reducing agents = S. mammosum extract pH 9 by NaOH at 35˚C (± 1) temperature for 30 minutes	Size: 10 - 14 nm Shape: Spherical	Biosensor	[96]
		Precursor = Silver nitrate Reducing agents = Quercetin (QUC,3,3Q,4Q,5,7-pentahydroxyflavone) (50 mM) at pH 7	Size: 5 - 8 nm Shape: Spherical	Biosensor	[97]
		Precursor = Silver nitrate (0.1 M) Reducing and capping agents = Orange peel extract Irradiated by Microwave (700 W) for 15 min	Size: 1 – 56 nm (95% < 30 nm) Shape: Spherical	Anti-bacterial	[98]
		Precursor = Silver nitrate (2.0 mM) Reducing agent = saffron (Crocus sativus L.) wastages extract Ultrasonic irradiation at room temperature for 3 h	Size: 12 - 20 nm Shape: Spherical	Anti-bacterial	[99]
	Microbial reduction	Precursor = Silver nitrate (3.5 mM) Reducing agent = Airborne bacteria (Bacillus sp.) Nutrient agar containing silver nitrate solution is incubated at room temperature for 7 days	Size: 5 - 15 nm Shape: Spherical	Anti-bacterial	[100]
		Precursor = Silver nitrate (3.5 mM) Reducing agent = fungus (C. Cladosporioides) Fungi and nutrient containing silver nitrate solution is incubated at 27°C temperature for 78 h	Size: 10 - 100 nm Shape: Spherical	Anti-bacterial	[101]
		Precursor = Silver nitrate (0.1 g/L) Reducing agent = Bacillus licheniformis at pH 8 Incubated at 27°C temperature for 24 h	Size: 10 - 80 nm Shape: Spherical	Anti-bacterial	[102]

Physicochemical properties of Ag NPs depend largely on the production process and reducing or capping agents used. Each of the synthesis methods produces a colloidal solution of Ag NPs with a specific size and shape. Ag NPs can be produced in a variety of shapes such as nanospheres, necklaces, nanobars, nanocubes, nanoprism, bipyramids, nanostars, nanowires, triangular, hexagonal, nanorice, and flower-shaped [69, 93, 103]. However, according to Table 1, the spherical shape is the most common shape obtained from many of the synthesis processes. The morphology of Ag NPs determines the efficiency of their end application [93]. For example, triangular / nanoprisms shapes are suitable for biosensors, Surface Enhanced Raman Spectroscopy (SERS), and Metal-Enhanced Fluorescence (MEF) [4]. In electronic circuit printing and catalytic usages, Ag NPs size is more important than shape, ultrafine particles with a size ranging from 2 nm to 8 nm are appropriate for these applications [87].

Crystallinity is also an important property of Ag NPs. A higher degree of crystallinity of Ag NPs shows a high quality of SPR by doubling the dephasing time of localized surface plasmons [104]. A study also suggests that single-crystalline Ag NPs showed a three times higher response than polycrystalline Ag NPs on the absorption cross-section of N719 dye [105]. X-ray diffraction data of produced Ag NPs reveals that the face centred cube crystalline structures are (111), (200), (220), and (311) lattice planes [106, 107].

The stability of the colloidal solution of Ag NPs often depends on Zeta potential [108, 109]. Zeta potential is defined by the charge of the particles in a colloidal system [110]. In general, a minimum value of ±30 mV zeta potential is required for a stable colloidal system [111]. The ionic nature or polarity of capping agents or stabilising agents can also influence the physicochemical behaviour of the colloidal solution, such as zeta potential [112].

In summary, each production method has some advantages and some disadvantages. Depending on the applications, Ag NPs are required to have different shapes and purity. For instance, the laser ablation method is suitable to produce Ag NPs for electronics use, where purity is one of the most important properties. However, this physical method may not be suitable for other applications because of its high production cost. Similarly, considering the low environmental impact, green synthesis (biological) methods are promising, but for cheap and bulk production of Ag NPs, pure chemical routes are cost-effective where the synthetic chemicals are used as reducing and stabilising agents. Ag NPs produced from the green

synthesis method has less aggregation behaviour than the Ag NPs produced from direct chemical synthesis, thus retains higher toxicity for a longer time [80]. However, a requirement in terms of the shape of Ag NPs may dictate the selection of the synthesis method.

2.3 Applications of silver nanoparticles

Silver nanoparticles have numerous applications in healthcare, consumer products, information, and communication technology (ICT), food industry, environmental health, and agriculture sectors [54, 57, 70]. Figure 2 shows the main nano silver applications, 30% of silver nanoparticles are used in medical products, 25% in paints and coatings, 15% in functional textiles, and 15% in cosmetics or personal care products [113].

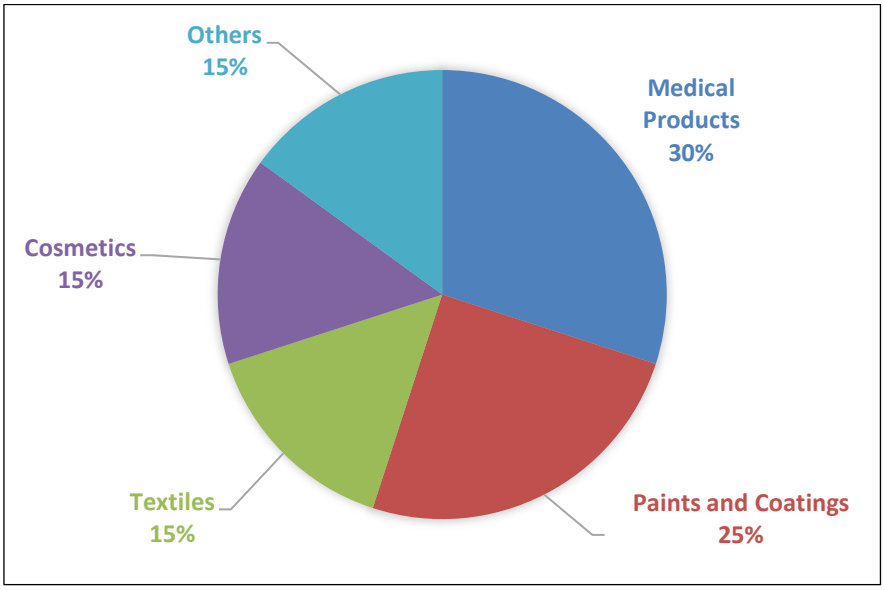

Figure 2: Major applications of silver nanoparticles [113].

Before the discovery of antibiotics, silver compounds were widely used to treat wounds or burns [114, 115]. As infection or diseases caused by bacteria, viruses, or fungi can lead to critical conditions for any patient regardless of age and gender, it is important to prevent any possible microbial activity in a wound. Due to silver's unique antimicrobial properties to fight viruses [116], bacteria, and fungi, silver nanoparticles have been used in diverse healthcare products, such as antimicrobial dressing/bandages, wound care products, breathing tubes, and catheters [70, 117, 118]. Ag NPs are also used in various implantable medical devices, for instance, Ag NPs deposited polymeric composite coatings (single or multi-thin layer) on dental

implants, contact lenses, orthopaedic implants, and cardiovascular implants [119-121]. Direct deposition of Ag NPs on surgical equipment and titanium implants is also a common practice [122-124]. Silver nanoparticles have good potential to be also used as antitumor agents to treat human lung cancer cells [125, 126]. Also, Ag NPs have proven inhibitory effects on HIV1 (human immunodeficiency virus) cells [127-129].

Antibiotic resistance is one of the greatest concerns raised by health experts and WHO [130-132]. Particularly, where antibiotics fail to destroy microorganisms to control the infection or to treat a wound [133]. In those cases, silver nanoparticles containing medication can be beneficial [134-136]. Recent studies have also revealed a synergetic effect of silver nanoparticles when applied with selective antibiotics, such as penicillin G, amoxicillin, erythromycin, vancomycin, and clindamycin [10, 30, 54, 70].

Furthermore, silver nanoparticles have good optical properties such as Surface Plasmon Resonance (SPR), which makes nano silver suitable to be used in biosensors, diagnostics, drug delivery, and imaging [3, 137]. Other examples of applications include analytical sensors in Surface Enhanced Raman Spectroscopy (SERS) [4], Metal-Enhanced Fluorescence (MEF), immune sensing of biological probes, and biological markers where nanoparticles are used [138].

Silver nanoparticles are abundantly used as an ingredient in many consumer products, such as cosmetics, soaps, pastes, antimicrobial textiles, and plastic coatings [17]. The main reason may be the intrinsic antimicrobial effect of silver nanoparticles, even when present in low concentrations [118]. For instance, silver-containing deodorants or socks (functionalised textiles) help to diminish bacterial growth on the skin [133]. In addition, due to very low electrical resistivity [4] and increased stability, silver nanoparticles are used in electronics products such as high conductive pathways, transistors, photonic and antireflective materials, and optical fibres [12, 29, 139].

Preservation of packed foodstuff is still challenging as bacteria or fungi can grow during the storage period. Silver nanoparticles are used in packaging containers and wrapping consumables to prevent and/or control food spoilage and extend the shelf-life [10, 140]. On the other side, organic preservatives are available and widely used in full processed foods; however, they are not suitable for semi-processed foods as they can be converted into toxic

substances under various food processing conditions such as high temperature [70]. A few food supplements also contain silver nanoparticles in low concentrations that are safe for humans, but sufficient to kill microorganisms [70, 141].

Drinking water must also be free from any form of microorganisms. Therefore, the disinfection of potable water is as equally important as filtering. Silver nanoparticles have been used in membrane filters to disinfect drinking water [142, 143]. Similarly, silver nanoparticles are used in the filter of a heating, ventilation, and air conditioning (HVAC) system to disinfect air [70, 144].

Silver nanoparticles are also used as a catalyst for several chemical processes, in particular, their photocatalytic behaviour allows silver nanoparticles to catalyse several chemical reactions, such as hydrogenation of organic compounds and some oxidation reactions [3, 145, 146]. However, some researchers claim that the high surface area and surface energy dominate the catalysis process [4, 29].

Functional textiles often contain silver nanoparticles that are embedded in textiles, but the washing process releases most of the silver nanoparticles [147, 148]. However, silver leaching from the textiles during the washing cycle is driven by several factors, such as nanoparticle size, water quality, hardness, detergent quality, and attachment of silver nanoparticles within textiles [149]. A study in Norway found that washing machines using a 'nano-wash' feature can release silver nanoparticles or silver ions up to 11 μg/L into the water during its operation [147].

Building materials, including paints, contain silver nanoparticles to protect against microbial activity [17]. Figure 3 demonstrates the wide variety of silver nanoparticles applications discussed in previous paragraphs.

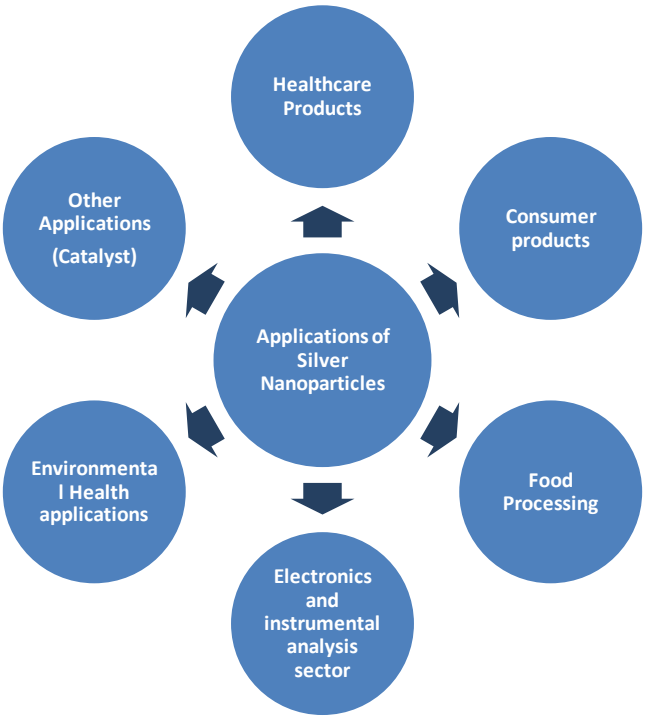

Figure 3: Main applications of silver nanoparticles.

2.4 Consequences and chemical transformation

The environmental and human health consequences of growing production and extensive use of silver nanoparticles are inevitable [150]. Different production methods produce toxic residues, and some of them are even carcinogenic and can cause allergic reactions or bioaccumulate in aquatic organisms [30]. In contrast, ultimately all silver nanoparticles enter into the aquatic environment either through Wastewater Treatment Plant (WWTP) or Sewage Treatment Plant (STP) with the discharged effluents, as can be seen in Figure 4 [3, 17]. For instance, many consumer products and healthcare products release silver nanoparticles that enter into the aquatic environment through the sewage disposal system. Biosolids from WWTPs, STPs, and the ash/residue from Waste Incineration Plant (WIP) have been applied in agriculture as soil amendments, from where silver can leach out and enter again into the surrounding environment [20]. Silver nanoparticles used in building materials can run off and accumulate in the soil [30]. Figure 5 shows that the estimated nano silver flow and the discharge in the aquatic system after wastewater treatment is 13% of total production [151].

Therefore, the study of the toxic effect on organisms and ecosystems gained substantial interest among researchers in recent years.

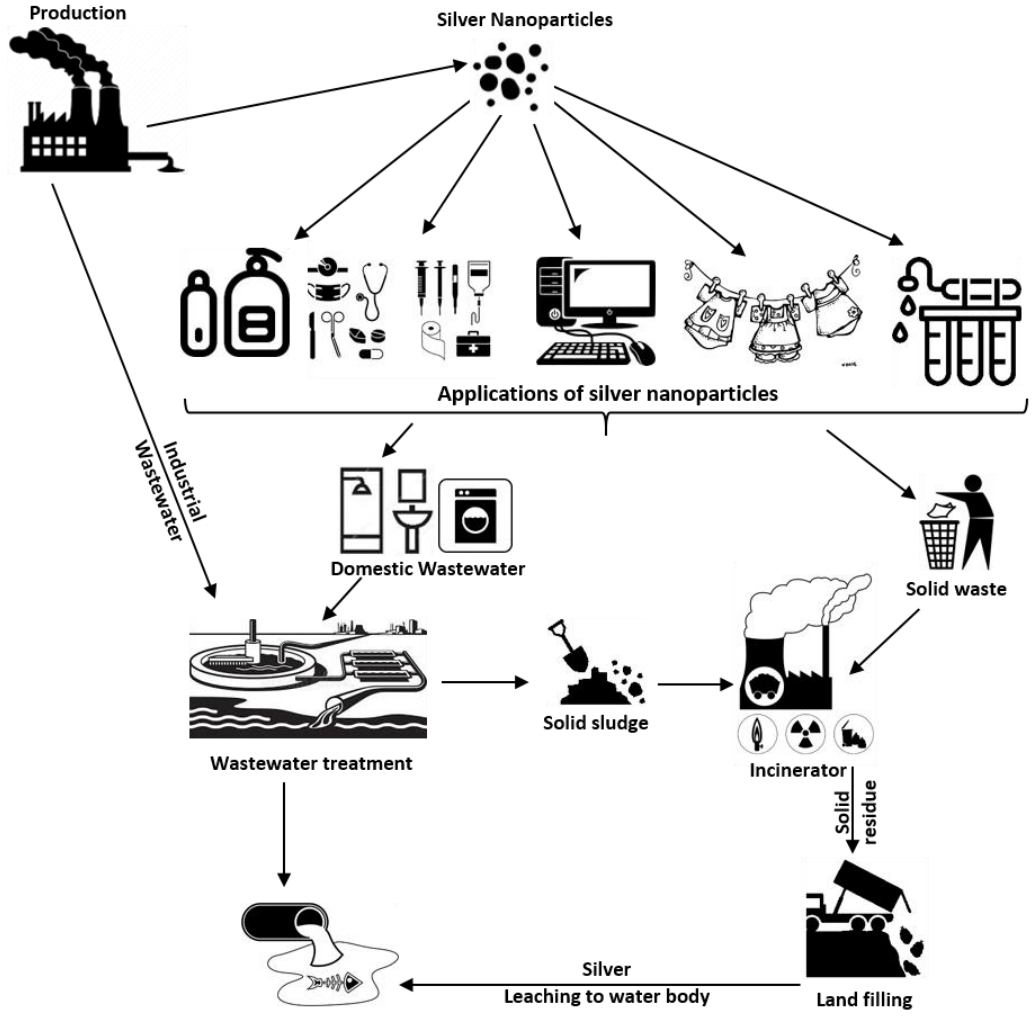

Figure 4: The life cycle of silver nanoparticles.

When the silver nanoparticles come to the open surface water environment, the interaction between Ag NPs and other natural organic materials (NOM), such as fulvic and humic acids create a coating on the surface of Ag NPs and subsequently settles as sediments [152-154]. These coated Ag NPs are analogous to the protein corona [32, 155]. This transformation often contributes to change the aggregation behaviour and toxicity of Ag NPs [156].

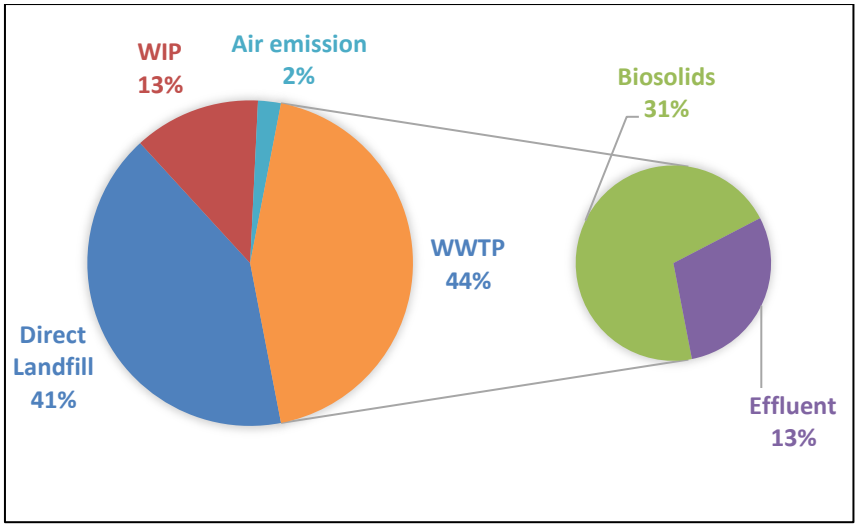

Figure 5: Global material flow for silver nanoparticles [151].

However, silver in wastewater is a mixture of silver nanoparticles, nanoparticle aggregates of silver sulphide, and silver ions [16]. Over time, chemical transformation often occurs, including oxidation, reduction, dissolution, and/or sulfidation [3, 17, 18]. Nevertheless, the dissolution of silver nanoparticles depends on several factors, including the type of surface coating of Ag NPs and surrounding water parameters, such as pH, dissolved organic matter (DOM), dissolved oxygen (DO), coexisting electrolytes, hardness, particle size and exposure time [157-159]. Due to its ionic behaviour, silver ions can bioaccumulate in the organism through cell membrane ion transporters [17]. In contrast, DOM can lead to the reduction of silver ion (Ag^{+}) into silver (Ag^{0}) nanoparticles under sunlight [18, 158, 160]. Therefore, both phenomena demonstrate a direct impact on the aquatic ecosystem. In acidic conditions, silver nanoparticles produce silver ions as demonstrated by reactions (1) and (2) [30]:

$$4Ag_{(s)} + O_{2(aq)} + 4H^{+}_{(aq)} = 4Ag^{+}_{(aq)} + 2H_2O_{(l)} \quad (1)$$

$$Ag_2S + 2H^{+} \rightleftharpoons 2Ag^{+} + H_2S_{(aq)} \quad (2)$$

However, recent studies suggest that the aggregation rate of Ag NPs is directly proportional to the concentration of cations (e.g., Na^{+}, Ca^{2+}), and the presence of humic acid (DOM) expedites the aggregation [161, 162]. Despite the low concentration of DOM in seawater, Ag NPs still show a higher aggregation rate because of the concentration of the cations in the seawater [161]. This aggregation of Ag NPs not only decreases the rate of silver ion (Ag^{+}) release but also helps to decrease the toxic effect of Ag NPs [163, 164]. However, other researchers suggest

that both pH and electrolyte density are mostly responsible for the aggregation, and the presence of DOM inhibits the aggregation because of the biomolecular corona effect [80].

Ag NPs having higher specific surface area show a higher dissolution rate, thereby higher toxicity than Ag NPs having low surface area regardless of particle shape [165]. However, the surface area often depends on the shape of the particles. A study suggests that truncated triangular Ag NPs have more antibacterial properties to the gram-negative organisms than Ag NPs with other shapes [166]. However, another study showed that human alveolar epithelial cells were strongly affected by the wire-shaped Ag NPs, whereas spherical Ag NPs showed no effect [167]. Optical properties are also influenced by the geometrical shape of the particles, but further investigation is required to better understand the impact of the particle shape on other usages of Ag NPs [61].

Silver nanoparticles can contaminate air from the HVAC filters where they are used. These airborne silver nanoparticles can be inhaled by humans [30]. However, researchers show that the potential routes of exposure are mainly oral, inhalation, or transdermal [4, 57]. It is reported that overexposure to silver nanoparticles causes severe skin decolouration to bluish-grey) in humans [57]. However, specific toxicity to humans is yet to be explored [168]. Quantification and comprehensive risk assessment of ecotoxicity need to be carried out.

Silver nanoparticles can be adsorbed by plant species that are growing in soil amended with mostly silver-containing biosolids. In WWTP, usually, silver nanoparticles and silver nitrate ($AgNO_3$) are converted into Ag_2S according to reaction (3) [169, 170], which has low bioavailability in the soil [171].

$$4Ag + O_2 + 2HS^- \rightleftharpoons 2Ag_2S + 2OH^- \quad (3)$$

Silver intake by plant root (wheat, rape) was increased by a high concentration of Cl^- in the soil, but plant growth was not impacted [172, 173]. However, as the silver is adsorbed by plants, consumption of fresh produce loaded with silver compounds may pose a health risk to humans. Additionally, the toxicological studies on phytoplankton (e.g., *Hydrilla Verticillate*), zooplankton (e.g. Daphnia Magna), fish (e.g. zebrafish, rainbow trout, Japanese medaka) showed clear ecotoxicity by silver nanoparticles in different environmental conditions [174, 175]. Therefore, silver bioaccumulation in fish and plant species can be transferred into the food chain [21].

Capping/stabilising agents or chemical coatings have not only a direct influence on the particle size, shape, and aggregation behaviour, but also have a vital role in dissolution and induced cytotoxicity [176]. These coatings are fundamental for the final application. For instance, chitosan derived polysaccharide coated Ag NPs demonstrate significant antimicrobial properties without showing any toxicity to eukaryotic cells [177]. On the other hand, PEG-coated Ag NPs demonstrated a higher dissolution rate than PVP coating [178]. However, the dissolution of any coating or capping agents also depends on the surrounding environment [179].

2.5 Silver Toxicity

Several studies found that silver nanoparticles show toxicity to bacterial growth, cell-based in vitro systems, algae, fishes [10, 11], water plants, and the human reproductive system [12]. Even though many of those studies have been done under controlled laboratory conditions, a short duration of time, and with a relatively higher concentration of silver ions than the real-life situation. Additionally, the natural aquatic ecosystem has a complex dynamic among the inhabitants, surrounding environment, other nanoparticles, and pollutants, and chemical transformation of the different forms of silver at their extremely low concentration (ng/L to µg/L) over a long period of time. Therefore, detailed environmental and health risks associated with silver nanoparticles in a realistic situation are yet to be done [21]. However, recent studies prove that a concentration as low as 10^{-2} to 10 µg/mL silver has shown antibacterial activity [77, 180].

The toxicity of silver nanoparticles can be explained by various mechanisms. The majority of silver toxicological studies show that elemental silver (Ag^0) and monovalent silver (Ag^+) are the most common forms of silver that have demonstrated toxicity. However, the toxic effect of silver is determined by the amount of free silver ions released from the silver substrates [54]. Elemental or zero-valent silver can enter cells and react with oxygen to produce toxic silver ions and reactive oxygen species (ROS), which can cause DNA damage [181, 182].

Human exposure to silver nanoparticles can occur through skin contact with silver nanoparticles containing products, food that contains or is in contact with silver nanoparticles packaging, disinfected drinking water, swimming pools and antifouling, nasal and throat sprays, and other forms of medicines [10, 57]. If the silver ion is ingested by a human, it is

deposited in the subcutaneous fat cells [13, 14]. Excessive exposure can cause argyria, in which human skin turns greyish blue [133, 183]. Silver can also inhibit Na^+ and Cl^- uptake, which may lead to failure of electrolyte balance in body fluid [49]. Airborne silver nanoparticles can enter the lungs and cause chronic health problems, which can become serious for people with preconditions such as asthma or chronic obstructive pulmonary diseases [184].

Silver ion oxidises thiol group of enzymes, thus interrupting the electron-transport chain and DNA reproduction. Ag^+ can also directly interact with DNA [57] and denature DNA and RNA [3]. However, in some cases, the dissolution of silver nanoparticles into silver ions may produce reactive oxygen species (ROS), which can deactivate microorganisms [21, 185]. Therefore, silver nanoparticles are usually more toxic than silver ions in the same environment. Figure 6 summarises the different routes of exposure of silver nanoparticles in the environment, including human exposure.

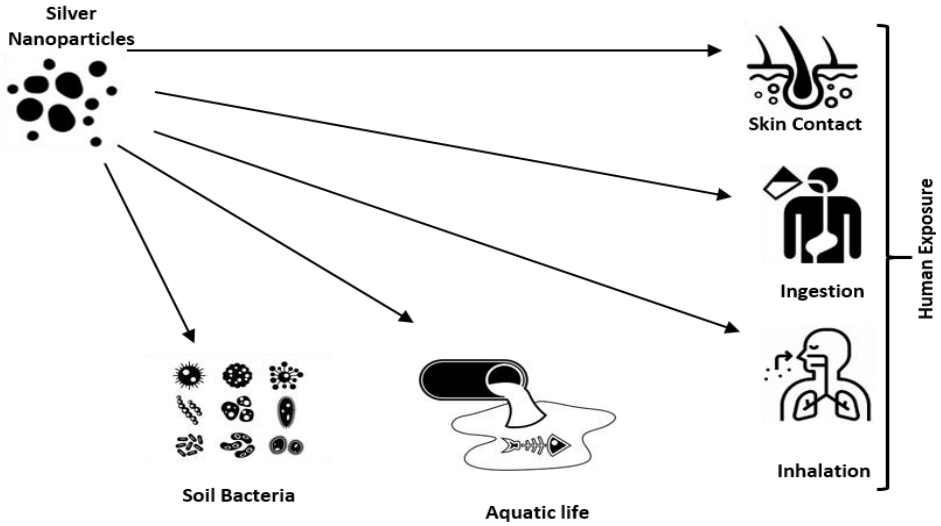

Figure 6: Route of exposure of silver nanoparticles.

Recent studies have demonstrated that all forms of Ag NPs toxicity are size-dependent instead of shape or morphology. Particle size less than 20 nm is more toxic than other larger particle sizes of Ag NPs [186, 187]. Because smaller particle size offers a higher specific surface area which increases the rate of Ag^+ release.

2.6 Regulation

Silver nanoparticles can be released from silver-containing products to wastewater during the production process or after use. Scientists have warned about the widespread use of Ag NPs, in-vitro studies have demonstrated a highly toxic effect on aquatic organisms and the possibility to be environmentally persistent [188, 189]. This growing concern raises awareness among the regulatory bodies and policymakers around the world to control the usage of silver nanoparticles and to ensure the appropriate treatment of wastewater. However, the regulation guidelines provide a maximum acceptable concentration of elemental forms of metals in surface water, groundwater, and drinking water. There is no separate guideline value of discharge for nanoform of silver or other metals in EPA, REACH (Registration, Evaluation, Authorization, and Restriction of Chemicals), EU, UK, Australia, and New Zealand [190]. Despite the evidence of bioaccumulation and cellular toxicity, in vivo and environmental toxicity data of Ag NPs is insufficient for the short and long run. Thus, further investigation is necessary on the impact of Ag NPs under present and future exposure scenarios for both aquatic and terrestrial ecosystems. Nevertheless, all the regulatory bodies are researching detailed toxicity data to set a separate regulation for Ag NPs disposal limits. Regulatory bodies worldwide set the maximum allowable limit for silver; these values are presented in Table 2. The maximum limit for drinking water is 0.1 mg/L for the USA, Australia, and Switzerland, while for Germany and China is 0.08 mg/L and 0.05 mg/L, respectively. The maximum limit for freshwater and marine waters is slighter lower than for drinking water and varies between 0.1 to 7.5 µg/L depending on the country's regulation (Table 2).

Table 2: Permissible limits of silver in water according to various standards.

Country	Regulatory Body	Area	Maximum Limit	Reference
USA	National Secondary Drinking Water Regulations (NSDWR)	Drinking water	0.1 mg/L	[14, 191]
USA	U.S. Environmental Protection Agency (U.S. EPA)	Freshwater and saltwater	3.2 µg/L and 1.9 µg/L	[191]
USA	Toxicity Characteristic Leaching Procedure (TCLP)	Leachate as a hazardous waste	5.0 mg/L	[191]
Australia	ANZECC*	Freshwater and Marine waters	0.1 µg/L and 1.0 µg/L	[192]
Australia	NHMRC**	Drinking water guideline	0.1 mg/L	[15]
Canada	Canadian Water Quality Guidelines for the Protection of Aquatic Life	Freshwater and Marine waters	0.25 µg/L and 7.5 µg/L	[193]
Germany	German Federal Environment Agency (GFEA) (1990)	Drinking-water regulations	0.08 mg/L	[194]
China	National Standard of the People's Republic of China	Drinking water	0.05 mg/L	[195]
Switzerland	WHO	Drinking water	0.1 mg/L	[196]

* ANZECC: Australian and New Zealand Environment Conservation Council

** NHMRC: National Health and Medical Research Council

In this section, a global regulatory point of view on Ag NPs is discussed. **In the USA:** Different US federal agencies such as U.S. EPA, U.S. FDA, and U.S. NIOSH (National Institute for Occupational Safety and Health) work to regulate the environmental and public health impacts of Ag NPs [188]. According to the recent recommendation, NIOSH proposed the maximum exposure limit (REL) of 0.9 $\mu g/m^3$ for silver nanoparticles and 10 $\mu g/m^3$ for any other form of silver [197]. On the contrary, the US Conference of Governmental Industrial Hygienists sets the threshold limit values for metallic silver and soluble silver as 0.1 mg/m^3 and 0.01 mg/m^3, respectively [198]. However, the absence of effective methods for detailed hazard assessment of Ag NPs makes regulation of Ag NPs a difficult task [199]. U.S. EPA and scientists elsewhere urged to develop a comprehensive risk assessment to further investigate the potential health and environmental impacts of all forms of nanomaterials [200].

In the European Union (EU): Like in the USA, the European Food Safety Authority (EFSA) is working to set a separate risk assessment followed by authorisation of nanomaterials. EFSA published a guidance report on risk assessment of the application of nanoscience and nanotechnologies in the food and feed chain in 2018. According to that guidance report, EFSA pointed out that the existing authorisation process is not adequate to cover the safety aspects of a nanomaterial or a corresponding non-nanomaterial [201]. However, the Joint Research Centre (JRC) published a NANoREG framework for the safety assessment of nanomaterials policy document to make a common ground to understand the environmental health and safety (EHS) aspects of nanomaterials under the current European regulatory framework focused on REACH [202]. REACH Regulation 1907/2006 focuses on both applicability and regulatory acceptance of nanomaterials and conventional or bulk substances. Nevertheless, these guidance documents suggest to take specific approaches for Ag NPs to carry out a further risk assessment and uncertainty analysis for future recommendations [203, 204].

In Australia: Despite the growing scientific concern on some nanomaterials which may pose potentially serious health and environmental impacts, the regulatory bodies are yet to place a separate guideline for the nanomaterials in food and agriculture. Food Standards Australia New Zealand (FSANZ), TGA (Therapeutic Goods Association), APVMA (Australian Pesticide and Veterinarian Medicines Association), and the Department of the Environment are working together to assess the public and environmental health and safety of nanomaterials. However, a comprehensive regulation of any nanomaterials and their environmental release control measures have not been addressed yet [205].

2.7 Mitigation

In previous sections, the consequences of silver nanoparticles were discussed. This section focuses on gathering and discussing the potential solutions to mitigate silver pollution as well as the impact on the ecosystem. In recent years, several treatment processes have been explored by researchers. Sequencing Batch Reactor (SBR) [206], activated sludge process [207], anaerobic treatment, membrane filtration, reverse osmosis, and ion exchange can remove most of the silver nanoparticles and silver compounds from wastewater. However, simplicity of operation and cost-effectiveness lead to investigating suitable sustainable alternatives such as adsorption. Several studies have been carried out on different adsorbents such as activated carbons, clays, biowaste materials, cellulosic materials, zeolites, graphene, and biochar. The

adsorption capacity of an adsorbent depends on several physicochemical factors, such as specific surface area (BET), pore size, pore volume, and surface functional groups [208]. More specifically, specific surface area and surface functional groups are the two most relevant contributors to physical and chemical adsorption respectively [23, 209]. The advantages and disadvantages of these various types of adsorbents are discussed in the following sub-sections.

2.7.1 Activated Carbon

Activated carbon is the most popular carbonaceous material used for numerous applications, including wastewater treatment, drinking water purification, air and gas filtration, catalysts, catalyst support, hydrometallurgical processes, and gas mask for personal protection [210]. In general, activated carbon has a very high specific surface area between 200 to 2,500 m^2/g [211, 212] and high pore volume, which makes this adsorbent suitable for adsorbing a wide range of organic and inorganic pollutants, including silver. Activated carbon is one of the widely used commercial adsorbents for air and water purification [49].

Activated carbon can be produced from coal (mineral carbon) or agricultural waste biomass, or naturally available abandoned lignocellulose materials [43, 213]. The production process involves either physical or chemical activation to convert biomass into activated carbon [214, 215]. In both processes, carbonisation is carried out at a temperature from 300°C to 600°C and activation at around 500°C to 900°C in an inert environment [213, 216]. Chemical activation demands an excessive amount of chemicals from 1:1 to 1:6 for the mass ratio of feedstock to activating agent [217, 218]. While physical activation requires CO_2 or steam, chemical activation requires the use of inorganic salts and acids such as $ZnCl_2$, K_2CO_3, HNO_3, H_2SO_4, H_3PO_4, KOH, or NaOH [216, 219].

Finely porous structure and hydrophilic surface functional groups are key characteristics that make activated carbon a good adsorbent [220]. The electrostatic interaction between functional groups presents in the activated carbon and ionic species such as silver ion is responsible for high adsorption [221]. For instance, oxygen anions (O^{2-}) present in the activated carbon forms a bond with silver ions to produce Ag_2O. However, chemical modification of activated carbon introduces strong acidic groups, and increases the density of total surface functional groups, such as –CHO, =CO, –COOH, $–SO_3H$, thus, increasing adsorption capacity [49, 222]. As shown in Table 3, chemical modification of activated carbon by sodium hydroxide treatment

can double the silver adsorption capacity, even in a short contact time [49]. As presented in Table 3, all experiments are favourable at room temperature and for a low initial concentration of silver. Low concentration acid solution (e.g., HNO_3) can be used for silver recovery from the used adsorbents [222]. Adsorption of silver nanoparticles on activated carbon depends largely on the conversion of silver nanoparticles into silver ions [223].

Despite having a large specific surface area which mainly comes from the microporous structure (<2nm) [224, 225], activated carbon cannot utilise those pores to adsorb Ag NPs as Ag NPs are larger than the pore diameter of activated carbon. The main limitations of using activated carbon for silver removal are the activation mechanism, regeneration of activated carbon, and overall cost-effectiveness [214, 216, 226]. The chemical modification involves the additional usage of chemicals, which is not environmentally and economically sustainable. Another limitation is the low or acidic working pH (Table 3). Semi-treated wastewater, which is the input for activated carbon adsorption, exhibits neutral pH after coagulation. Acidification is initially required, which uses extra chemicals to bring the pH down, then neutralising demands more chemicals to meet the discharge limit of pH, 6 to 9 [192, 227-229]. In addition, silver nitrate solution has been used to measure the adsorption capacity except for one case where a mixture of silver ions and silver nanoparticles was used, which would be a more realistic scenario of silver in wastewater. However, the selectivity of silver among other pollutants, and the possibility of scaling up to a continuous process are yet to be explored.

2.7.2 Functionalised biowaste materials

Multiple researchers find that adsorbents having sulphur and nitrogen-containing groups can show a higher affinity to silver ions as both have lone pair electrons [230]. Therefore, absorbents functionalised by amino or thiol groups can have good silver adsorption efficiency from an aqueous solution [231].

Table 3: Summary of silver adsorption capacity by different types of adsorbents from aqueous solution (mainly silver nitrate solution).

Type of Adsorbents	Adsorbent	Pre-treatment / modification	Adsorption capacity (mg/g)	pH	Initial concentration of silver (mg/L)	Contact time	Temp (°C)	Reference
Activated Carbon	Colloidal carbon nanospheres (CNS)	Sodium hydroxide	152	3-9	0.098 - 202	6 min – 32 hrs	Room Temp	[49]
	Activated carbon (Norit® CA1)*	No	65	3-9	50 - 105	12 hrs	20	[223]
	Coconut shell activated carbon	Washed in deionized water	60 - 80	3 - 5	100 - 500	200 min	30 - 50	[232]
	Peat-based activated carbon**	Washed with water	37.2	1.5 - 4.5	120	5 hrs	25	[220]
Biowaste Materials	Trimercaptotriazine-functionalized polystyrene chelating resin	-	187.1	0.0	820	4 hrs	Room Temp	[233]
	Chelamine	-	129.4	6	20 - 700	24 hrs	22±0.5	[234]
	Thiourea-modified chitosan resin	-	406.6	4	1,698	4 - 12 hrs	25 - 55	[235]
	Chitosan	-	42.0	6	50	1 - 96 hrs	20±0.1	[236]
	Hexanedioyl thiourea chelating resin (HTR)	-	491.8	6.9	5,393 (0.05M)	12 hrs	20	[237]
	Ion-imprinted chitosan gel beads	-	89.2	5	353	1 - 48 hrs	25	[238]
Modified celluloses	Magnetic cellulose xanthate	-	166	1	10	5 min – 1 hr	Room Temp	[239]
	L-cysteine functionalized cellulose	-	66.67	6.9	160	1 - 10 hrs	25	[240]
	Mercerized coconut fiber	-	64.93	7.5	169.8	30 - 340 min	30±1	[241]
	Pristine coconut fiber	-	54.15	7.5	25.4	30 - 340 min	30±1	[241]

	Cellulose nanocrystals (CNC)	-	34.35	6.39	107.8	2 hrs	20	[242]
	Chitin nanocrystals (ChNC)	-	19.80	6.63	107.8	2 hrs	20	[242]
	Cellulose nanofibers (CNF)	-	15.45	5.45	107.8	2 hrs	20	[242]
Clays	Modified vermiculite	-	69.2	4	10,000	30 sec - 16 hrs	10 - 20	[243]
	Montmorillonite	-	63.29	6	200	1 - 5 hrs	25	[51]
	Calcined bentonite	-	61.48	-	50 - 200	3 - 120 min	Room Temp	[244]
	Hectorite	-	49.5	4	27	60 min	Room Temp	[245]
	Saponite	-	48.3	4 - 8	2,000	5 hrs	23	[246]
	Raw Vermiculite	-	46.2	4	10,000	30 sec - 16 hrs	10 - 20	[243]
	Perlite	-	8.46	6.5	5 - 50	2 hrs	20 - 50	[19]
Biochars	Biochar-supported nanoscaled zero valent iron (nZVI)	zero valent iron (nZVI)	745.5 and 534.5	-	25 - 300	24 hrs	22±0.5	[33]
	Bamboo biochar	No	640	-	0-3000	24 hrs	22±0.5	[13]
	Engineered biochar from biofuel residue	No	90.06	-	20.7	10 min - 24 hrs	Room Temp	[52]
	Vineyard biochar	No	88.9	5.0± 0.1	50 - 500	70 min	19±2	[23]
	Paulownia tree biochar	No	75.2	5.0± 0.1	50 - 500	70 min	19±2	[23]
	Tobacco biochar	No	72.5	5.0± 0.1	50 - 500	70 min	19±2	[23]
	Biochar produced from biosolids	No	41.5	-	100 - 1000	10 min - 45 hrs	22±2	[50]

* Citrate-coated silver nanoparticles

** Silver sulphate media

Grapefruit peel modified by urea to create an amino group-containing organic matrix refers as bio-template showed 72.33 mg/g silver adsorption from an aqueous medium [230]. Functional groups primarily form silver complexes thereby higher adsorption is achieved. However, strong bond energy between adsorbent and silver ions does not allow full regeneration of the adsorption, which negatively affects the feasibility of the process [230]. Adsorption performances of a few functionalised biowaste materials are shown in Table 3, showing that chelating and chitosan resins demonstrated a high silver adsorption capacity while chitosan has the lowest adsorption rate. The main limitation of using resins and chelating agents is that the initial concentration of heavy metals in secondary or semi-treated effluent has to be more than 100 ppm to make the treatment process workable and feasible [247].

2.7.3 Cellulosic materials

Cellulose is the most abundant natural polymer [248], which is made of D-glucose repeating units [249], a six-carbon ring, also known as pyranose [250]. Structurally cellulose contains several hydroxyl groups that have a substantial impact on adsorption behaviour towards a wide range of water pollutants such as heavy metals (silver, copper, gold, zinc, lead, iron, and chromium), organic dyes, protein, and pesticides [239]. Adsorption capacity and selectivity for a specific target pollutant can be enhanced by chemical and/or physical modification [251].

Silver, along with other heavy metals adsorption studies by modified cellulose, gained considerable interest in recent years. For instance, L-cysteine modified cellulose can provide three surface functional groups (– COOH, $–NH_2$, and –SH), which shows a high silver adsorption capacity of 66.67 mg/g in a batch process and 41.23 mg/g in a continuous column method exhibiting high selectivity towards silver ion in a multiple metal ions environment and good reusability of the adsorption column [240]. Magnetic cellulose xanthate can show up to 166 mg/g silver adsorption capacity from an acidic solution with three cycle adsorption-desorption and has a huge advantage of easy magnetic separation after adsorption [239]. Magnetic celluloses often contain zero-valent iron atoms, which have reductive and complexation tendencies and therefore increase the adsorption capacity [252]. Adsorption behaviour of modified cellulose for silver removal from aqueous solution is summarised in Table 3, showing an adsorption capacity between 15 and 166 mg/g. Table 3 also indicates that cellulosic materials can work at neutral effluent pH, which does not require extra chemicals to

adjust pH. However, adsorbent modification usually requires a chemical treatment that can produce subsequent wastewater and increase the environmental impact of the overall process.

2.7.4 Inorganic adsorbents

Inorganic adsorbents such as zeolite and clay possess good adsorption properties. Zeolites have a porous framework of crystalline hydrated aluminosilicates [253]. Common types of natural zeolites are clinoptilolite, stilbite, natrolite, analcime, mordenite, phillipsite, chabazite, and laumontite. However, several zeolites are synthesised, such as zeolites A, X, Y, and ZMS-5 [254, 255]. Both natural and synthetic zeolites are widely used due to their unique high cation exchange property, molecular sieving, catalytic, and adsorption behaviour [253]. Natural zeolites have been used to remove heavy metal ions and ammonium ions from groundwater and wastewater [256]. Among natural zeolites, clinoptilolite is the most abundant and naturally available with a typical chemical formula of $Na_6[(AlO_2)6(SiO_2)30].24H_2O$, and has shown a silver adsorption capacity of 33.23 mg/g [257]. Chemical modification of zeolites enhances its adsorption capacity and extends the property to adsorb anions and organic pollutants from an aqueous medium [253]. Although the application of zeolites for various heavy metals removal is well studied, very few research has been done on silver adsorption by zeolites. Synthetic zeolite produced from green tuff stone cake showed a maximum silver adsorption capacity of 118.6 mg/g while the H-Na-ZSM-5 zeolite showed 61.4 mg/g [247, 258].

Clay is another example of inorganic adsorbents that have been used for heavy metals removal from an aqueous solution even at a low concentration due to a good adsorption capacity [259]. Clay is a mixture of silica, alumina, metal oxides, water, and other minerals. Scientists classify clays into different groups depending on the quality and minerals present in them, such as kaolinite, montmorillonite, saponite, illite, pyrophyllite, vermiculite, and serpentine [260]. However, most of the clays contain anions and cations that give strong ion-exchange properties to remove inorganic and organic pollutants from wastewater [261]. In contact with water, clays can produce negative charges, which can undergo complex reactions with the positively charged species such as silver, copper, lead, mercury, zinc, chromium, cadmium, manganese, and arsenic to remove them from their aqueous solutions [260, 262].

The main advantage of using clay as an adsorbent is naturally available on the earth's surface, is low-cost, non-toxic, and abundantly available [245]. Nevertheless, scientists urged for pre-

treatment and modification of clay with metallic oxides, such as MnO_2, Al_2O_3, Fe_2O_3, TiO_2, Fe_3O_4, $MnFe_2O_4$, to increase the adsorption capacity and selectivity towards a specific heavy metal or pollutant [243]. Previous researchers demonstrated that modified clay exhibits better results than natural clay (Table 3). For instance, modified vermiculite and raw vermiculite showed a silver adsorption capacity of 69.2 mg/g and 46.2 mg/g, respectively [243], and the pH dependency is moderate. Inorganic materials can work in a wide pH range from 4 to 8. However, the silver adsorption capacity by clays is significantly lower than other adsorbents.

2.7.5 Graphene

Graphene is a single atomic layer of sp^2-hybridized carbons, which are hexagonally arranged [263]. Graphene has drawn substantial scientific attention in recent years for its exceptional physical and chemical properties and multipurpose usages such as energy storage, hydrogen storage, nanocomposite, and nanoelectronics [264]. The large theoretical surface area of approximately 2,630 m^2/g [265] favours graphene to be used as a promising adsorbent to remove pollutants from aqueous media. However, chemical modification helps to improve the surface properties and increase the density of oxygen functional groups [263]. For instance, triethanolamine modified graphene oxide showed a silver ion adsorption capacity of about 410 mg/g after four cycles of reuse [266].

Nevertheless, graphene can aggregate irreversibly by π–π bonding and Van der Waals interactions to form graphite and consequently reducing its adsorption capacity and reusability [267]. The production cost of graphene is still high, and its production processes may have a high carbon footprint. Recently, significant research has been carried out on the preparation of graphene containing biochar that has demonstrated good performance in the adsorption of different pollutants [268].

2.7.6 Biochar

Biochar is the solid carbonaceous by-product from the pyrolysis of biomass, which consists of unconverted organic solids and ash, a mineral fraction of the biomass pyrolysis process [250, 269-271]. Depending on the potential use, pyrolysis parameters can be controlled to produce biochar with desired properties for a specific use. For instance, at a high temperature, volatile materials are removed quickly, which results in high micro-pore volume in the biochar [272].

Micro-porous structure and a large surface area make biochar appropriate for diverse use such as soil quality enhancement and carbon storage [273-277], wastewater treatment [47, 50, 278-284], pesticide remediation [285], fuel and catalyst in energy recovery technologies [286, 287], activated carbon production [215, 288], removal of SO_2 and NO_x from flue gases [271].

Micro-pore volume is the main physical property defining the adsorption capacity of biochar. Surface functional groups are also important for the adsorption of certain pollutants. Pyrolysis temperature is the main processing variable impacting on both properties, surface functional groups decrease at high-temperature (> 600°C) while micro-pore volume increases with pyrolysis temperature [289]. The adsorption capacity of biochar is also affected by properties of contaminants such as ionic nature, polarity, and processing conditions [287]. Therefore, it is fundamental to understand the key biochar properties for adsorption of each compound or element and then define the biochar production. For instance, BET surface area, pore size, pore-volume, surface functional groups, surface charge, pH, and mineral components play a key role in adsorption [290, 291]. For example, pore size has an important influence on metal adsorption; biochar with a small pore size cannot trap large adsorbate particles, regardless of their charges or polarity [290]. Oppositely, favourable polarity or surface charge allows adsorbate particles to enhance their contact with biochar.

Heavy metals (e.g., As, Cr, Cd, Hg, Pb) recovery by biochar is dominated by various mechanisms such as electrostatic interactions, cation exchange, complexation, reduction, and precipitation [290]. Silver adsorption is also driven by different mechanisms depending on the biochar quality and the adsorption conditions. Chemical and/or physical modification is often carried out to increase the density of surface functional groups or to add minerals, reducing agents, and nanoparticles [290]. Surface functional groups such as –COOH, $–NH_2$, and –OH have a strong influence on metal adsorption capacity [292]. Biochar is often treated with alkali, reducing agents, oxidizing agents, carbonaceous materials, metal ions, acid, steam, and gas purging to modify its properties according to a specific use [272].

Biochar has several added advantages compared to other similar adsorbents. For instance, relatively low temperature and less chemically intensive process make biochar less complicated and inexpensive compared to activated carbon. Biochar production is an effective method for carbon-sequestering from waste biomass, which would produce greenhouse gases by

conventional disposal (landfilling) [24]. Therefore, biochar has limited environmental footprints compared to activated carbon.

The application of low-cost adsorbents to remove heavy metals, particularly modified biochar, has attracted much attention in recent years [13, 51]. However, the low-cost sustainable modification and application of biochar to mitigate silver nanoparticles pollution has not been well explored so far. Table 3 compiles all projects where biochar was used for silver removal. According to Table 3, the modification of biochar enhances adsorption efficiency to a great extent. For instance, biochar supported nanoscale zero-valent iron (nZVI) showed up to 745.5 mg/g silver adsorption capacity [33]. The silver adsorption process by biochar can work under a wide range of initial concentrations at room temperature. However, the pH dependency of the adsorption process has not been studied yet.

Firstly, the data shown in Table 3 indicates that only one modification (by zero-valent iron) was studied. Secondly, the pH dependency of the adsorption processes was not monitored and reported. Thirdly, all the experiments were done on silver nitrate solution prepared with double distilled water except for one case. According to the literature, silver can be presented in various forms in wastewater, such as silver nitrate, silver chloride, silver sulphide nanoparticles, and silver nanoparticles. A study demonstrated that the biochar could break the PHBV (polyhydroxybutyrate-co-valerate) composites containing Ag NPs to release silver ions and eventually adsorb in a tropical soil environment [178]. Therefore, biochar adsorption should be tested for other silver forms that are available in aqueous solutions.

In summary, the adsorption capacity of different adsorbents (Table 3) depends on the initial concentration of silver, modification and/or activation of adsorbents, contact time, and solution pH. In general, biowaste materials and biochars are the type of materials with higher silver adsorption capacity. The adsorption capacity of biowaste materials varies between 42 mg/g (for chitosan) and 407 mg/g for thiourea-modified chitosan, showing that the modifying agent/process plays a key role in the adsorption capacity of adsorbents. This is also confirmed by the biochar adsorption results, the biochar modified with the zero-valent iron demonstrated the highest adsorption capacity of 745.5 mg/g. Bamboo biochar has also confirmed a high silver adsorption capacity and is a promising low-cost adsorbent for nanosilver mitigation as well as for other contaminants.

2.8 Conclusions

Water pollution is the greatest threat to the entire ecosystem. Increasing the production and use of silver nanoparticles are going to be an additional toxicity risk for the aquatic environment. Therefore, it is crucial to develop an economically and environmentally feasible process to mitigate silver pollution. Adsorption research has gained significant interest in recent years because of its cost-effectiveness and suitability for bulk effluent treatment. The present review explored the effectiveness of silver adsorption by different adsorbents.

Silver can be present in various forms in wastewater. For instance, silver nitrate, silver chloride, silver sulphide nanoparticles, and silver nanoparticles. However, most of the research has been carried out on silver nitrate, which has not demonstrated the effectiveness of the process in a realistic environment. Modified activated carbon shows good adsorption capacity under certain conditions, such as low working pH. Activation mechanisms to produce activated carbon in order to enhance its adsorption rate as well as regeneration processes to extend the adsorption cycles have been investigated. However, these conditions make the treatment process more complex, more chemically intensive, and cost intensive. The selectivity of silver from other pollutants and the possibility of scaling up to a continuous process are yet to be explored.

Some of the functionalised organic/biowaste materials, such as resins and chelating agents, can work at a neutral pH. However, the initial concentration of silver has to be more than 100 ppm which is impractical compared to the real-life situation where the silver ion concentration is less than the mg/L level. Cellulosic materials can also work at a neutral effluent pH and provide significant adsorption capacity, but the modification of these materials requires chemical treatment, which can produce subsequent wastewater. Inorganic adsorbents, such as zeolites and clay, demonstrated an adsorption capacity significantly lower than the other adsorbents, but they can work under a wide range of pH: 4 to 8. Another promising adsorbent, graphene, has drawn research interest recently, but susceptibility to aggregate and to forming graphite is still a challenge to be further explored. Additionally, the current production methods of graphene have a high carbon footprint due to the high energy demand, which again impacts on the production cost and environment.

Biochar has several advantages compared to other similar adsorbents. For instance, relatively low processing temperature and less chemically intensive production processes make biochar

a low-cost adsorbent compared to activated carbon. Additionally, biochar production from biomass waste helps to capture carbon rather than producing greenhouse gases. However, the low-cost sustainable modification and application of biochar to mitigate silver nanoparticles pollution should be further explored. A few key prospective areas of interest in silver removal may include, but are not limited to:

- selection of appropriate biomass as the composition of biomass often drives the physical and chemical properties of biochar,
- low-cost modification of biochar to increase the adsorption capacity and to extend the reusability of used biochar,
- assessment of the adsorption capacity under a realistic environment, especially the effect of other co-existing chemical compounds or elements,
- experimentation on selectivity and recyclability,
- scaling up of the adsorption process – from batch method to a continuous process,
- in-depth cost study to demonstrate the economic viability of the overall process.

3 IMPACT OF BIOMASS FEEDSTOCKS AND PYROLYSIS KINETICS

Abstract

Thermogravimetric, spectroscopic, and pyrolysis kinetics studies were performed to investigate the influence of biomass composition (spent coffee grounds (SCGs), sawdust, and algae) and pyrolysis temperature (500, 700 and 900ºC) on biochar properties, and their impact on silver (Ag) adsorption capacity. Biomass feedstocks were characterised by proximate and ultimate analysis and thermogravimetric analysis (TGA). TGA results showed that the 10°C/min heating rate provided the highest decomposition rate. Activation energy fluctuation over the decomposition period revealed that the algae had a more complex composition compared to SCGs and sawdust. The characterisation of biochars was carried out to examine their surface area and porous properties, crystallinity, and presence of various chemical groups. Elemental composition results revealed that increasing the temperature from 500° to 900°C increased the surface area of algae biochar (4.06-46.62 m^2/g), but decreased the surface area of biochars obtained from SCGs (40.1-3.4 m^2/g). Sawdust biochars obtained at 700°C and 900°C resulted in the highest surface area of 345.7 m^2/g and the lowest surface area of 127.4 m^2/g, respectively. High temperature increases the decomposition of the volatiles from the biomass and produces biochar with more micropores leading generally to an increase in the surface area of the biochar. Silver concentrations before and after the adsorption in water solutions were determined by inductively coupled plasma-atomic emission spectroscopy (ICP-AES). Results revealed that algae biochar produced at 700°C showed the highest Ag removal capacity of 196.2 mg/g, while SCGs biochar produced at 500°C and sawdust biochar produced at 700°C achieved the maximum adsorption capacities of 25.13 mg/g and 24.68 mg/g, respectively with 99% silver removal rate. Silver precipitation by inorganic halides in the algae was a potential barrier to quantify the actual adsorption by algae biochar. Although the adsorption capacities difference between the SCGs and sawdust was not very high, SCGs biochar produced at low pyrolysis temperature (500°C) could be a promising commercial adsorbent to mitigate silver ion and silver nanoparticles (Ag NPs) pollution and a value-added alternative for landfilling of SCGs waste.

Keywords: silver removal; kinetics; algae; sawdust; coffee; Pyrolysis; Py-GCMS

Highlights

- Biomass type impacted on biochar quality and adsorption capacity
- Pyrolysis temperature influenced biochar yield and physicochemical properties
- Chemical adsorption was leading over the physical adsorption for silver removal
- Inorganic constituents in macroalgae affected biochar yields and adsorption of silver
- SCGs is a promising biomass for producing value-added products

As to be submitted in: Islam, M. A., Dada, T. K., Parvin, M. I., Duan, A. X., Sarmah, A. K., Antunes, E., "A thermogravimetric and kinetic study of biomass feedstocks for the production of value-added chemicals and biochar for silver removal from wastewater", Journal of Environmental Chemical Engineering.

3.1 Introduction

Biomass wastes are defined as biodegradable and produced as a by-product of various activities by different industries, such as agro-industries, seaweeds, food processing, wood processing, municipal wastes, and wastewater treatment plants [25]. Biomass consists of a complex composition of hemicellulose, cellulose, lignin, moisture, and small amounts of other extractives [26]. The proportion of cellulose, hemicellulose and lignin varies on the species, age, sources, and climate of the grown area [293]. Approximately 140 gigatonnes of biomass wastes are generated every year, with a significant increase each year [27]. Proper management of biomass wastes is a great challenge, and most of them go to landfills that develop detrimental environmental impacts, including greenhouse gas emissions. The conversion of biomass waste into high value-added chemicals or energy fuels reduces the load on landfills [28]. Biomass waste is considered a potential feedstock for various products, such as renewable energy products, biochar, chemicals, and building materials. To employ a circular economy approach reusing the biomass waste to generate valuable products can be a problem-solving solution to sustainably manage the biomass waste and reduce the environmental risks. Therefore, pyrolysis is considered a promising approach to ensure a circular economy for biomass waste and help to convert biomass waste into valuable products for further applications.

Pyrolysis is a thermochemical process that consists of simultaneous and successive reactions, while organic materials go through a heat treatment process in an inert environment [294]. Pyrolysis of biomass gives a variety of products depending on biomass compositions and pyrolysis operating parameters [295]. In this process, organic components in the biomass start decomposing from 300°C and go up to 1000°C in the absence of external oxygen [296]. This is an irreversible process and produces numerous chemical compounds in the form of pyrolysis vapours and solid residue [250]. Pyrolysis of biomass produces non-condensable gases (syngas) such as CO_2, CO, CH_4, H_2, C_2H_6, C_2H_4, a condensable fraction comprising mainly oxygenated compounds, water, and solid residue called biochar [297]. This condensable fraction forms a coffee brown viscous liquid that is often termed bio-oil or pyrolysis oil [298], possesses a higher heating value in the range of 15-25 MJ/kg, comparatively lower than conventional fossil fuel [299].

Depending on the heating rate and residence time at peak temperature, pyrolysis can be classified into three types: slow or conventional, fast, and flash pyrolysis [300]. Consequently,

the relative distribution of products varies in three different phases. For instance, lower temperatures and longer vapour residence time produce high yields of biochar. In contrast, higher temperatures and longer residence time are favourable for high yields of pyrolytic gases, and a moderate temperature and short residence time are optimum for bio-oil production [250].

Biochar (often called char) is the solid carbonaceous by-product of biomass pyrolysis, which comprises residual organic solids and ash or a mineral fraction of biomass pyrolysis [280]. The yield and quality of biochar mainly depend on the process parameters. For instance, biochar obtained from high temperatures contains a higher carbon percentage and higher surface area. At high temperatures, volatiles are removed quickly and produce high microporous volume in the biochar matrix [272]. Micropores offer a large specific surface area, which is one of the key properties of the adsorption process. However, at high temperatures, the char yield decreases, and most of the functional groups tend to disappear [301]. Pyrolysis conditions can be controlled to produce desired quality biochar depending on the potential end-use. Separation of biochar is also important to avoid the catalytic effects on secondary cracking reactions of pyrolytic vapours [302]. Furthermore, biomass chemical composition plays a promising role in biomass conversion rate and resultant composition of biochar (presence of elements and functional groups) as well as its physicochemical properties, such as specific surface area and the number of pores [303].

Biochar has been successfully used for numerous beneficial usages, such as the removal of emerging contaminants, heavy metals, antibiotics, dyes and phosphorous [304]. Besides, biochar can be used for carbon storage, soil fertility, mitigating soil and water pollution, application in direct carbon fuel cells, greener fuels for electric arc furnaces, and activated carbon production, including removal of pollutants such as SO_x and NO_x from flue gases [271].

A large number of studies have successfully demonstrated the application of biochar for mitigating heavy metal pollution and also reported the adsorptive removal of silver metal by biochar from an aqueous solution [305]. However, the effect of physicochemical properties of biochar on silver removal from aqueous solution has not been thoroughly investigated. It is well understood that the composition of the biomass can play a decisive role in biochar chemical composition and surface properties, while the operating parameters of the pyrolysis process may alter the physicochemical characteristics, indicating that the selection of a

feedstock and optimisation of the pyrolysis process is critical to obtain the biochar with attractive characteristics for enhanced adsorption of silver.

Therefore, the overarching aim of this study is to have some insights into the selection of a feedstock, the effect of pyrolysis temperature on chemicals production, biochar's physicochemical properties, and the application of char for adsorptive removal of silver from wastewater. To achieve this, three different types of feedstocks, such as spent coffee grounds (SCGs), algae, and sawdust were selected. These biomasses exhibit different chemical compositions and are expected to produce biochar with varying physicochemical properties. For example, sawdust contains a higher percentage of lignin and cellulose that can favour biochar production with a high specific surface area [306]. Algae contain a wide variety of chemicals, such as lipids, carbohydrates, and proteins [307]. In general, algae have also lower carbon content, but often have high nitrogen, phosphorus, and other nutrients (S, K, P, Ca, and Mg) [308], which might influence biochar quality for silver removal. SCGs have high fixed carbon and various organic compounds, such as hemicellulose, cellulose, lignin, lipids, fatty acids, and other polysaccharides that can provide surface functional groups on biochar for better adsorption [309]. All three feedstocks were pyrolysed at 500, 700, and 900°C to investigate the effect of feedstock compositions on the physicochemical characteristics of biochar, and consequently, on the removal of silver metal.

3.2 Materials and methods

3.2.1 Materials

SCGs were collected from a local coffee shop at the James Cook University, Townsville Bebegu Yumba campus (Juliette's Espresso). Pelletised dry algae (*Ulva Ohnoi*) were collected from the Marine and Aquaculture Research Facilities Unit (MARFU), James Cook University, Townsville, Australia. Sawdust was a mixture of different hardwood, mostly Australian gum trees, collected from a local business in Townsville. All the biomass samples were dried in an oven at 105°C overnight to remove residual moisture. Silver nitrate ($AgNO_3$), 99.99% wt/wt, was outsourced from Sigma-Aldrich (S6506-25G, lot#MKCJ2718).

3.2.2 Methods

3.2.2.1 Characterisation of biomass wastes

The composition of biomass wastes plays a vital role in the final properties of biochar, particularly the textural properties like surface area and pore volume that enhance the adsorption of a contaminant. Therefore, proximate and ultimate analyses of all three biomasses were carried out to determine the percentage of moisture, volatiles, fixed carbon, ash content, elemental carbon (C), hydrogen (H), and nitrogen (N) content. Oxygen (O) content was calculated from mass difference and considering the total mass of 100.

Ultimate or elemental analysis (EA) was done in a Costech Analytical Elemental Analyser 4010 (Valencia, California, USA) fitted with a zero-blank auto-sampler. The analyser uses dumas combustion to form CO_2 and N_2 that are detected by a thermal conductivity detector (TCD). Standards were used to formulate a calibration curve from which the C and N percentages of the biomass samples were determined.

Thermogravimetric analysis (TGA) is an important technique to understand the thermal decomposition behaviour of a substance. The 'Discovery TA/SDT650' analyser was used for thermogravimetric analyses of the three biomass samples. All thermal analyses were carried out in a nitrogen environment (nitrogen flow rate, 50 ml/min) from 25°C to 1000°C with a heating rate of 10°C/min. The TGA curves were obtained from the plot of a residual mass percent against temperature. The moisture content (%) and volatile matters (%) were calculated from the TGA curves of the individual biomass. Moisture content (%) was calculated from the mass loss to 200°C, and volatile matters (%) were calculated from the mass loss from 200°C to 500°C. To study pyrolysis kinetics, TGA and DTGA (derivative TGA) curves were further recorded at three different heating rates, 5°, 10°, and 15°C/min for all three biomass wastes. For each TGA analysis, about 20 mg of the biomass sample was analysed.

Ash content was determined by heating around 10 g of each biomass sample (dry sample) at 600°C for 6 h in a conventional furnace (air atmosphere). At room temperature, samples were removed from the furnace and cooled in a desiccator for an additional hour, then weighed. Ash content was calculated from Eq. (1):

$$Ash\ content\ (\%) = \frac{B - C}{A - C}\ x\ 100\% \quad (1)$$

where B is the mass of crucible plus mass of biomass after heat treatment, A is the mass of crucible plus the mass of initial biomass, and C is the mass of crucible.

Fixed carbon content (%) was calculated as below:

$$Fixed\ carbon\ content\ (\%) = 100\% - (Moisture\ \%\ +\ Volatiles\ \% + Ash\ \%) \quad (2)$$

3.2.2.2 Pyrolysis gas chromatograph mass spectrometer (Py-GCMS)

A pyrolysis gas chromatograph mass spectrometer (Py-GCMS) is an excellent equipment to elucidate the product distribution resulting from biomass pyrolysis. Identification of the chemical composition of pyrolysed vapour is crucial to optimise the actual pyrolysis conditions for retaining potential functional groups in the biochar. The CDS 6150 pyrolyser aligned with an Agilent 6890 GC 5973N MS was used to carry out the analysis. The pyrolyser was set at an initial temperature of 25°C with a heating rate of 1°C/millisecond to reach the final temperature of 550°C and held for 30 seconds. The interface, valve oven, and gas chromatography (GC) transfer line were all set at 300°C. In addition, a GC was equipped with an HP-5MS column in which the inlet was set at 250°C with a split ratio of 80:1. GC oven started at 40°C, was held for 1 minute, and then reached up to 300°C with a heating rate of 10°C/min and held for 20 minutes. Finally, a mass spectrometer (MS) fitted with an electron impact ion source scanned a range of 25-550 m/z with the quad temperature at 150°C and the source temperature at 230°C.

3.2.2.3 Pyrolysis Kinetics analysis

The pyrolysis of biomass is often assumed as a single step reaction as described below:

$$Biomass\ \rightarrow\ Volatiles + Biochar \quad (3)$$

where *Volatiles* is the sum of the bio-oil and syngas, and *biochar* is the solid residue after pyrolysis.

The rate of reaction from solid-state to volatiles is frequently described as,

$$\frac{d\alpha}{dt} = k(T)\, f(\alpha) \tag{4}$$

where $k(T)$ is a function of temperature, *(T),* and termed as reaction rate constant; $f(\alpha)$ is a function of the reaction model.

For the heterogeneous function of the uniform kinetic reactions, $f(\alpha)$ is expressed as:

$$f(\alpha) = (1-\alpha)^n \tag{5}$$

where n is the order of reaction, the degree of conversion of biomass, (α) can be calculated from its relative weight loss as follows,

$$\alpha = \frac{m_0 - m_t}{m_0 - m_\infty} \tag{6}$$

where m_0 is the initial mass of biomass (mg), m_t is the residual mass (mg) at reaction time t, and m_∞ is the residual mass (mg) at equilibrium.

The kinetic reaction rate constant, *k(T)* can be described by the Arrhenius equation as,

$$k(T) = A\, e^{\left(\frac{-E_\alpha}{RT}\right)} \tag{7}$$

where A, E_α, R, and T are a pre-exponential factor (min^{-1}), the apparent activation energy (kJ mol^{-1}) of the decomposition reaction, the universal gas constant (8.314 J mol^{-1} K^{-1}), and the absolute temperature (°K), respectively.

By substituting Eqs. (5) and (7) in Eq. (4), the heterogeneous solid-state reaction can be obtained,

$$\frac{d\alpha}{dt} = k(T)\, f(\alpha) = Ae^{\left[\frac{-E_\alpha}{RT}\right]} (1-\alpha)^n \tag{8}$$

The constant heating rate (β), in a non-isothermal process, is defined as,

$$\beta = \frac{dT}{dt} = \frac{dT}{d\alpha} \times \frac{d\alpha}{dt} \tag{9}$$

From the Eq. (4), (7) and (9), and after some mathematical manipulation, we obtain

$$\frac{d\alpha}{dT} = \frac{A}{\beta} e^{\left[\frac{-E_\alpha}{RT}\right]} f(\alpha) \tag{10}$$

By integrating the above Eq. (10) results:

$$g(\alpha) = \int_0^{\alpha} \frac{d\alpha}{f(\alpha)} = \frac{A}{\beta}\int_{T_0}^{T} e^{\left[\frac{-E_\alpha}{RT}\right]} dT \tag{11}$$

where *g(α)* is the integrated form of the reaction function. Eq. (10) does not have an exact solution and thereby requires some approximation to find a solution. Therefore, International Confederation for Thermal Analysis and Calorimetry (ICTAC) highly recommends iso-conversional methods to determine the apparent activation energy (E_α). The parameters $f(\alpha)$, E_α, and A are often called as kinetic triplets [310]. In this study, based on Arrhenius equation, activation energy (E_α), pre-exponential factor (A), and order of reaction (n) were determined from the TGA/DTGA analysis data. Several methods are available to analyse solid-state kinetic data. However, Ozawa-Flynn-Wall (OFW) and Kissenger-Akahira-Sunose (KAS) methods were used to determine the kinetic triplet considering the limitation of model-fitting methods for complex and simultaneous pyrolysis reactions [311].

Ozawa-Flynn-Wall- (OFW) method:

By Doyle's approximation, the OFW method is expressed as [312]:

$$\ln(\beta) = \ln\left[\frac{AE_\alpha}{Rg(\alpha)}\right] - 5.331 - 1.052\left(\frac{E_\alpha}{RT}\right) \tag{12}$$

Activation energy E_α can be obtained from the slope $-1.052\left(\frac{E_\alpha}{R}\right)$ of the plot ln(β) vs $\frac{1}{T}$.

Kissinger-Akahira-Sunose (KAS) method:

The KAS method is represented as follows [310]:

$$\ln\left[\frac{\beta}{T^2}\right] = \ln\left[\frac{AR}{E_\alpha g(\alpha)}\right] - \frac{E_\alpha}{RT} \tag{13}$$

where the apparent activation energy, E_α can be calculated from the slope, $-\frac{E_\alpha}{R}$ of the straight line obtained by plotting $\ln\left[\frac{\beta}{T^2}\right]$ vs $\frac{1}{T}$.

Since these methods provide the overall activation energy at different heating rates, the pre-exponential factor (A) can be calculated from the activation energy obtained from OFW and KAS methods, at each conversion from the below Eq. (14) [313]:

$$A = \beta E_\alpha \frac{e^{\left[\frac{E_\alpha}{RT}\right]}}{RT^2} \quad (14)$$

3.2.2.4 Pyrolysis Thermodynamic analysis

Thermodynamic analysis of biomass pyrolysis is also important to understand the pyrolysis mechanism and determine the feasibility of the overall pyrolysis process. Therefore, crucial thermodynamic parameters, such as enthalpy (ΔH), entropy (ΔS), and Gibbs free energy (ΔG) were calculated from the following Eq. [310]:

$$\Delta H = E_\alpha - RT \quad (15)$$

$$\Delta S = \frac{\Delta H - \Delta G}{T} \quad (16)$$

$$\Delta G = E_\alpha + RT \ln\left(\frac{K_B T}{hA}\right) \quad (17)$$

where K_B is the Boltzmann constant (1.381×10^{-26} kJ K^{-1}), h represents Plank constant (6.626×10^{-37} kJ s), and T is the peak temperature (°K) at the degree of conversion α.

3.2.2.5 Pyrolysis experiments and characterisation of biochar

Pyrolysis of the three biomass wastes was done in a nitrogen environment (flow rate, 3 L/min) using a fixed bed reactor, a conventional electrical tube (quartz) furnace–Termolab (Portugal). For each experiment, about 10 g of individual biomass waste was weighed in a quartz crucible and placed in the tube furnace. All three biomass samples were pyrolysed at 500°, 700°, and 900°C, with a heating rate of 10°C/min and a residence time of 2 h to find the best biomass feedstock for biochar production. At least three pyrolysis experiments were performed for each biomass waste and pyrolysis condition. After each pyrolysis experiment, biochar was weighed, grounded, and collected for characterisation and adsorption testing. A schematic diagram of the pyrolysis process is shown in Figure 7.

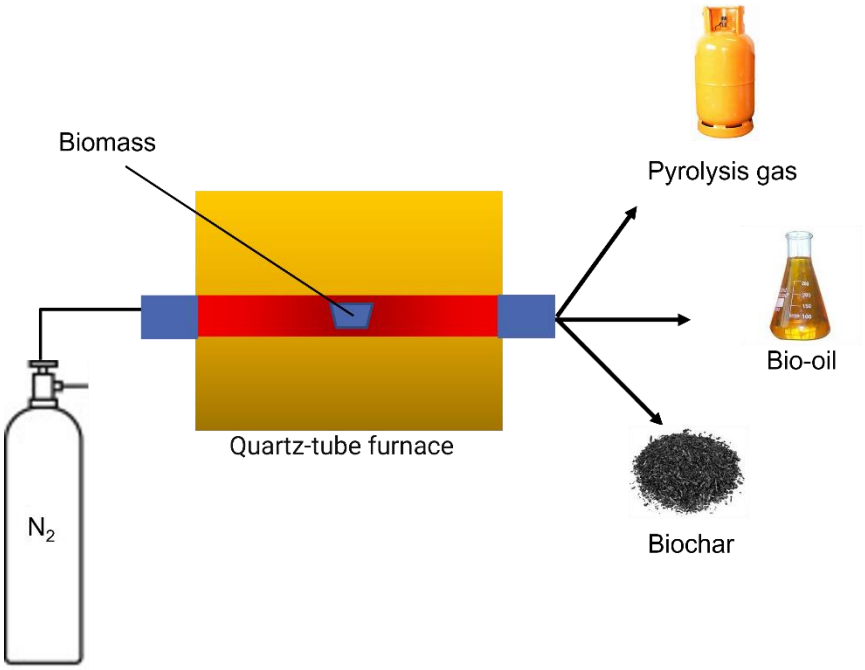

Figure 7: Schematic diagram of pyrolysis of biomass.

Biochar yield (%) was calculated after each pyrolysis by the following Eq. (18):

$$\boldsymbol{Biochar\ yield} = \frac{\boldsymbol{BC}}{\boldsymbol{DBW}} \times \mathbf{100\%} \tag{18}$$

where BC is the weight of dry biochar and BDW is the weight of dry biomass feedstock.

The ***pH*** of biochar often influences the pH of adsorption media, which might impact on the performance of the adsorbent. To determine the pH of each biochar sample, 0.5 g of biochar was mixed in 10 ml of double-distilled water and shaken in an ultrasonic bath for 90 min to ensure good contact between the biochar and water [301]. The pH was then measured and recorded by the Thermo Scientific (Model: Orion Star A215) pH meter with an Orion 8157BNUMD probe.

Specific surface area (Brunauer-Emmet-Teller, BET surface area) is a key property of any adsorbent material [314]. BET surface area, total volume, and pore size of pores were measured by a N_2 adsorption and desorption phenomena using the Quantachrome Autosorb iQ3 gas adsorption analyser. Approximately 0.2 g of biochar was used for each run, and all biochar samples were analysed at least twice. Prior to each analysis, the sample was firstly degassed under vacuum conditions overnight at room temperature and then at 250°C for an hour. The

BET model was used to calculate specific surface area and the BJH (Barrett-Joyner-Halenda) adsorption model for pore size and total pore volume.

A ***Fourier transform infrared (FTIR)*** is the equipment for identifying surface functional groups, which attribute the surface polarity or the surface charge for chemisorption [315]. A Thermo Science i7ATR- FTIR analyser was used to estimate chemical functional groups presented in different biochar samples. Prior to the experiment, biochar samples were manually grounded to improve the homogeneity and obtain a fine powder (less than 75 µm) for the chemical analysis. A small amount of powdered sample was placed on a diamond ATR sample holder, and a total of 64 scans were collected per sample between 500 and 4000 cm^{-1}.

X-ray diffraction (XRD) analysis was used to understand the structural arrangement or the crystallinity of biochar obtained after pyrolysis. The Bruker Phaser D2 X-ray Powder Diffractometer, Cu radiation was used. XRD spectra were obtained from 5° to 65° with a scan step size of 0.02° and a time step of 1 s.

3.2.2.6 Silver adsorption performance of biochars

After the physicochemical characterisation, biochar samples were tested to determine the silver adsorption capacity under different conditions. Accurately weighed silver nitrate was dissolved in double distilled water to prepare 50, 200, and 400 mg/L silver solutions. All the silver adsorption experiments were carried out in a batch process at room temperature (22° ± 2°C). To understand the impact of different variables on silver adsorption, the Taguchi method was used to design the experiment and analyse the processed data. Five variables, such as type of biomass, pyrolysis temperature, initial silver concentration, agitation intensity (in rotation per minute (RPM)), and quantity of biochar were tested. All variables were tested at three levels as shown in Table 4. A certain amount of biochar was added to 100 mL of silver solution and stirred at a specific speed for 5 h. After the adsorption process, around 10 mL of solution was drawn into a syringe and filtered using a 0.22 µm membrane to measure the residual silver concentration.

Table 4: Variables and respective levels considered for the Taguchi experimental design.

Variables/ levels	Biomass Feedstock	Pyrolysis temperature (°C)	Initial Ag Concentration (mg/ml)	Agitation Intensity (RPM)	Quantity of biochar (g)
Level 1	Algae	500	50	200	0.1
Level 2	SCGs	700	200	350	0.2
Level 3	Sawdust	900	400	500	0.3

Silver concentration in the aqueous solution was measured before and after adsorption by inductively coupled plasma-atomic emission spectroscopy (ICP-AES). An Agilent 5100 Varian Liberty Series II (Singapore) was used, and a series of silver standards were measured at a wavelength of 338.289 nm to calibrate the instrument. An independent silver standard solution was measured along with every batch of sample solutions for quality control and quantification purposes. The silver adsorption capacity (Q_t in mg/g of biochar) at a given time *t,* was calculated by the Eq. (19):

$$Q_t = \frac{(C_0 - C_t) \times V}{m} \tag{19}$$

where, C_0 (mg/L) is the initial concentration of the silver in the aqueous solution, C_t (mg/L) is the concentration after adsorption at time *t*, V (L) is the volume of the solution and m (g) is the amount of biochar used. The silver removal percentage (%) was obtained by the Eq. (20)

$$\%\ of\ silver\ removal = \frac{(C_0 - C_t)}{C_0} \times 100 \tag{20}$$

3.3 Results and discussion

3.3.1 Characterisation of biomass wastes

The results of ultimate and proximate analyses of the three biomass samples are presented in Table 5. The ultimate analysis data indicate that sawdust and SCGs contained a similar high elemental carbon (C), approximately 48.9% and 47.5%, respectively, whereas algae contained 28.9% of carbon. These carbon content values obtained in this study were consistent with

previous studies that showed nearly similar values [316], but in general, the values are higher than in other agricultural biomass [317]. In contrast, low carbon percentages in algae were confirmed for *Ulva Ohnoi* and other macroalgae in previous studies [318]. In addition, algae had 4.1 % nitrogen (N), higher than sawdust and SCGs, indicating the increased presence of protein molecules in algae [319].

SCGs had the lowest oxygen (O) content, approximately 43.7%, which might be advantageous to produce the bio-oil with a high heating value [320]. On the other hand, the proximate analysis revealed that sawdust and SCGs contain the highest amount of fixed carbon (22.0 and 18.8%), volatile matter (67.1 and 71.5%) and the lowest ash content, indicating their suitability for biochar production via pyrolysis. Algae showed the highest moisture and ash contents. High moisture content might make this feedstock unsuitable for bio-oil production, and the high ash content could lead to high biochar yields with ash from the pyrolysis process [321]. Based on the ultimate and proximate analysis results, sawdust feedstock that contains the highest fixed carbon content might be the suitable biomass to produce biochar with minimum ash. In contrast, algae exhibited significantly different thermal decomposition that is attributed to its unique composition, such as the presence of a high number of nitrogen-containing compounds. However, the silver adsorption capacity was the main determinant to identify the best biomass for biochar production.

Table 5: Composition of biomass wastes determined by proximate and ultimate analysis.

Biomass	**Proximate analysis (%)**				**Ultimate analysis (%)[a]**			
	Moisture[a]	**Volatiles[a]**	**Ash[a]**	**Fixed carbon[a]**	**C**	**H**	**N**	**O[b]**
Algae	20.7	40.6	23.2	18.6	28.9	5.0	4.1	62.0
SCGs	7.2	71.5	2.5	18.8	47.5	6.4	2.5	43.7
Sawdust	9.8	67.1	1.1	22.0	48.9	5.9	0.2	45.1

[a] Values on a dry weight basis

[b] Calculated by weight difference

TGA and DTGA analyses in Figure 8 show the thermal decomposition behaviour of the three biomass feedstocks. From these results, it can be estimated that SCGs and sawdust showed a nearly similar decomposition pattern in all three stages, which can be attributed to the presence of a nearly similar percentage of fixed carbon and volatile matters in the two biomasses. In

contrast, algae exhibited significantly different thermal decomposition that is attributed to its unique composition, such as the presence of a high number of nitrogen-containing compounds. For all biomass samples, TGA and DTGA curves can be separated into three stages, as shown in Table 6. Stage 1 (up to 200°C) is mainly attributed to the loss of moisture and other volatile substances extractable from water. For instance, algae released the highest moisture of 20.7%, whereas SCGs and sawdust released 4.73% and 10.38%, respectively.

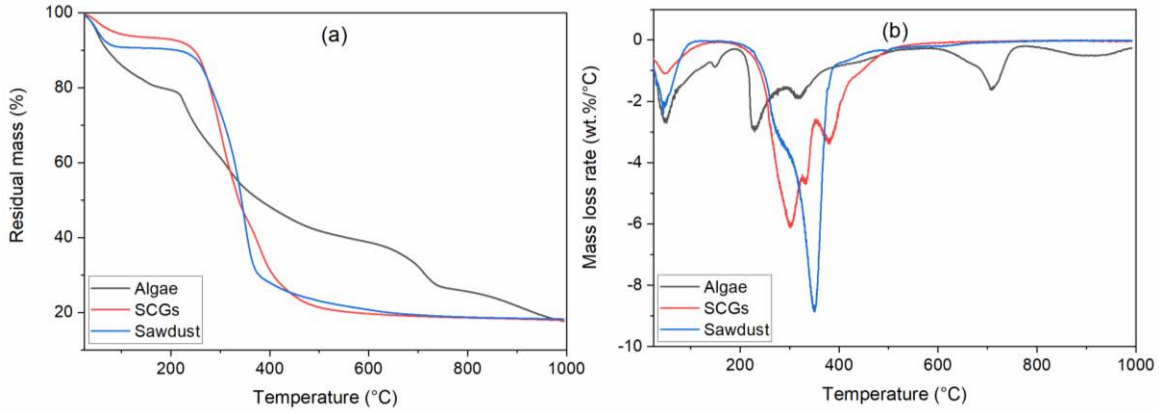

Figure 8: (a) TGA spectra of algae, SCGs, and sawdust; (b) DTGA spectra of algae, SCGs, and sawdust.

Stage 2 is considered as the main stage where the majority of the weight loss occurs, contributing to the depolymerisation of biomass components, such as hemicellulose, cellulose, and lignin. Hemicellulose is known to be completely depolymerised at 350°C, while the degradation of cellulose starts above 180°C and is completely degraded at 400°C [322]. In contrast, depolymerisation of lignin polymers starts above 180°C and is completely decomposed by 800°C [316]. For the algae sample, stage 2 was marked from 200° to 400°C, where algae decomposed their main constituents such as carbohydrates, proteins, and lipids [323]. At this stage, algae released 27.34% of volatiles. A steep weight loss between 200°C and 550°C could also be ascribed to the degradation of carbohydrates and proteins constituents presented in algae, while above 550°C, lipids and other compounds are decomposed into their secondary constituents [323]. In stage 2, SCGs and sawdust had a mass loss of 72.40% and 64.03%, respectively, corresponding to the temperature range of 200°-550°C and 200°-450 °C, respectively. A mass loss of 75% for SCGs was reported by Li et al. [322]. In addition, SCGs mass loss of up to 330°C was attributed to hemicellulose decomposition, and the last DTFA peak was found at 392°C, which is associated with the decomposition of higher lignin and

lipids [324]. However, sawdust had a single DTGA sharp peak at 351°C which corresponds to the maximum decomposition of hemicellulose and cellulose in stage 2 [325]. The last stage, up to 800°C, is attributed to solid decomposition, where the weight loss rate is slower, and a slight weight loss could be due to char consolidation [326]. For instance, final stage weight loss for algae, SCGs, and sawdust were 21.72%, 1.95%, and 6.63%, respectively.

Table 6: Thermal decomposition steps and parameters of algae, SCGs, and sawdust at a heating rate of 10°C/min.

Stages	Parameters	Algae	SCGs	Sawdust
Stage – 1 (Moisture removal)	T_{range} (°C)	25-200	25-200	25-200
	DR_{max} (wt%/min)	2.45	0.50	1.87
	T_{max} (°C)	65	70	60
	W_{loss} (%)	20.45	4.73	10.38
Stage - 2	T_{range} (°C)	200-400	200-550	200-450
	DR_{max} (wt%/min)	2.82	5.79	8.64
	T_{max} (°C)	230	300	350
	W_{loss} (%)	27.34	72.40	64.03
Stage - 3	T_{range} (°C)	400-800	550-800	450-800
	DR_{max} (wt%/min)	1.51	0.11	0.19
	T_{max} (°C)	722.89	600	600
	W_{loss} (%)	21.72	1.95	6.63
% Residual weight at 800°C	W (%)	30.49	20.92	18.95

3.3.2 Product distribution in the pyrolysis process based on Py-GCMS

Py-GCMS analysis for the three biomass wastes was carried out and fitted with the National Institute of Standards and Technology (NIST) library and reported in Figure 9 while a detailed list of compounds was placed in Appendix 1 (Table A1, Table A2, Table A3, and Table A4). Pyrolysis vapours from the three biomass wastes pyrolysis were combined in different chemical groups, such as phenols, acids, ketones, aldehydes, and hydrocarbons. Out of the wide variety of chemicals, phenols, acids, ketones, and aldehydes compounds were the higher molecular weight compounds that could impact the biochar quality as well as silver adsorption potential. SCGs produced the highest quantity of fatty acids (49.6%), while sawdust produced maximum phenolic compounds (28.7%). Previous studies also reported high acidic content in SCGs [327] and high phenols, ketones, and aldehydes in sawdust [328]. However, combined acids and phenols compounds were higher in SCGs (59.7%) than in sawdust (49.5%). These findings indicated that pyrolysis of SCGs could offer more acidic functional groups in the

biochar during pyrolysis, which would enhance silver adsorption. In addition, hydrocarbons are high heating value compounds that determine the usability of bio-oil [329]. Therefore, algae that contained high 19.4% hydrocarbons, was the best biomass among the three for solely bio-oil production, whereas SCGs and sawdust produced 7.2% and 1.6% of hydrocarbons, respectively. Similar high hydrocarbon content in macroalgae pyrolysis products was identified in past studies [330].

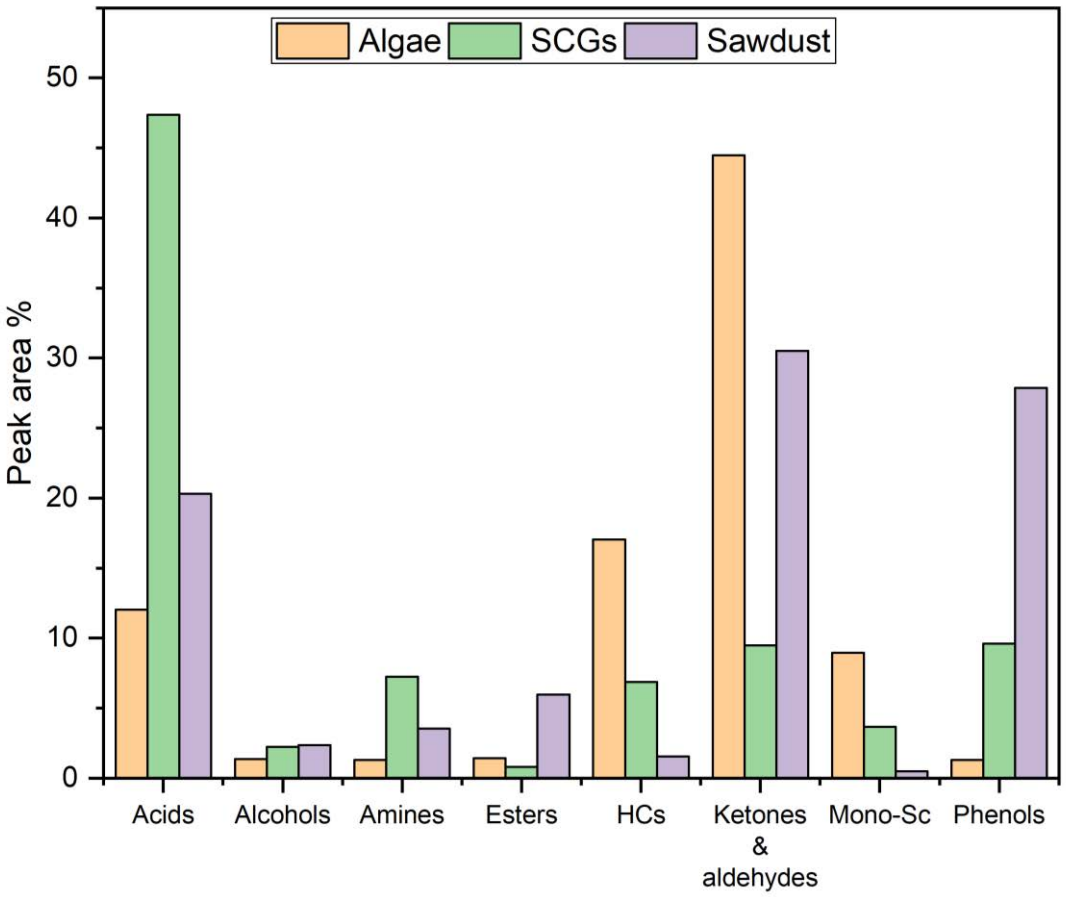

Figure 9: Pyrolysis vapour product composition from the three biomass wastes analysed by Py-GCMS.

3.3.3 Kinetics analysis of biomass pyrolysis

3.3.3.1 Effect of heating rate

TGA and DTGA curves of algae, SCGs, and sawdust were recorded at three different heating rates of 5, 10, and 15°C/min. Figure 10 shows the effect of heating rates on TGA and DTGA curves. The decomposition behaviour was different as individual biomass wastes have different

compositions. Various DTGA peaks in different stages were found, which was expected since biomasses degraded at different stages with various reaction rates. It can be observed from Figure 10 that the DTGA peaks reached the maximum value at 10°C/min except for algae, and the DTGA curves shifted to a higher temperature zone while increasing the heating rates. These findings indicated the uneven heat transfer through the particles of each biomass. For instance, the temperature in the centre of the biomass particles is lower than the temperature on the surface [331]. The heat transfer efficiency was poor at a high heating rate compared to a low heating rate. These results were in line with previous studies as a similar shift of DTGA curves at higher heating rates was recorded [332].

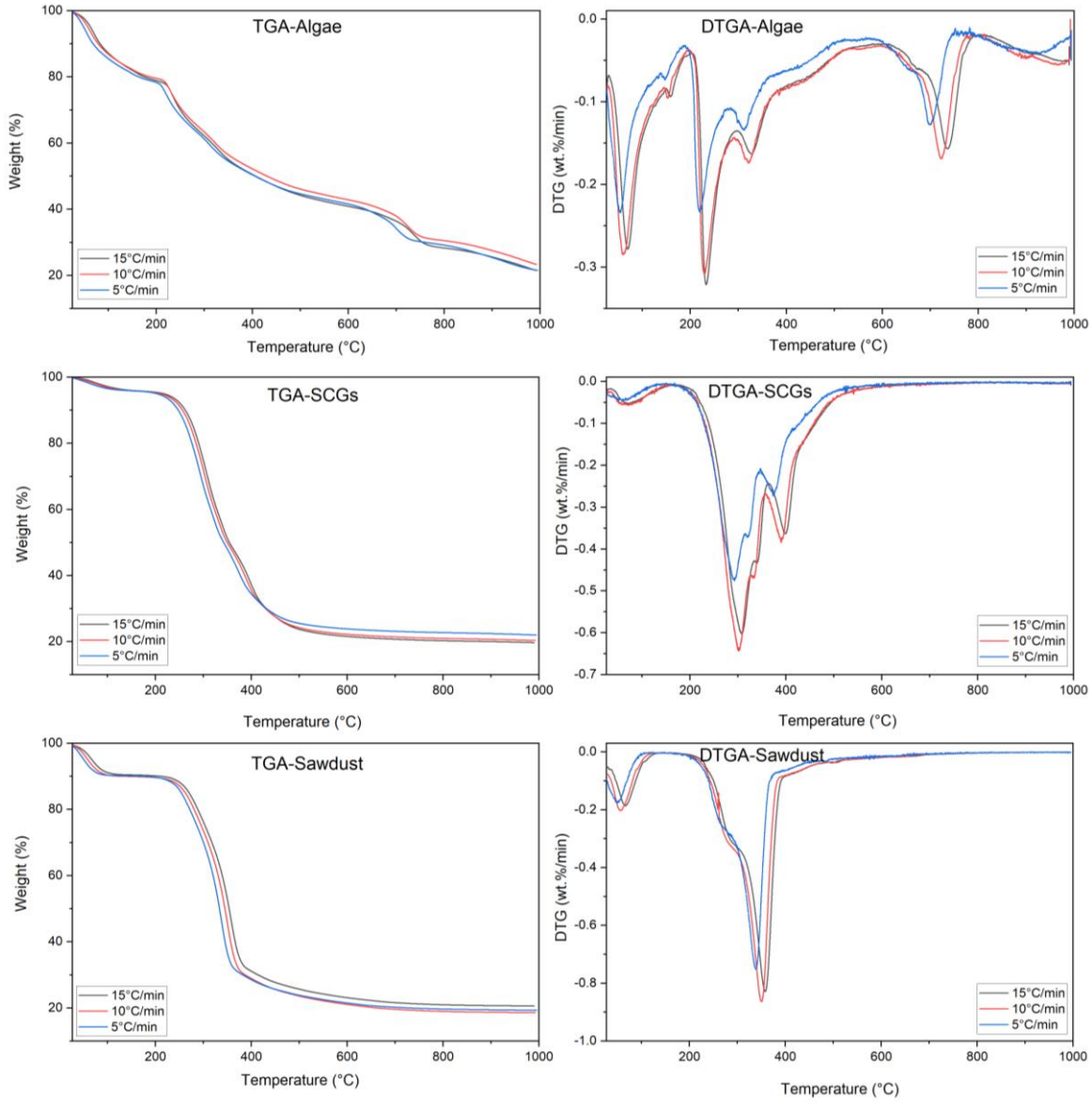

Figure 10: TGA and DTGA curves of three biomass wastes at heating rates of 5, 10, and 15°C/min.

3.3.3.2 Determination of activation energy

TGA and DTGA data at three different temperatures and three biomass wastes were used to derive the kinetic parameters using model-free methods, as shown in Figure 11. To calculate the iso-conversion plot of activation energy, E_α with a degree of decomposition α, the degree of decomposition was considered up to 90% with a 10% size of each step according to the recommendation by the Kinetics Committee of the International Confederation for Thermal Analysis and Calorimetry (ICTAC) [333].

Activation energy, $E_{\alpha,}$ is the minimum energy that is required to initiate a chemical reaction. The high activation energy of a reaction means that this reaction requires a long residence time or high reaction temperature to start the reaction. Ozawa-Flynn-Wall (OFW) and Kissinger-Akahira-Sunose (KAS) methods were used to obtain kinetic plots, results are shown in Figure 11, and the calculation details are reported in Appendix 1 (Table A5). The calculated activation energies for algae by using the OFW method ranged from 57.20 to 285.33 kJ.mol^{-1} with an average of 173.83 kJ.mol^{-1}, while by the KAS method, ranged from 54.57 to 284.01 kJ.mol^{-1} with an average of 173.00 kJ.mol^{-1}. Similarly, the activation energy for SCGs using the OFW method varied from 143.80 to 269.74 kJ.mol^{-1} with an average of 188.59 kJ.mol^{-1}, and by the KAS method varied from 142.69 to 271.98 kJ.mol^{-1} with an average of 188.38 kJ.mol^{-1}. In addition, the activation energies for sawdust by using the OFW method varied from 58.41 to 226.45 kJ.mol^{-1} with an average of 166.88 kJ.mol^{-1}, and by the KAS method varied from 55.61 to 226.69 kJ.mol^{-1} with an average of 165.94 kJ.mol^{-1}. In this study, the average values of activation energy calculated by both the OFW and the KAS methods were similar to previous studies [334]. Interestingly, the regression coefficients (R^2) of the fitting for both methods for SCGs and sawdust were better than the algae. This implied that algae had a more complex pyrolysis reaction than the other two biomass wastes. Overall, all kinetic parameters calculated by the two methods for the three biomass wastes were in good compliance with each other and could be used to simulate the decomposition process under a specific condition.

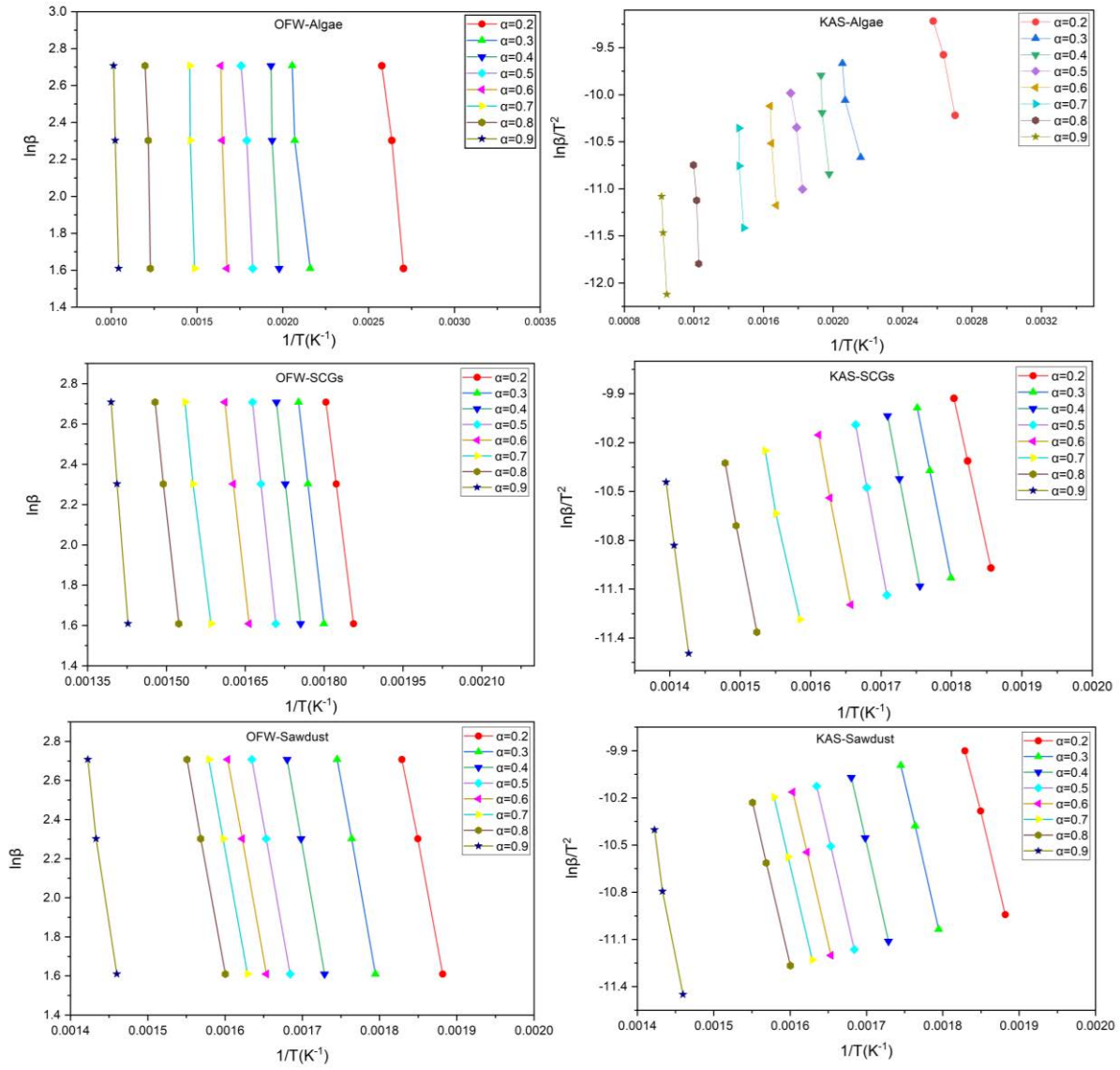

Figure 11: Kinetic plots obtained from OFW and KAS methods for algae, SCGs, and sawdust.

According to Figure 12, the required activation energies for algae and sawdust were lower than SCGs, which indicated the removal of extra moisture at this stage. However, after the first 0.2 degrees of conversion, the activation energy for pyrolysis of SCGs was very similar to the sawdust. Activation energy fluctuation in the algae decomposition indicated their complex chemical composition compared to the SCGs and sawdust.

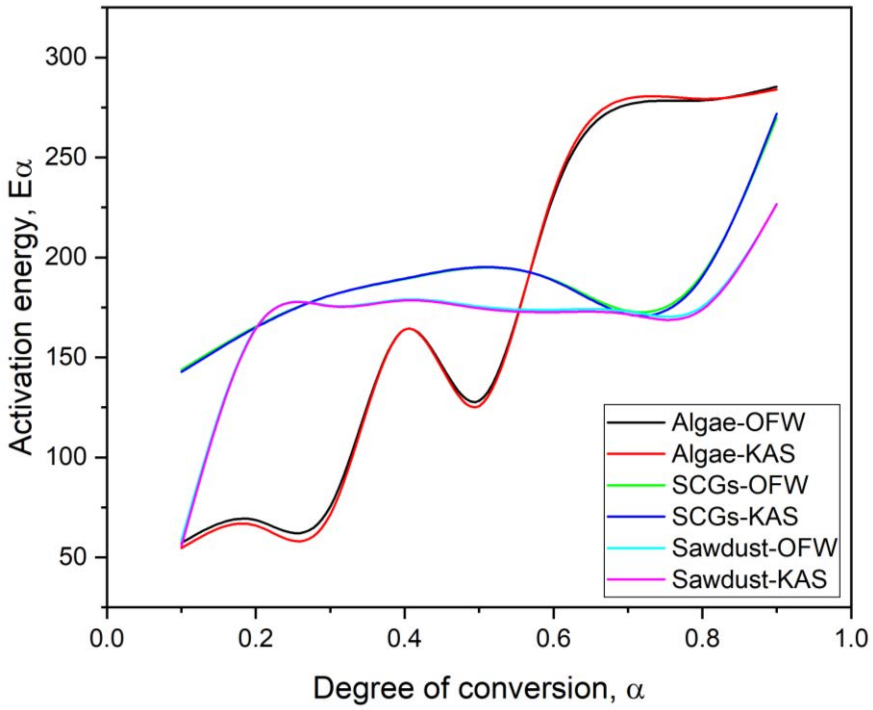

Figure 12: Variation of required activation energy during pyrolysis decomposition of biomass wastes (SCGs, sawdust and algae).

3.3.3.3 Pyrolysis thermodynamics analysis

The apparent activation energies, E_α calculated from the KAS method were used to derive the thermodynamic parameters, such as pre-exponential factor (A), the kinetic reaction rate constant, k, Enthalpy (ΔH), entropy (ΔS), and Gibbs free energy (ΔG) as shown in Appendix 1 Table A6. Pre-exponential factor (A) values exhibited wide variations for a range of conversion degrees from 10^9 to 10^{23} (Table A6), which was attributed to the complex composition of biomass wastes as well as complex decomposition reactions during the thermal conversion. The low pre-exponential factors (A <10^9 min^{-1}) also imply surface reaction, whereas the high pre-exponential factors ($A \geq 10^9$ min^{-1}) indicate the formation of the activated complex, which probably restricts rotation compared to the initial decomposition [313]. Especially in algae, a high value of A in the middle of the reaction suggests that decomposition becomes slow, which requires high energy to increase molecular collisions. However, similar values of pre-exponential factors were reported in previous studies [335].

The enthalpy changes (ΔH) demonstrate the energy difference between the reactant (biomass) and decomposition products [336]. Positive enthalpy indicates that the reaction is endothermic,

while negative enthalpy indicates an exothermic reaction [334]. The enthalpy changes (ΔH) at various decomposition stages are presented in Appendix 1 Table A6 with average values of ΔH for algae, SCGs, and sawdust as 167.98, 183.29, and 161.05 kJ·mol^{-1}, respectively, and the required heat energy for pyrolysis followed an order: sawdust<algae<SCGs. It is important to note that Py-GCMS analysis in this study and previous research showed that higher molecular weight compounds were identified in SCGs, and require higher energy to decompose [324]. In addition, a small difference (~5 kJ·mol^{-1}) in average activation energy derived from both methods was observed for all three biomass wastes, which demonstrated that thermal decomposition is a favourable conversion process [337].

The Gibbs free energy changes (ΔG) are also presented in Appendix 1 Table A6, and the average values are 132.24, 133.15, and 165.55 kJ·mol^{-1} for algae, SCGs, and sawdust, respectively. Gibbs free energy mainly indicates the total energy increase during the decomposition reactions [313], where a gradual increase of ΔG was reported with the degree of decomposition.

Entropy (ΔS) represents the degree of disorderness of the reaction system. The smaller value of ΔS indicates the system is near to its thermodynamic equilibrium, which also suggests the system is less reactive. In contrast, a high value of ΔS suggests the higher reactivity of the system to form an activated complex [313]. According to Table A6 in Appendix 1, negative values of ΔS in algae and sawdust imply a low degree of disorderliness in the system after decomposition and formation of more stable pyrolysis products than the biomass [338].

3.3.3.4 Production and characterisation of biochars

Table 7 summarises biochar yields obtained from the pyrolysis process and their physicochemical properties such as pH, surface area, pore size, and pore volume. An increase in the temperature from 500° to 900°C resulted in decreased biochar yield consistently for all biomass feedstocks. For example, algae provided the maximum biochar yield (43.89% at 500°C) and the lowest yield of 27.75% at 900°C. Similarly, SCGs and sawdust generated the highest biochar yield at 500°C and the lowest at 900°C. This is mainly attributed to the higher pyrolysis temperature (> 600°C) promoting the conversion of bio-oils and biochars into gaseous products due to the dominance of secondary cracking reactions, leading to higher yields of pyrolytic gases and decreasing the biochar yield [339]. It was further observed that

algae feedstock at 500°C generated the highest biochar yield among all the samples, irrespective of the type of biomass wastes and pyrolysis temperatures.

As mentioned previously, biomass composition and ash content play a significant role in biochar production. During the pyrolysis of sawdust and SCGs at 500°C, the major constituents like cellulose, hemicellulose are completely decomposed and primarily contribute to the formation of bio-oil and gases, while a considerable portion of lignin is depolymerised into its monomer units. On the contrary, pyrolysis of algae at 500°C decomposes mainly carbohydrates and proteins, while the dominant portion of lipids and other inorganic compounds is depolymerised between 550° and 750°C, as demonstrated by TGA results [340]. This indicates a substantial decrease in biochar yield for algae samples when the temperature was increased from 500° to 900°C, while a small decrease in biochar yield was observed for sawdust and SCGs. The comparatively higher biochar yield for algae can also be due to the presence of greater ash content and the lowest volatile matters, as indicated by the proximate analysis.

Table 7: Summary of yields and properties of biochars obtained from the different biomass wastes pyrolysis at different temperatures.

Biomass wastes	Pyrolysis temperature (°C)	Biochar Yield (%)	pH	BET (m^2/g)	Pore Volume (cc/g)	Pore size (nm)
Algae	500	43.89	10.59	4.06	0.024	3.18
	700	30.18	11.49	17.35	0.082	9.58
	900	27.75	10.85	46.62	0.122	6.57
SCGs	500	25.95	10.02	40.1	0.019	3.28
	700	23.82	9.77	1.56	0.009	3.82
	900	21.86	10.20	3.4	0.005	17.55
Sawdust	500	29.16	10.48	257.97	0.040	3.52
	700	25.24	10.28	345.69	0.023	3.41
	900	24.36	10.51	127.40	0.034	4.31

Adsorption is a surface phenomenon and thus greatly depends on the surface properties of biochar [341]. Therefore, the textural properties, such as surface area, pore size, and pore volume of the produced biochar samples were examined, and the results indicated that except for algae biomass, the change in pyrolysis temperature did not show a particular trend in the textural properties of the biochars (Table 7). For example, the increase in temperature from

500° to 900°C consistently enhanced the surface area from 4.06 to 46.62 m^2/g and the pore volume from 0.024 to 0.122 cc/g of algae biochar. The change in pore volume and the specific surface area is dependent on the release rate of volatile matters from the biomass sample during the pyrolysis process [23]. Therefore, it can be suggested that the increase in temperature promoted the release of volatile compounds from the biomass and created an enhanced number of pores that directly contributed to the increase in the surface area [305]. Alternatively, sawdust biochar achieved the highest specific surface area of 345.69 m^2/g at 700°C, and for SCGs, the highest surface area of 40.1 m^2/g was obtained at 500°C, while biochars obtained at other temperatures exhibited lower surface areas.

The above findings for the sawdust sample demonstrated that partial release of volatile matters at 500°C produced a lower number of pores and a low surface area, while at 700°C, the uniform rate of mass loss contributed to a slow and consistent release of volatile matters to create a high number of small size pores and eventually a higher surface area. In addition, the low surface area at 900°C can be attributed to the merging of the smaller pores into larger pores due to the further thermal decomposition of sawdust [342].

SCGs biochars produced at 700°C and 900°C are characterised by low surface area. This can be partially attributed to the extremely low porosity of SCGs biomass samples that might restrict the passage of N_2 molecules during the BET surface area analysis [343]. Consequently, a very smaller number of N_2 molecules could be adsorbed by the biochar surface and showed low surface area. From an adsorption point of view, average pore diameter determines the accessibility of heavy metals (for example, silver metal particles in this study), while specific surface area plays a major role in the adsorption capacity of heavy metals [344]. Therefore, this analysis indicates that the biochar sample of sawdust that exhibited the highest surface area and pore volume could be advantageous to achieve greater adsorption capacity for silver species.

The pH of the adsorption medium greatly influences the adsorption of heavy metals, such as silver. For instance, acidic or low pH (<6) increases the concentration of H^+, which blocks the ion-exchanged sites in the adsorbents, such as biochar. In contrast, a very high mutual pH (>8) was found to force the precipitation of heavy metals, thus reducing the adsorption capacity [345]. The pH results of each biochar sample presented in Table 7 indicate that biochars from all three biomass feedstocks were highly alkaline (pH 9.77–10.85) in nature. The higher

presence of inorganic nutrients (Na, K, Ca, Mg) along with the alkaline functional groups in algae may contribute to the high alkaline pH of biochar samples [346]. On the contrary, alkalinity increased with an increase in pyrolysis temperature, which was in agreement with a study reported by Shang et al. [281], thus demonstrating that the increase in pyrolysis temperature decreases the organic functional groups, such as –OH, and –COOH, and consequently the biochar pH increases [347].

Figure 13a shows the FTIR of three biomass feedstocks, indicating that various functional groups were present in each biomass. For instance, algae biomass showed the first two peaks at wavenumbers 598 and 612 cm^{-1}, indicating the presence of halo groups, such as C–I and C–Br. In contrast, medium peaks were observed in algae, SCGs, and sawdust biomasses from wavenumbers 1050 to 1085 cm^{-1}. These peaks demonstrate the presence of C–O groups, but the quantity of C–O groups varies and could be ordered as algae > sawdust > SCGs biomass, indicating the presence of carboxyl-containing compounds such as esters, ketones, and carboxylic acids. However, the wavenumber range (1050–1085 cm^{-1}) was overlapped with 1030 to 1070 cm^{-1}. Therefore, the peak at 1054 cm^{-1} in algae and a peak at 1034 cm^{-1} in sawdust might be the cause of S=O stretching/sulfoxide group/H-N-H or amino group [348]. The peaks at 1402 cm^{-1} indicate the presence of carboxylic acids (O-H), and the peaks at 1639 cm^{-1} in algae represent alkene (C=C) groups [49]. SCGs biomass showed two peaks at 2851 and 2925 cm^{-1} that are assigned to the presence of alkene (C-H) groups [349]. A broad peak at 3292 cm^{-1} in algae biochar confirmed the presence of the carboxylic group that is also presented in SCGs and sawdust at low intensity [350].

FTIR spectra of biochars are shown in Figure 13b-d, demonstrating that functional groups presented in biomass disappeared as the pyrolysis temperature increased, which can be attributed to the enhanced reactions such as dehydration, decarboxylation, and decarbonylation during biomass pyrolysis [339]. For example, very few functional groups were identified in the biochars produced at 500°C, but biochars produced at 700 and 900°C had hardly detectable functional groups except for algae. Algae biochars produced at 500, 700, and 900°C did not show any peak before 600 cm^{-1}, but 611, 626, and 627 cm^{-1} had minor peaks, indicating the removal of C–I and retention of C–Br groups [351].

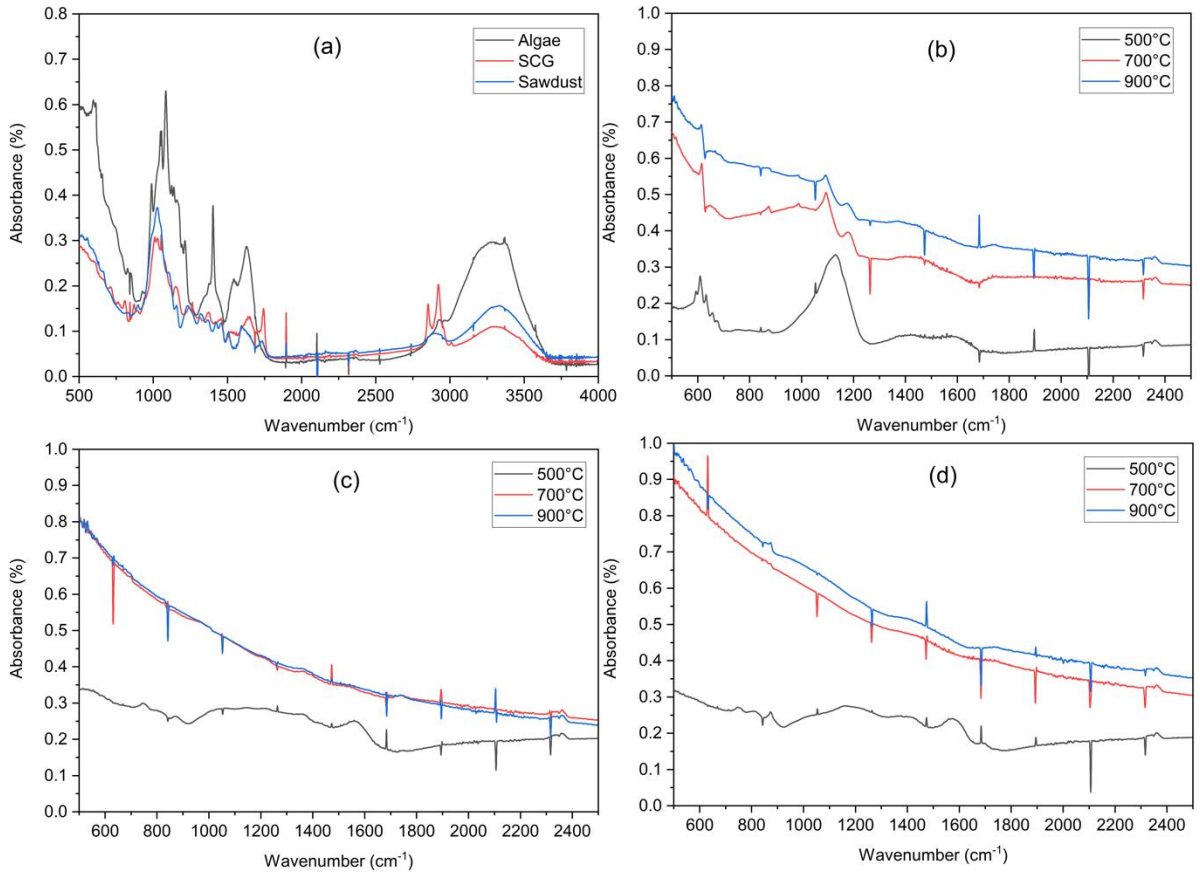

Figure 13: (a) FTIR spectra of algae, SCGs, and sawdust biomasses; and FTIR spectra of biochar samples obtained from (b) SCGs, (c) algae, and (d) sawdust at different pyrolysis temperatures (500, 700, and 900°C).

With the increasing pyrolysis temperature, C–O alcoholic or ester groups decreased, but remained at a low intensity even in biochar produced at 900°C; that was supported by the peaks at 1054 and 1098 cm^{-1} [23]. However, functional groups (C–H and O–H) in biomass material at wavenumbers 2851 to 3292 and 2925 cm^{-1} were completely decomposed from all three biomasses during pyrolysis because of their instability at high temperatures [301]. Narrow bands at 2369, 1564, 1264, and 881 to 755 cm^{-1} indicated the presence of O=C=O, –COOH, C–O, and C–H in SCGs biochar produced at 500°C, respectively [352].

In sawdust biochar, produced at 500°C, minor absorbance peaks at 2370, 1683, 1585, and 886 to 760 cm^{-1} appeared due to vibrations of O=C=O, C=O, –COOH, and C-H bonds, respectively [351]. The presence of oxygen-containing functional groups, such as –COOH, –OH, –COR plays a vital role in chemisorption of any heavy metal ion [353]. The analysis suggests that higher pyrolysis temperature reduces the number of surface functional groups in biochars.

Since functional groups play a pivotal role in the adsorption of heavy metals, the presence of inadequate functional groups may decrease the silver removal from wastewater. Hence, low temperature (<500°C) pyrolysis should be employed to produce biochar that retains the maximum number of functional groups, that could enhance adsorption capacity for heavy metals.

The degree of crystallinity of different biochar samples was determined by XRD, and the results are presented in Figure 14. Algae biochar produced at 500°C showed moderate crystallinity at 2θ of 22° to 34° (Figure 14(a)), and the crystallinity decreased in biochar produced at 700°C, however, it increased again at 900°C biochar. In contrast, at 2θ of 46°, crystallinity was persistent in all three biochar temperatures. However, 900°C algae biochar exhibited additional small peaks from 44° to 49°, which can be attributed to the presence of metallic salt presented in algae. SCGs and sawdust biochars produced at 500, 700, and 900°C provided the XRD spectra of corresponding amorphous carbon (Figure 14(b), (c)). A similar amorphous structure of SCGs and sawdust biochars was reported in previous studies [354]. In contrast, a broad peak at approximately 24° indicated the tendency to form a graphitic structure in the biochar matrix at higher temperatures [352]. The XRD of biochar after adsorption Figure 14(d) has three sharp peaks at 2θ of 38.06° (111), 44.2° (200), and 64.4° (220), which corresponds to the presence of silver nanoparticles and thus demonstrates that during adsorption process silver ions were reduced and produced Ag NPs on the biochar surface.

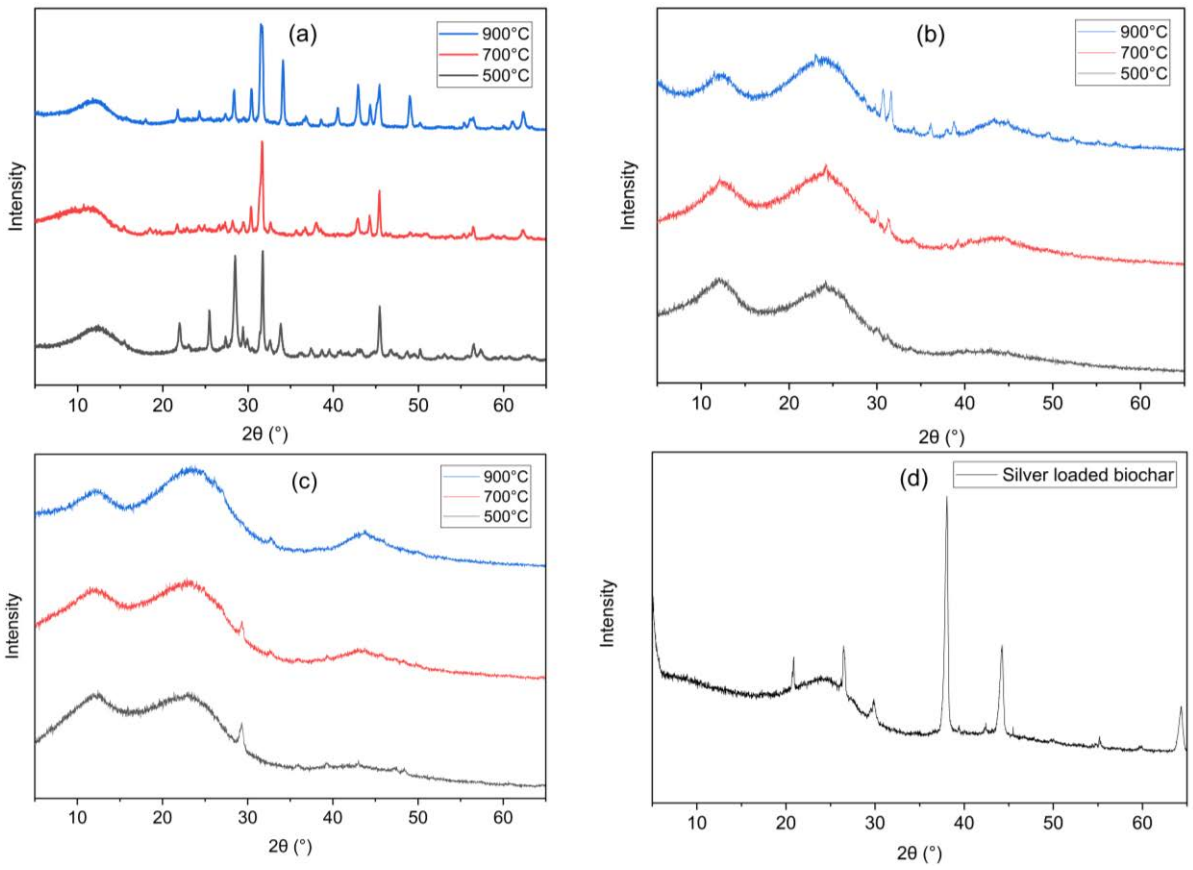

Figure 14: XRD spectra of biochar obtained at different pyrolysis temperatures from different biomass feedstocks (a) algae, (b) SCGs, (c) sawdust, (d) SCGs biochar produced at 500°C after silver adsorption.

3.3.3.5 Adsorptive removal of silver

Biochars produced from the three biomass feedstocks at varying pyrolysis temperatures were tested for silver adsorption capacities under different parameters, such as the quantity of adsorbent, concentration of silver, and speed of agitation. The concentration of silver in the initial and final solutions after adsorption was determined by ICP-AES. All experimental data were analysed by the miniTAB software and presented in Appendix 1 Table A7. The Taguchi analysis (in Appendix 1 Figure A4) showed that silver adsorption decreased against the increase in the quantity of biochar. When a certain amount of biochar removed the total silver from the solution, additional biochar did not have free silver for adsorption and increased the denominator of the Eq. (19) and eventually decreased the adsorption capacity (mg/g ratio). In the majority of the samples, the adsorption capacity for silver decreased with an increase in the mass of biochar. For example, 0.1 g of SCGs biochar obtained at 500°C showed an adsorption

capacity of 25.13 mg/g, which was reduced to 8.23 mg/g when 0.3 g of the biochar was used. Similarly, algae biochar obtained at 500°C achieved 99.71 mg/g adsorption capacity that decreased to 33.12 mg/g when applying 0.3 g of the adsorbent. However, the quantity of adsorbent did not affect the adsorption capacity for some biochar samples. For instance, SCGs biochars produced at 900°C showed the adsorption capacity of 43.98 and 43.42 mg/g, employing 0.1 and 0.3 g of biochar, respectively. In contrast, silver adsorption was improved by increasing the initial silver concentration. Increasing the initial silver concentration increased the driving force between silver concentration in solution and silver in biochar, supplied sufficient silver in the solution that allowed the maximum utilisation of the adsorption capacity of a certain amount of biochar. However, the type of biomasses, pyrolysis temperature, and agitation speed (RPM) had no linear effect on silver adsorption by biochar.

Silver adsorption study also demonstrated some correlation among the different conditions. For instance, at a low initial silver concentration (50 mg/L), the adsorption capacity was gradually decreased by increasing the quantity of biochar. At a low silver concentration, a low quantity (0.1 g) of biochar was capable of removing all the silver from the solution, so adding more biochar was not beneficial in terms of silver adsorption capacity as all silver in the solution was removed by a small amount of biochar. For example, algae biochar tested with the silver concentration of 200 mg/L and using either 0.1 or 0.3 g of biochar achieved an adsorption efficiency of 99.97%. Based on the experimental data, algae biochar produced at 700°C provided the highest adsorption capacity of 196.2 mg/g for a 400 mg/L initial silver concentration using 0.1 g biochar in 100 ml solution for 5 h. However, it was observed during the experiments that by adding algae biochar into the silver solution, the solution turned slightly white, indicating that part of the silver reacted and precipitated because of the presence of inorganic salts in algae biochar.

SCGs biochar produced at 700°C showed the highest adsorption capacity of 46.1 mg/g for a 200 mg/L initial silver concentration by using 0.1 g biochar. Finally, 900°C sawdust biochar achieved the adsorption capacity of 55.3 mg/g for a 200 mg/L initial silver concentration by using 0.1 g biochar in a 100 ml solution for 5 h. The results showed that the silver adsorption capacity of biochar was not proportional to the specific surface area of biochar. This indicated that the surface functional groups might have also played a vital role in overall silver adsorption from aqueous solution, so both chemical and physical adsorption processes are essential. Silver adsorption capacities of other biomass derived biochar varied, but modified biochars provided

extra adsorption capacity, as demonstrated in previous research work [22]. Considering the energy required for pyrolysis and having a blend of large surface area and surface functional groups, SCGs biochar produced at 500°C could be more suitable than the other two biochars. This approach could be an alternative safe re-use of SCGs to reduce GHGs emissions and close the loop of the circular economy.

3.4 Conclusions

This study investigated the effect of feedstocks on biochar production using different biomass wastes. TGA results showed that 10°C/min was the optimum heating rate for the pyrolysis, and pyrolysis GC-MS analyses revealed the main composition of pyrolysis vapour and the potentiality of using any of the tested biomass to produce bio-oil or value-added chemicals. Based on the characterisation results, biochar produced from sawdust at 700°C showed the highest specific surface area of 345.7 m^2/g, whereas a surface area of 40.1 m^2/g was obtained from SCGs biochar produced at 500°C. In addition, biochar obtained (at 700°C) from sawdust showed a silver adsorption capacity of 24.68 mg/g while SCGs biochar produced at 500°C provided adsorption capacity of 25.11 mg/g with 99% silver removal efficiency. SCGs biochar that is characterised by low surface area demonstrated the highest silver adsorption because of the presence of surface functional groups such as –COOH, –OH, –COO. However, algae biochar showed the highest silver removal capacity, 196.2 mg/g, which was obtained not solely by adsorption, rather mainly by precipitation of silver salts. Therefore, SCGs is the best biomass waste among the three samples to produce biochar for silver removal since it showed the highest silver adsorption capacity and was cheaper to produce, the pyrolysis temperature was only 500°C. Biochar production from SCGs can be also a safe disposal option, avoiding any hazardous consequences from the landfilling of SCGs. Subsequently, the produced biochar could be a sustainable and cost-effective adsorbent for the effective mitigation of silver pollution.

4 INVESTIGATING THE IMPACT OF PYROLYSIS CONDITIONS AND MECHANISMS OF SILVER ADSORPTION BY BIOCHAR

Abstract

This study aims to investigate the impact of pyrolysis temperature on spent coffee grounds (SCGs) biochar properties and its impact on silver adsorption. Biochars were produced from SCGs at temperatures between 500 and 1000°C. SCGs derived biochars were then characterised by different analytical methods, such as Brunauer-Emmet-Teller (BET), Fourier transform infrared (FTIR), X-ray diffraction (XRD), and investigated for silver removal. Results revealed that the biochar produced at 500°C offered a maximum surface area of 40.1 m^2/g with a yield of 23.48% biochar and the highest silver adsorption capacity of 49.0 mg/g with 99.9% silver removal efficiency. However, biochar produced at higher temperatures gradually lost the surface area as well as the silver adsorption capacity. The morphology of adsorbed silver on biochar was determined by using Scanning electron microscopy-Energy dispersive X-ray spectrometry (SEM-EDS) and XRD analyses, which showed an even distribution of silver on the biochar surface. Further, X-ray photoelectron spectroscopy (XPS) confirmed that part of the silver ions was reduced to form metallic silver (Ag^0)/silver nanoparticles (Ag NPs) during adsorption. The kinetics and isothermal evaluation suggested that silver adsorption was dominated by pseudo-second-order model and Langmuir isotherm, which means that silver adsorption was mainly dominated by chemisorption and monolayer on biochar surface. Overall, this study suggests that the 500°C is the best pyrolysis temperature to produce SCGs derived biochar with suitable physicochemical properties that can efficiently adsorb silver species from wastewater.

Keywords: silver removal; adsorption kinetics; biomass pyrolysis; coffee biochar applications; heavy metal removal

Highlights

- SCGs biochar produced at 500°C exhibited the highest silver adsorption capacity
- Silver adsorption mechanism was dominant by monolayer chemisorption phenomena
- Strong affinity/interaction between the adsorbent and adsorbate
- XPS analysis confirmed the chemical transformation of silver ions during adsorption.

As submitted in: Islam, M. A., Dada, T. K., Parvin, M. I., A. K., Kumar, R., Antunes, E., "Optimisation of pyrolysis temperature to produce spent coffee grounds (SCGs) derived biochar for silver adsorption and its validation by kinetic and isothermal modelling", Environmental Research.

4.1 Introduction

Approximately 359 billion cubic metres of wastewater are produced each year around the globe, out of which only 63% of the wastewater is collected and 52% is properly treated, while 48% of the wastewater remains untreated and subsequently released into the environment [355]. Primarily, in developing countries, wastewater management is considerably poor due to inefficient infrastructures and lack of financial resources. At the same time, both rapid urbanisation and industrialisation result in an increase in the annual production of wastewater. Wastewater generated from domestic and industrial sources is generally contaminated with potentially toxic heavy metals such as Lead (Pb), Chromium (Cr), Cadmium (Cd), Mercury (Hg), Silver (Ag), and other hazardous pollutants [356, 357]. Though several techniques are employed to remove the contaminants, including heavy metals, during the wastewater treatment process (WWTP), a major portion of heavy metals remains in the treated effluent that finally goes into the water bodies [358, 359]. In addition, treated or untreated wastewater is widely used for agricultural and landscape irrigation [355]. Thus, heavy metal pollution becomes a serious threat to the global aquatic environment and human health [360, 361]. For instance, direct exposure to silver (Ag) can cause human health problems, such as liver and kidney disorders, eye and skin irritation, chronic problem in respiratory tract, and silver can also bio-accumulate in the food chain [362-364]. The toxicity of silver (ions and nanoparticles) towards living cells, including human cells, has been demonstrated by several studies [21, 365]. Therefore, to ensure the safety of human health and ecosystem, it is highly important to treat the wastewater to eliminate heavy metals like silver and other contaminants in wastewater prior to its further applications or final discharge.

Several advanced technologies, such as the activated sludge process, sequencing batch reactor (SBR), ion exchange, and reverse osmosis, are available to eliminate silver from wastewater, but most of these technologies are considered highly expensive and inefficient to remove silver particles completely from the wastewater. In addition, current wastewater treatment facilities cannot completely remove silver due to its low concentration (µg/L level) and the toxicity of the bacteria dominant treatment process [21, 44, 45, 366]. Adsorption has been gaining substantial interest for the efficient removal of silver from aqueous media, mainly because it is a simple, economical, and eco-friendly process [50]. Recently, many natural and synthetic adsorbents have been investigated for silver adsorption, for instance, activated carbons [223, 232], clays [243, 244], biowaste materials [236, 238], cellulosic materials [241, 242], zeolites

[247, 258], graphene [266], and biochar [50, 179]. However, compared to other adsorbents, biochar has been demonstrated as a promising adsorbent for heavy metals because of its low production cost, negligible environmental footprint, and significantly high adsorption capacity [22].

The primary interactions between biochar and heavy metals adsorption constitute electrostatic interactions, ion exchange, precipitation, and chemisorption [50]. Biochar is known to contain a net negative charge and can bind to positively charged silver ions, thus could ultimately play a key role in silver adsorption [367]. The presence of functional groups on the biochar surface help in the reduction of heavy metals. For example, a study confirmed that carboxyl groups in the biochar reduced Cr^{IV} into Cr^{III} [368]. In contrast, physicochemical properties of biochar such as pore size, particle size, surface area, and the number and type of functional groups affect the adsorption capacity of heavy metals. For instance, high surface area and porosity may provide additional sites and enhance the adsorption of silver species [52]. Overall, it can be suggested that the application of biochar could be highly advantageous to remove silver contamination from wastewater and mitigate its environmental risks.

Spent coffee grounds (SCGs) are the waste by-product of the coffee industry. Coffee grounds (CGs) are coffee beans that have been crushed to a powder. Coffee is prepared by forcing boiling water through the CGs. After the water has been forced through, what remains is SCGs. Half of the SCGs produced come from cafes, while the other half is produced by the soluble coffee industry in the making of 'instant' coffee [369]. An average cafe in a large Australian metropolitan area in 2016 produced over three tonnes of SCGs (wet weight) per year, over 90% of which directly went to landfilling as SCGs do not have significant market value [370]. Landfilling of SCGs or any organic/food waste causes greenhouse gas emissions that are a key concern for climate change through global warming [322]. A circular economy approach for SCGs could not only reduce the environmental impact by eliminating pollution from landfilling but also transform SCGs into new products.

Pyrolysis is an alternative thermal conversion method to degrade the volatile organic content of the biomass into oil, gases, and biochar [26, 310, 371-373]. Oil yields greater than 35 wt% (dry oils) have been achieved using pyrolysis in a fluidized bed with a high total energy efficiency [322, 374]. Therefore, pyrolysis of SCGs is an environmentally sustainable process to convert waste into value-added resources [343], which is also a potential route of safe

disposal of about eight million tonnes of SCGs per year [352, 375]. Optimisation of pyrolysis conditions, such as pyrolysis temperature, can improve the physicochemical properties of biochar to enhance adsorption capacity. Moreover, the bio-oil fraction can alleviate the pyrolysis energy cost and make the process economically more viable.

According to a review of the literature, firstly, silver removal by any biochar has not been well studied, and secondly, this is the first study that uses SCGs derived biochar for silver adsorption. In this study, SCGs were pyrolyzed at a wide range of temperatures between 500 and 1000°C, biochar physicochemical properties were analysed, and the silver adsorption performance was investigated. A detailed adsorption kinetics evaluation and isothermal study of silver adsorption were also done to better understand the adsorption mechanisms of monolayer or multilayer and physisorption or chemisorption.

4.2 Materials and methods

4.2.1 Materials

SCGs were collected from Juliette's Espresso, a coffee shop at the JCU Townsville Bebegu Yumba campus. SCGs samples were dried in an oven at 105°C overnight to remove residual moisture. The sequence of steps used in the preparation of SCGs derived biochar is shown in Figure 15. Silver nitrate ($AgNO_3$), 99.99% wt/wt, was outsourced from Sigma-Aldrich (S6506-25G, lot#MKCJ2718).

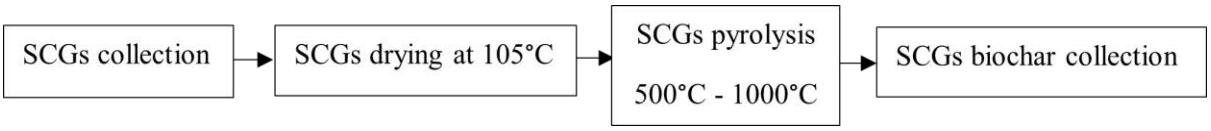

Figure 15: A process flow diagram for SCGs biochar production.

4.2.2 Methods

4.2.2.1 SCGs biochar production and characterisation

To understand the impact of pyrolysis temperature on biochar surface area and functional groups, SCGs were pyrolysed at 500°, 600°, 700°, 800°, 900°, and 1000°C with a heating rate

of 10°C/min and dwelling time of 2 h to find the best pyrolysis temperature for SCGs biochar production to be posterior used for silver adsorption. This wide temperature range was selected based on our previous studies and literature review. After producing the biochar at each temperature, biochar yield (%), elemental analysis (EA), pH, specific surface area (Brunauer-Emmet-Teller, BET surface area), surface functional groups by Fourier transform infrared (FTIR), X-ray diffraction (XRD) were analysed by using the same methods as discussed in previous work [301]. The particle size distribution of SCGs biochar produced at 500°C was measured by the Malvern Mastersizer 3000.

4.2.2.2 Silver adsorption performance of SCGs biochar

To evaluate the silver adsorption capacity, 0.1 g of each biochar was added into 50 mL of 50 mg/L silver solution. Finally, adsorption capacity and silver removal percentage were determined from the silver concentrations before and after adsorption measured by ICP-AES.

After silver adsorption, biochar produced at 500°C was separated from the liquid phase by using filter paper that was then dried at 105°C overnight and analysed by XRD at room temperature. Scanning electron microscopy combined with Energy-dispersive X-ray spectroscopy (SEM-EDS) was used to examine the microstructure and silver distribution on biochar before and after adsorption tests. A Jeol JSM5410LVA SEM was used for the analysis where a beam of high-energy electrons was scanned across the surface of a sample to obtain high magnification and high-resolution images.

X-ray photoelectron spectroscopy (XPS) analysis was carried out to reveal the elemental composition and oxidation states of biochar surfaces and adsorbed silver measurements. A Kratos Axis Supra connected with a monochromated Al Kα X-ray source and a helium lamp for UPS measurements were used. The binding energy was calibrated by the C 1s peak at 284.6 eV. XPS peak processing software was used to deconvolute the peaks and identify different species of the same element.

4.2.2.3 Kinetic and isothermal study of silver adsorption by SCGs biochar

For the silver adsorption kinetics study, 0.25 g of SCGs biochar produced at 500°C (which demonstrated the highest silver removal in the preliminary experiments) was added to 250 mL

of silver solution with an initial silver concentration of 50 mg/L, which was stirred at 350 RPM for different contact times (5 min to 24 h). To understand the time dependency on silver adsorption, after each time interval (5, 10, 15, 20, 30, 40, 60, 90, 120, 180, 240, 300, 450, 600, and 1440 minutes), around 10 mL of solution was taken by a syringe and filtered by using a 0.22 µm membrane and then analysed by inductively coupled plasma-atomic emission spectroscopy (ICP-AES).

For the isothermal study and to reveal the impact of initial concentration on adsorption, 25, 50, 100, 150, 200, and 400 mg/L silver solutions were prepared by dissolving accurately weighed silver nitrate in double-distilled water. Silver adsorption experiments were carried out using the batch process at room temperature (22 ± 2°C). About 0.10 g of biochar that showed the highest silver removal (biochar produced at 500°C) was added to 100 mL silver solution of each initial concentration and stirred for 5 h at 350 RPM as more than 95% silver was adsorbed within the first 5 h according to the kinetics study. After each experiment, around 10 mL of solution was filtered using a 0.22 µm membrane for further analysis.

All experiments were done at least two times. If the relative difference between the two replicates was greater than 5%, one more repetition was carried out. Average of all repeats were presented only.

4.3 Results and discussion

4.3.1 Impact of pyrolysis temperature on SCGs derived biochar properties

Table 8 shows the results of biochar yields and textural properties of the produced biochars at the studied temperatures. Results revealed that increasing the temperature gradually decreased the biochar yield. The highest SCGs conversion into biochar was at 500°C pyrolysis, which produced 23.5% biochar, and the lowest was at 1000°C pyrolysis producing 21.8% biochar. However, the change in biochar yield from 500°C to 1000°C was not significant and was expected according to TGA analyses [316, 376]. These results from our study are consistent with previous studies that demonstrated the decrease in biochar yield with an increase in temperature [270]. Therefore, it could be suggested that lower pyrolysis temperature could be helpful to achieve higher biochar yield and could be comparatively more economical since less energy would be used for pyrolysis. However, in addition to biochar yield, it is critical to obtain

biochar with suitable textural properties, such as high surface area, pore volume, and physicochemical properties like high acidic functional groups to achieve high adsorption capacity.

Elemental analysis results of SCGs biochars produced at different temperatures between 500°C and 1000°C are summarised in Table 8. As expected, carbon content was found to increase with the pyrolysis temperature, while oxygen content decreased. The maximum carbon content of 83.53% was reached in the biochar produced at 1000°C, and the minimum carbon content of 70.5% was found in the biochar produced at 500°C. In contrast, the oxygen content of 22.94% was the highest in biochar produced at 500°C and the lowest of 12.42% in the biochar produced at 1000°C. These findings demonstrated that oxygen-containing groups were decomposed at high temperatures either in the form of pyrolytic gases like CO_2, CO, or NO_x and eventually decreased the oxygen content and increased the carbon proportion in the residual biochar [316]. Similar elemental composition of SCGs biochar was observed in previous studies [348, 352].

Table 8 presents the pH results of SCGs biochar produced at various pyrolysis temperatures. Based on the experimental results, all SCGs biochars were alkaline in nature as the pyrolysis process led to the formation of alkaline minerals from micronutrients in the biomass [344] with a slightly nonlinear change with temperature. However, alkalinity was slightly increased with the increase of pyrolysis temperature, which indicates a decrease of acidic functional groups, such as – OH, and – COOH [281, 347, 377].

Specific surface area (BET), pore-volume, and pore size results of each SCGs biochar sample are presented in Table 8. SCGs biochar has a very low surface area compared to other lignocellulosic origin-derived biochar, such as biochar produced from sugarcane bagasse and wood pyrolysed at 500°C that reported surface area of 202 and 316 m^2/g, respectively [378], whereas SCGs pyrolysed at 500°C previously reported only 1.46 m^2/g [352]. One of the reasons might be the smaller number of microspores in the biochar matrix. For instance, SCGs biochar produced at 500 and 800°C provided a pore volume of 0.019 and 0.003 cc/g, respectively, but BET surface area of 40.1 and 5.2 m^2/g, respectively. A maximum BET surface area of 40.1 m^2/g was found for the biochar produced at 500 °C, and the minimum was 3.4 m^2/g at 900 °C.

Additionally, biochar produced at 500 °C had a minimum pore size of 3.28 nm with a maximum pore volume of 0.019 cc/g. These results were significantly higher than in the previous study under the same pyrolysis conditions for SCGs [379]. The pore size increased with the increase in pyrolysis temperature. Biochar produced at 900°C had the largest pore size of 16.04 nm diameter, providing the lowest surface area. This might be a result from collapsing of pores, which leads to the formation of larger pores, but at 1000°C, these pores might shrink again. Pore size increased gradually till 900°C, then again decreased to 7.13 nm at 1000°C. These results indicate the weakness of the BET surface area measurement technique, such as the N_2 adsorption-desorption process, where complete desorption might not be able to be achieved and, consequently, is unable to accurately measure the surface area of SCGs biochar. For instance, BET analysis of these biochars took a long time, and the results provided a non-linear BET curve and a non-equilibrium system of adsorption-desorption of N_2, which might be responsible for less accurate results [343]. Degassing the pore and high burn-off degrees or long residence time might be responsible for widening the micropores, thus providing low surface area [348]. In addition, the BET technique is not valid for macroporous materials, and SCGs biochar might be one of these materials based on SEM images.

Table 8: SCGs derived biochar yields at different pyrolysis temperatures and their physicochemical properties.

Pyrolysis temperature (°C)	Elemental analysis (%)				Biochar yield (%)	pH	Surface area[a] (m^2/g)	Pore volume[b] (cc/g)	Pore size[c] (nm)	Silver adsorption capacity (mg/g)	Silver removal (%)
	C	H	N	O[x]							
500	70.5	2.87	3.69	22.94	23.48	10.29	40.1	0.019	3.28	49.0	99.9
600	75.82	2.89	4.63	16.66	22.74	10.4	31.3	0.012	5.18	47.3	96.0
700	76.29	2.61	3.23	17.87	22.14	11.02	33.5	0.013	6.01	48.4	99.7
800	77.73	1.16	3.26	17.85	22.33	10.38	5.2	0.003	8.14	28.7	57.7
900	80.08	0.87	3.83	15.22	21.86	11.27	3.4	0.005	16.04	25.3	51.5
1000	83.53	2.01	2.04	12.42	21.78	10.53	7.5	0.005	7.13	23.6	48.1

x = Calculated bythe difference, a = BET surface area, b = MP (Micropore analysis proposed by Mikhail) method, c = BJH (Barrett, Joyner & Halenda) method.

Peaks identified in FTIR spectra of different SCGs biochar samples are summarised in Table 9. The results revealed that lower pyrolysis temperatures produced biochar with a larger number of functional groups, demonstrating the presence of a variety of organic compounds in the biochar. For example, biochar produced at 500°C showed peaks at 1050, 1470, and 1890 cm^{-1}, which can be attributed to the presence of oxygen-containing alcoholic groups, aliphatic C−H groups, and aromatic C−H stretching, respectively. Conversely, increasing pyrolysis temperature started consistently decreasing the number of functional groups in the biochar, suggesting the volatilisation of organic compounds into pyrolytic gases and their condensation into the bio-oil. For instance, biochar formed at 600°C showed peaks at 1470, 1900, and 2100 cm^{-1}, which can be ascribed to the occurrence of organic compounds with aliphatic C−H, aromatic C−H, and C≡C, respectively. In addition, 1000°C temperature produced biochar with only aromatic compounds C−H. The analyses show that higher pyrolysis temperature enhances the decomposition of organic compounds into pyrolytic gases and bio-oil, leaving the biochar with a very few less or a negligible number of functional groups that are necessary for the adsorption of heavy metals. Therefore, lower pyrolysis temperatures should be applied for biochar production to generally result in a variety of functional groups in biochar, which could play a pivotal role as adsorption sites.

Table 9: Functional groups confirmed by FTIR analysis in the biochar produced at different temperatures.

Pyrolysis temperature (°C)	**Frequency (cm^{-1})**	**Alignment**	**Reference**
500	1050	O−H stretching alcoholic groups -CO-O-CO- stretching anhydride	[380, 381]
	1470	Methylene C−H groups vibrations	[379]
	1890	Aromatic C−H stretching	[23]
600	1470	Methylene C−H groups vibrations	[379]
	1900	Aromatic C−H stretching	[382]
	2100	C≡C stretching alkyne	[382, 383]
700	1900	Aromatic C−H stretching	[382]
	2100	C≡C stretching alkyne	[382, 383]
800	841	Alkene C=C stretching and aromatic C−H stretching	[23]
	1470	Methylene C−H groups vibrations	[379]
	2100	C≡C stretching alkyne	[382, 383]
900	2100	C≡C stretching alkyne	[382, 383]
1000	1900	Aromatic C−H stretching	[382]

The XRD analysis spectra of different biochars produced under different pyrolysis temperatures are presented in Figure 16 (a). XRD patterns showed nearly amorphous structures of all biochars. A slight increase in intensity of peaks at 2θ of 24.5° and 43° regions indicate amorphous carbonaceous structures. However, at higher temperatures, amorphous carbonaceous structures rearranged to form a graphitic structure, indicated by broad peaks at 2θ of 24.5° [352, 354].

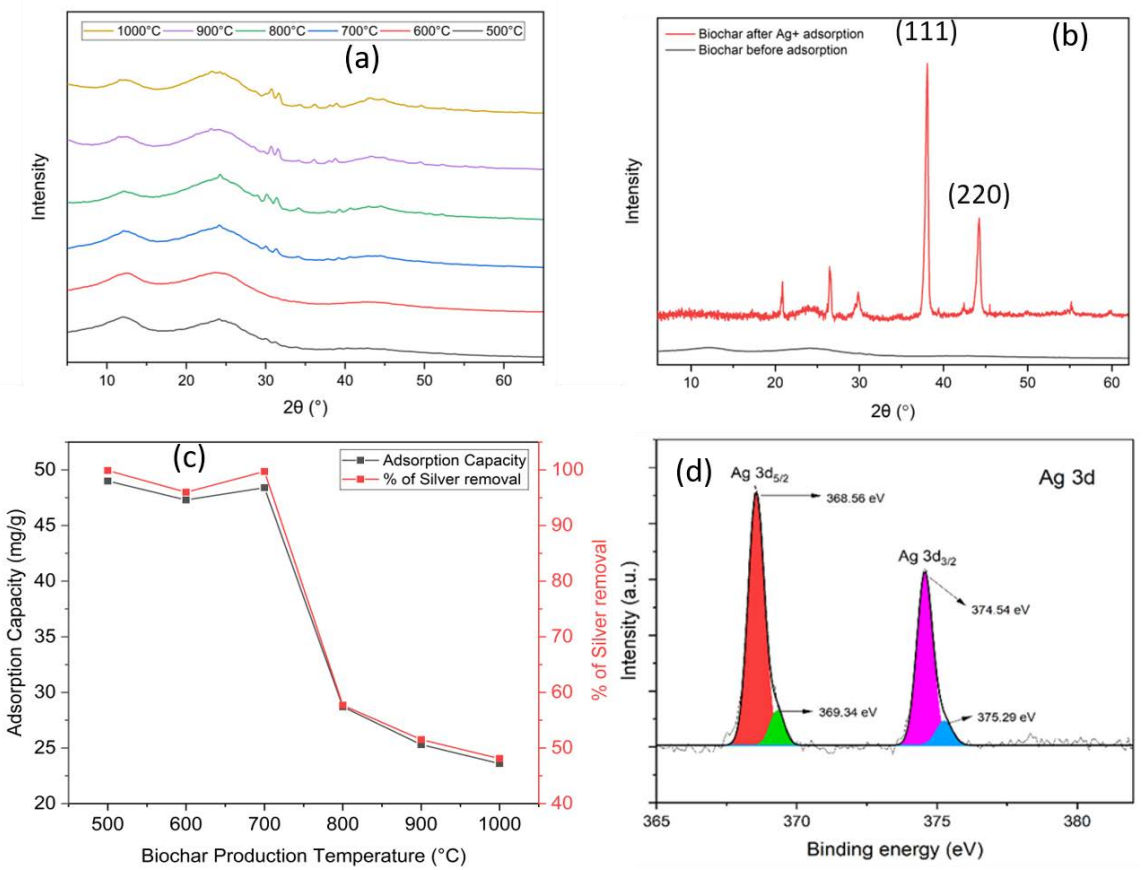

Figure 16: (a) XRD spectra of SCGs biochar obtained at different pyrolysis temperatures; (b) XRD analysis of SCGs biochar (500°C) before and after Ag+ adsorption; (c) Silver adsorption capacity and removal % of different SCGs biochar after 5 h; (d) XPS analysis of SCG biochar after Ag+ adsorption.

4.3.2 Silver adsorption study by SCGs biochar

The results of silver ions adsorption performance of SCGs derived biochar are shown in Table 8 and Figure 16 (c), which revealed that biochar produced at 500°C showed a maximum adsorption capacity of 49.0 mg/g and 99.9 % silver removal performance. In contrast, biochar produced at 1000°C provided the lowest adsorption capacity of 23.6 mg/g and 48.1% silver removal. In addition, SCGs biochar produced at 600 and 700°C provided the adsorption capacity of 47.3 mg/g and 48.4 mg/g with 96% and 99.7% silver removal, respectively. The decrease in adsorption capacity and % of silver removal with increasing pyrolysis temperatures can be attributed to textural properties, such as low surface area, pore volume and less required acidic groups in biochars. Since the biochars with a low surface area and negligible functional groups showed low adsorption capacity, it can be estimated that physisorption (that might include electrostatic forces and Van der Waal forces) played a role in silver removal [223]. At the same time, biochars that contained a significant number of functional groups also favoured the chemisorption mechanism for silver adsorption [384].

Therefore, based on silver adsorption performance, biochar produced at 500°C was selected and used to evaluate the kinetics and isothermal behaviour of silver adsorption from an aqueous solution. Despite having a low specific surface area, the SCGs biochar showed higher adsorption capacity (48.6 mg/g after 24 h) than biochar produced from biosolids (43.9 mg/g), which had a higher specific surface area (38 to 151 m^2/g) [50]. This observation demonstrated that surface functional groups played a major role in silver adsorption by SCGs biochar.

Table 10 also presents the comparison of silver adsorption capacities by biochars derived from different biomass wastes. According to Table 10, the maximum silver adsorption capacity achieved was 137.4 mg/g with a 2000 mg/L of Ag^+ solution, which was high compared to other studies. This difference can be explained by the direct impact of initial high concentration and different type of biomasses [385]. However, for a similar initial concentration of Ag^+, SCGs in this study offered the highest adsorption capacity.

Table 10: Comparison of silver adsorption capacity of different biomasses derived biochars.

Type of biomasses	Adsorption capacity (mg/g)	Initial silver concentration (mg/L)	Reference
Biofuel residue	90.06	50-100	[52]
Biosolids	43.9	100-1000	[50]
Sunflower husk	22.9		
Rapeseed	26.9	100-300	[349]
Wood waste	19.1		
Gracilaria R. algae	4.7	50-100	[386]
Pomelo peel	137.4	2000	[385]
Pine sawdust and bagasse	0.60–5.25	170	[345]
SCGs	46.2	50	[48]
SCGs	49.0	50	This study

Particle size distribution was measured for just the biochar produced at 500°C and is presented in Appendix 2, Figure A5. According to the results, 90% of SCGs biochar (produced at 500°C) particles were less than 371 µm, 50% were less than 184 µm, and 10% were less than 24 µm. These results demonstrated that SCGs biochar was composed of fine particles. Small particle size is generally considered favourable for greater contact between solid and liquid phases and could be advantageous to achieve enhanced adsorption capacity [387].

4.3.3 Characterisation of silver loaded biochar

All biochar samples studied for silver adsorption were characterised by XRD, SEM-EDS, and XPS to confirm the presence of silver in biochars after adsorption and prove their efficiency for the successful mitigation of silver pollution.

4.3.3.1 XRD analysis of biochar after adsorption

XRD spectrum of silver-loaded biochar is shown in Figure 16 (b). Three sharp peaks at 2θ of 38.06° (111) and 44.2° (200) were observed. All peaks can be attributed to the presence of crystalline silver nanoparticles [388, 389], which were otherwise absent in the biochars before

adsorption, as shown in Figure 16 (a). This finding demonstrates that the silver ions were reduced during adsorption and produced Ag NPs on the biochar surface.

4.3.3.2 SEM-EDS analysis of before and after adsorption

Figure 17 (a-c) illustrates the SEM images of SCGs biochar produced at 500°C before adsorption and shows that biochar had a rough, rigid, uneven, and irregular cracked surface. Figure 17 (d-f) shows SEM images of biochar after silver adsorption. Significant changes can be seen in the biochar surface compared to the untreated biochar samples, showing the homogeneous distribution of silver particles as white spots on the biochar surface. These white spots are silver nanoparticles that were confirmed by SEM-EDS analysis [223]. Small and large white spots on the surface indicated silver particles less than 100 nm in diameter. Large white clusters are the agglomerates of Ag NPs, which might be produced after the surface reduction of silver ions (Ag^{+}) [13].

In addition, EDS mapping (shown in Figure 17g) confirms the adsorption of silver by biochar, confirming the presence of 3.18 wt% silver on SCGs biochar. Other major elements such as carbon, oxygen, and trace amounts of other elements, such as magnesium, were also found in the biochar. The biochar samples successfully demonstrated the adsorption of silver, suggesting that biochar could be an efficient adsorbent for silver removal from wastewater.

The size of the deposited silver crystallite was calculated from the XRD data using the Scherrer Eq. (21):

$$D = \frac{K\lambda}{\beta \cos\theta} \tag{21}$$

Where, D is the mean size of the ordered (crystalline) domains (nm), K is the shape factor having the typical value of 0.9, λ is the wavelength of X-ray (0.154051 nm for Cu Kα radiation), β is the FWHM (full width at half maximum) of the diffraction peaks, and θ is the Bragg angle (°). The average size of silver particles on the surface of biochar was 20 nm based on the most intense XRD peak. This result is similar to the SEM results confirming that the newly deposited silver particles are nanoparticles.

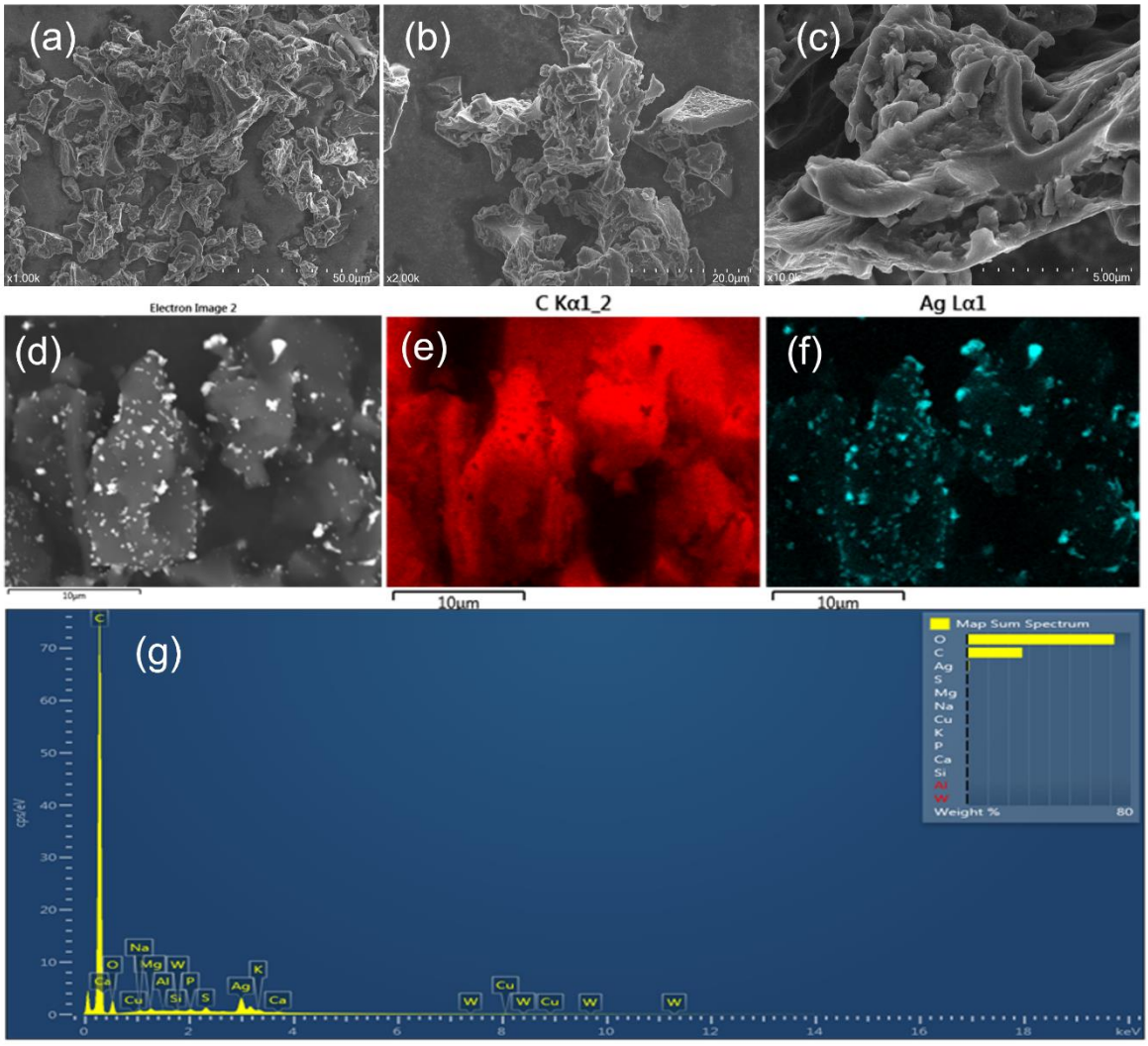

Figure 17: (a-c) SEM images of SCG biochar produced at 500°C before silver adsorption experiments; (d-f) SEM-EDS images of SCG biochar after silver adsorption; (d) backscattering image where the silver nanoparticles are the white spots; (e) refers to the carbon distribution in the biochar; (f) refers to the silver distribution on the biochar; (g) EDS-mapping spectra.

4.3.3.3 XPS analysis of biochar after silver adsorption

The presence of silver particles and their oxidation state in biochar samples was further confirmed by XPS analysis. Figure 16 (d) shows the results of XPS analysis for SCGs biochar before and after Ag^{+} adsorption, showing the electron binding energies of Ag $3d_{5/2}$ and Ag $3d_{3/2}$ orbitals. A separate table of XPS analysis can be found in Appendix 2 Table A8. For silver ions, Ag $3d_{5/2}$ and Ag $3d_{3/2}$ orbitals can be further divided into 368.56/369.34 and 374.54/375.29 eV, respectively [390]. The peaks at the binding energy of 368.56/369.34 eV

can be attributed to the presence of Ag^{+} in the biochar, while peaks at 374.54/375.29 eV can be ascribed to metallic Ag^{0} [391]. According to Table A8 in Appendix 2, 34.60% and 6.54% of atomic concentration of Ag^{+} were reduced to metallic Ag^{0} and Ag^{2+}, respectively. These findings again confirmed the chemisorption phenomenon, which was revealed by the kinetic and isothermal studies of silver adsorption by SCGs biochar.

4.3.4 Silver adsorption kinetics

Kinetic studies can provide vital information to understand the physicochemical mechanism of silver adsorption on the SCGs biochar. The adsorption capacity was measured by varying the contact time from 5 min to 24 h. Finally, the experimental data were compared with different kinetic models, such as pseudo-first-order (22), pseudo-second-order (23), Intraparticle diffusion (Weber and Morris) (24), and Elovich Eq. (25).

$$\ln(Q_e - Q_t) = \ln Q_e - k_t\, t \tag{22}$$

$$\frac{t}{Q_t} = \frac{1}{k_2\, Q_e^2} + \frac{t}{Q_e} \tag{23}$$

where Q_e (mg/g) and Q_t (mg/g) are the silver adsorption capacity at equilibrium, and time *t (h),* k_1 (h^{-1}) and k_2 (g/(mg h)) are the reactions rates constants.

$$Q_t = k_{id} t^{\frac{1}{2}} + C \tag{24}$$

where k_{id} (g/(mg $h^{1/2}$)) is the intraparticle diffusion rate constant and C (mg/g) is a constant.

$$t = \left(\frac{1}{\beta}\right)\ln(\alpha\beta) + \left(\frac{1}{\beta}\right)\ln t \tag{25}$$

where α (mg/g min) is the initial adsorption rate, and β (g/mg) is the desorption constant.

Kinetic study data were compared with theoretical model values in Figure 18 (a) and Table 11. The results suggest that the silver adsorption on the biochar surface occurred in two steps. For instance, the adsorption of silver ions was rapid at the beginning (up to 2 h contact time) and reached equilibrium after around 8 h. These findings demonstrate that silver ions were rapidly adsorbed by the adsorption sites on the outer surface of the biochar matrix, and after the first 2 h, silver ions diffused into the pores slowly. This second step could be explained by

intraparticle diffusion, which reduced the adsorption rate. The results confirm the contribution of both chemical (slow) and physical (rapid) adsorption phenomena.

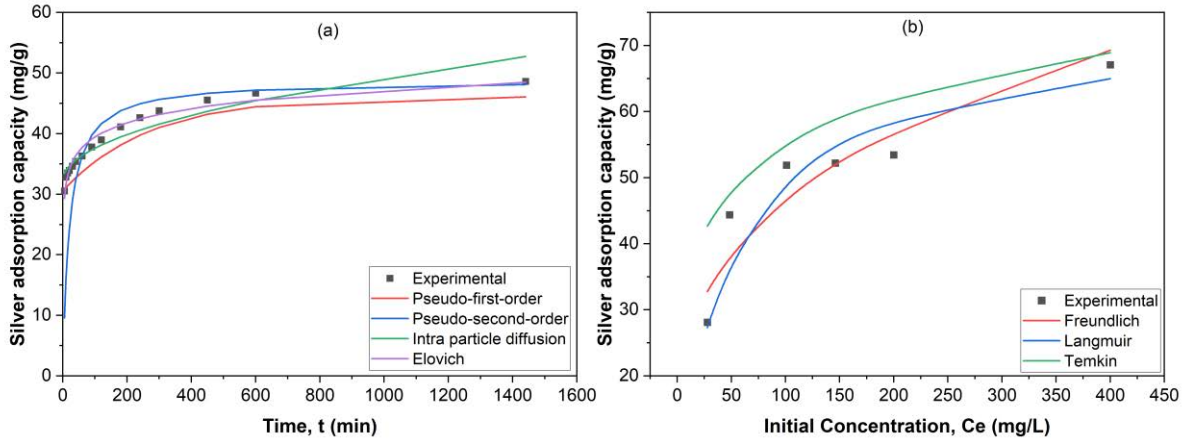

Figure 18: (a) Silver adsorption kinetics by SCGs biochar; (b) Adsorption isotherms of silver adsorption by biochar, including experimental data and theoretical models.

Figure 18 (a) and Table 11 show the comparison between experimental data and theoretical models for silver adsorption, where both the pseudo-first-order and pseudo-second-order models fit well with experimental curves having similar correlation co-efficient R^2 values of 0.9990 and 0.9895, respectively. However, the calculated adsorption capacity from the pseudo-second-order models was closer to the experimental value. Experimental data also showed that 61% silver was adsorbed in the initial 5 min. This attributed that the silver adsorption was mainly dominated by physisorption along with chemisorption. Additionally, a low k_2 value of 0.0010 g/(mg h) indicated that the adsorption process was driven by the number of unoccupied sites in biochar [353]. The pseudo-second-order model also explained the additional complex mechanisms, such as surface adsorption, external liquid film diffusion, and precipitation [50].

Table 11: Silver adsorption kinetic parameters derived by using different kinetic models.

Kinetic Models	**Reaction / diffusion rate constant**	**Constant, mg/g**	**R^2**
Pseudo-first-order	$k_1 = 0.0037\ h^{-1}$	$Q_e = 15.6192$	0.9895
Pseudo-second-order	$k_2 = 0.0010$ g/(mg h)	$Q_e = 48.7805$	0.9990
Intra particle diffusion	$k_{id} = 0.5408$ g/(mg $h^{1/2}$)	C = 32.2090	0.8960
Elovich	$\beta = 0.2954$ g/mg	$\alpha = 3912.2538$	0.8960

4.3.5 Silver adsorption isotherms

Adsorption isotherms were studied to understand the affinity between silver ions and biochar, and the results are shown in Figure 18 (b) and Table 12. The adsorption isotherms showed the impact of the initial silver concentration in the solution on silver removal capacity by biochar under a constant pH and isothermal condition (22°±2°C). The same biochar showed an adsorption capacity of 28.1 mg/g in 25 mg/L silver solution and 67.1 mg/g in 400 mg/L silver solution with the same retention time of 5 h. This finding indicates that higher concentration increases the driving force of mass transfer during the interaction between the solid and liquid phases.

The experimental data were compared with different isotherm models, such as the Langmuir model (26), Freundlich isotherm (27), and the Temkin isotherm (30) and (31). The Freundlich model assumed mathematically unlimited adsorption sites on heterogeneous adsorption surfaces [392]. As can be observed in Figure 18 (b) and by the R^2 value in Table 12, the Langmuir model fits better the experimental data, indicating monolayer adsorption on a homogeneous surface, which is in line with the adsorption kinetic results.

$$\frac{C_e}{Q_e} = \frac{1}{Q_m K_L} + \frac{C_e}{Q_m} \tag{26}$$

$$\ln Q_e = \ln K_F + \frac{1}{n} \ln C_e \tag{27}$$

where K_F $(L/g)^{1/n}$ and K_L (L/g) are the model constants, n is the Freundlich exponent, which represents the adsorption intensity, and Q_m (mg/g) represent the maximum adsorption capacity [50].

The equilibrium factor (R_L) can be calculated by Eq. (28), which is a dimensionless parameter used to determine whether the adsorption process is favourable or not.

$$R_L = \frac{1}{1 + K_L C_0} \tag{28}$$

where,

R_L=0 : adsorption is irreversible,

0 < R_L < 1 : adsorption is favourable

$R_L = 1$: linear nature of adsorption,

$R_L > 1$: adsorption is unfavourable

$$K = K_L M_{Ag} \tag{29}$$

where, R_L is the equilibrium factor, K_L represents the Langmuir constant, C_0 is the maximum silver concentration, K_L represent the Langmuir constant, M_{Ag} represents the molecular weight of silver in mg/mol, R is the ideal gas constant (8.314 J/mol K).

Temkin isotherm is a linear form expressed by Eqs. (30) and (31):

$$Q_e = B \ln K_T + B \ln C_e \tag{30}$$

$$B = \frac{RT}{b_t} \tag{31}$$

where, K_T (mg/g) is the Temkin isotherm constant, B is a constant associated with the heat of adsorption, and b_t is the Temkin isotherm constant.

Table 12: Silver adsorption isothermal parameters calculated by using different theoretical models.

Langmuir				**Freundlich**			**Temkin**		
K_L (L/g)	Q_m(mg/g)	R^2	R_L	K_F (L/g)	1/n	R^2	K_T (L/g)	*B* (J/mol)	R^2
0.0217	72.4638	0.987	0.1031	12.8507	0.2812	0.859	2.1755	12.6840	0.913

Silver adsorption by SCGs biochar was validated well with the Langmuir model as the R^2 value of the Langmuir model was the highest at 0.987, whereas Freundlich and Temkin's models provided R^2 values of 0.8589 and 0.9131, respectively (Table 12). This observation demonstrated that silver adsorption was a monolayer on a homogeneous biochar surface. However, studies showed that the Langmuir model was also used to simulate the adsorption process by chemical precipitation [13]. In addition, the equilibrium factor, R_L = 0.1031, was calculated by using the Eq. (28). R_L value was lower than 1, which indicated that the adsorption was favourable; thus, the affinity or bond strength was strong between the adsorbate and adsorbent [352].

4.4 Conclusions

This study investigated the effect of pyrolysis temperature from 500° to 1000°C on the properties of SCGs biochar and their implication for silver adsorption from water solution. Results revealed that biochar produced at 500°C provided the maximum yield of 23.48% biochar, the highest surface area of 40.1 m^2/g and pore volume of 0.019 cc/g. Also, the silver adsorption performance showed that the biochar produced at 500°C achieved a maximum adsorption capacity of 49.0 mg/g with 99.9% silver removal efficiency. In contrast, biochars produced at 1000°C achieved the lowest adsorption capacity of 23.6 mg/g with 48.1% silver removal efficiency. Low adsorption efficiency by biochars produced at higher temperatures could be attributed to their low surface area and pore volume, and the smaller number of functional groups. SEM-EDS results showed an even distribution of silver on the biochar surface. XPS analysis confirmed the presence of metallic silver (Ag^0) on the biochar surface, indicating the partial chemical transformation of silver ions during adsorption. The kinetic study validated that silver adsorption by SCGs biochar supported the pseudo-second-order model, which revealed the presence of chemisorption. Additionally, isothermal analysis established that the batch process of silver removal was dominated by homogeneous monolayer adsorption. This study indicates that biochar production from SCGs can be used as an adsorbent that is a sustainable approach to mitigate silver pollution while avoiding the hazardous consequences of landfilling of SCGs. However, further studies are required to evaluate the impact of activation of SCGs biochar on the silver adsorption performance with co-existing pollutants on silver removal. Investigation the impact of pH on Ag NPs adsorption by biochar can help to understand the transformation of silver and the binding process of silver to biochar as well as the overall Ag NPs adsorption process. A pilot-scale using a continuous adsorption column is required to better understand the capacity to handle large volumes of wastewater contaminated with silver species.

5 SILVER REMOVAL PERFORMANCE IN A FIXED-BED ADSORPTION COLUMN

Abstract

Even low concentration monovalent silver (Ag^+) and silver nanoparticles (Ag NPs) are emerging environmental threats, seeking an eco-friendly and cost-effective continuous treatment process to mitigate their pollution. In this study, an attempt has been made to investigate the potential of spent coffee grounds (SCGs) biochar in a fixed-bed adsorption column, to remove silver ions and silver nanoparticles from wastewater. A series (adsorption and desorption) of fixed-bed column experiments were performed under different operating conditions to determine the breakthrough curves (BTCs) and understand the effect of initial concentration (50–100 mg/L), the quantity of biochar (0.5–1 g), and the form of silver Ag^+ and Ag NPs on biochar removal capacity. Thomas and Yoon-Nelson models were applied to simulate different column parameters, such as breakthrough time, saturation time, the volume of treated effluent, and percentage of removal. These simulated results could assist in the scale-up of the process for an actual industrial operation. Experimental data showed good agreement with both Thomas and Yoon-Nelson models, where the simulated values were closely matched with the experimental values. Biochar was collected after the adsorption and characterised to confirm the morphology, crystal structure, and ionic state of silver. The saturated column was regenerated by 0.05 M HNO_3 as eluent and used at least 3 times with 15% capacity loss compared to initial performance, which demonstrated the viability and effectiveness of the biochar adsorption process.

Keywords: adsorption kinetics; biomass pyrolysis; Wastewater treatment; biochar; silver removal

Highlights

- First study on silver removal using biochar in a fixed-bed column on continuous mode
- Adsorption of silver using biochar is economical and effective
- Thomas and Yoon-Nelson models can be applied to simulate different column parameters
- Silver adsorption on biochar was partially dominated by chemisorption and silver transformation.

As published in: Islam, M. A., Dada, T. K., Parvin, M. I., Vuppaladadiyam, A. K., Kumar, R., Antunes, E. (2022), "Silver ions and silver nanoparticles removal by coffee derived biochar using a continuous fixed-bed adsorption column", Journal of Water Process Engineering, 48, 102935.

5.1 Introduction

Silver is one of the precious metals and is popular for its diverse industrial applications. Metallic silver or silver compounds have been used for various applications, such as mirrors, photographic plates, solar panels, radiography, jewellery, and high-value tableware. In addition, distinct physicochemical properties, such as antimicrobial action, very low thermal and electrical resistance, and special optical property (surface plasma resonance, SPR), make silver nanoparticles (Ag NPs) a useful addition to nanotechnology [223, 393]. However, environmental exposure to silver ions (Ag^+) and Ag NPs through waste streams raises concern about human health and the ecosystem [6, 7]. Biocidal products, such as anti-microbial textile and personal care and health care products, are the key source of silver (both Ag^+ and Ag NPs) in urban wastewater streams [394].

Usage of silver-based biocidal products is on the rise in the modern-day lifestyle. These externally used personal care products are often washed off during the day to day activities. Additionally, laundry of Ag NPs treated anti-microbial textiles cause silver leaching to domestic wastewater [395]. The production of Ag NPs increased by more than double in the last decade, and the trend is expected to continue in the near and long-term future. To date, >1700 products that contain Ag NPs are identified [2]. The source of Ag^+ is mainly from the photographic industries where Ag (I) waste is discharged as thiosulfate complex form mainly as $[Ag(S_2O_3)_2]^{3-}$. In addition, silver ions (Ag^+), AgCN, $[Ag(NH_3)_2]^+$ enter the waste stream from other industrial sources, such as mirror coating, electroplating, and mining [396]. Thus, a high quantity of silver enters the wastewater stream via various sources and increases the pollutant load in wastewater treatment plants (WWTPs) [397].

Although a good proportion (around 75%) of Ag^+ and Ag NPs can be removed by conventional or current WWTPs [398, 399], these silver species are a significant threat to the current treatment processes that are bacteria dominant. Anti-microbial silver can damage the bacteria and reduce the overall WWTPs efficiency [400]. Continuous discharge of residual silver contaminated effluent into natural water streams, or agricultural soil could be a potential threat to the environment [401]. Additionally, a significant proportion of the silver species are retained in the biosolids, which may later be used for land application. Thus, both routes are eventually releasing silver into the environment, resulting in a negative impact on the aquatic ecosystem and human health [402]. Furthermore, when these silver species (Ag^+ and Ag NPs)

come into wastewater streams, multiple transformations are expected to occur in a complex environment, such as WWTPs.

Understanding the aggregation and transformation behaviour of silver compounds and Ag NPs is fundamental to understand their transport phenomena and toxicity, which are greatly influenced by the chemistry of water streams [158, 162]. The transformation of Ag NPs in aqueous media is mainly driven by four mechanisms: oxidative dissolution, sulfidation, chlorination, and photoreduction, as presented in Figure 19 [18, 403]. Under oxygen-rich aqueous conditions, Ag NPs transform into Ag^+ that dissolves in water. However, Ag^+ can be converted back to Ag NPs in the presence of sunlight and dissolved organic matters (DOMs). A recent study demonstrated that Ag^+ could be reduced to Ag NPs by humic acid from natural organic matters (NOM) under dark conditions, ambient temperature (30°C), and high pH (6-9). In addition, the coexistence of formate, acetate, carbonate, or sulphate can accelerate the adsorption process [404]. However, neither the surface functionality nor the nature of the core structure can hinder the anaerobic transformation of Ag NPs or AgCl NPs to Ag_2S, which is more stable in a wastewater environment [169, 405]. Under such conditions, adsorption of NOM on Ag NPs surface limits the reduction reaction to produce toxic Ag^+ [406]. However, any further environmental change can destabilise the equilibrium and regenerate the toxic Ag^+.

In WWTPs with an HS^- rich environment, especially in domestic wastewater, both Ag NPs and Ag^+ can undergo sulfidation under anaerobic environments and produce an Ag_2S solid that is claimed as barely bioavailable and less toxic. However, a recent study found that the sulfidized species of silver showed toxic impacts on soil microorganisms [407]. In Cl^- rich environments, such as seawater, Ag NPs dissolve into Ag^+ and produce AgCl NPs and $AgCl_x^{(x-1)-}$ compounds.

A significant proportion of Ag NPs can be reduced to produce Ag^+ ions that transform into Ag_2S and AgCl. These sulphide and chloride species of silver are stable forms in terms of toxicity to a certain extent in the wastewater environment, but they are still bioavailable and toxic for some organisms, such as plants and *Caenorhabditis Elegans* [408]. Additionally, transformation reactions equilibrium can shift in to reverse direction based on the surrounding environment and contact time [409].

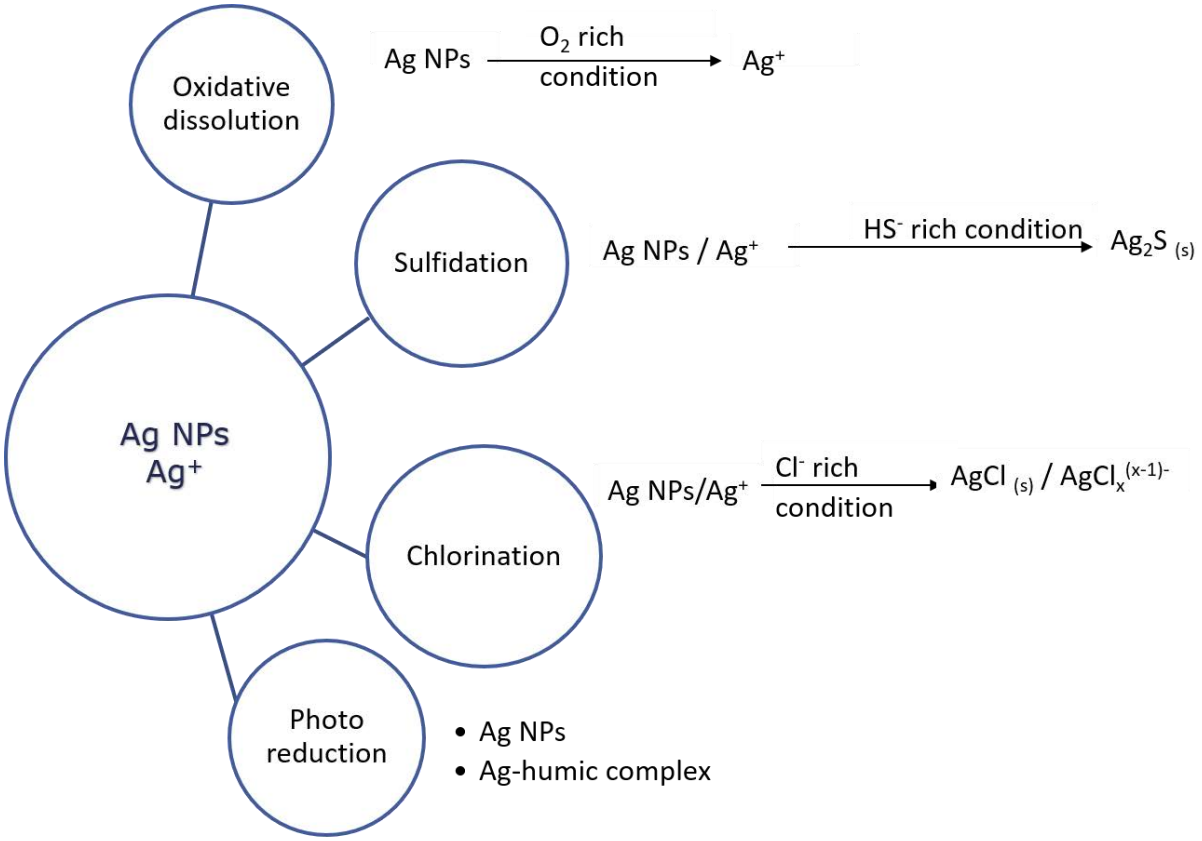

Figure 19: Transformation of silver ions and Ag NPs in a natural environment.

Proven silver removal technology is still not available to treat bulk scale wastewater. Some complex and economically unfeasible treatment processes such as reverse osmosis, membrane, and filtration are available for the total removal of silver [393]. Besides, a low concentration of silver makes the treatment processes more challenging. Adsorption by biomass waste-derived biochar can offer an effective solution to these challenges [410].

The adsorption process demonstrated tremendous success in removing several heavy metals from wastewater [341]. Biosorption is an adsorption process where the adsorbents come from biological origin to remove a wide range of contaminants, such as toxic metals. This technique is simple, sustainable, and cost-effective for handling a large quantity of wastewater with a low concentration of metals [411, 412]. Although activated carbon is the most widely used commercial adsorbent, multiple investigations of silver removal by activated carbon or other synthetic and natural adsorbents challenged the commercialisation of such technology due to the cost-effectiveness and environmental footprint [410]. Biochar has been successfully used to remove numerous contaminants, such as antibiotics removal [413, 414], phenols [415-417],

and heavy metals [418, 419] from wastewater. For example, a study investigated the application of biochar to adsorption of different heavy metals like copper, zinc and lead from the aqueous phase. The results revealed that the biochar achieved a maximum adsorption capacity of 128.7 µg/g for copper, 107 µg/g for zinc and 4.49 µg/g for lead [420]. Another study reported the generation of biochar from pyrolysis of digested sludge and applied to remove cadmium and lead from wastewaters [421]. The results showed that the biochar achieved excellent adsorption capacity for lead and cadmium, which were 0.75 and 0.55 mmol/g [421]. The adsorption capacity of the biochar was attributed to the presence of various functional groups on biochar surfaces and its porous structure; however, the higher adsorption capacity for the lead was ascribed to the increased affinity compared to cadmium [421].. In addition, biochar is a potential support matrix to immobilise nanoparticles [33], which can be advantageous for removing Ag NPs from wastewater. Due to the continuous generation of a large volume of wastewater, sustainable and cost-effective solutions are required. Therefore, continuous adsorption of silver species might mitigate silver pollution.

Spent coffee grounds (SCGs) are the waste residue generated from the production of instant coffee and coffee brewing [422]. The estimated generation of SCGs was >18.6 billion kg in 2016 [352]. Landfilling of these SCGs can be a burden because of the greenhouse gas (GHG) emissions [423]. Biochar produced from SCGs can be utilised to remove silver from wastewater. This approach can solve two problems with single technological innovation. According to the literature, only a few studies have been performed on silver (Ag^+ and Ag NPs) removal by using biochar produced from biomass waste, and most of them were limited to batch experiments. In most of the studies, Ag^+ ions were used for laboratory investigation. However, silver transformation reactions confirm that all Ag NPs are not converted into Ag^+, and sometimes Ag^+ ions are transformed into Ag NPs in a natural environment. Thus, it is crucial to evaluate the suitability of a process for both species of silver to ensure the complete removal of silver. Most importantly, only one study was found where biochar was used to adsorb Ag NPs for batch scale, and, to the best of our knowledge, there is no study reporting on the adsorption of Ag NPs using biochar in a continuous mode. Assessing the potential of SCGs biochar to remove silver (Ag^+ and Ag NPs) from wastewater in a continuous mode was the key objective of the present study to establish its industrial-scale applicability. In this study, for the first time, a laboratory-scale fixed-bed adsorption column was used to understand the potential of SCGs biochar in the adsorption of Ag^+ and Ag NPs from wastewater on a continuous mode. The performance of the dynamic adsorption column was evaluated by

varying process parameters such as initial concentration, the quantity of biochar, and the form of silver (Ag^+ and Ag NPs). Experimental column characteristic parameters were compared with the simulated values from Thomas and Yoon-Nelson. Models to establish the hypothesis; Morphology and chemistry of silver after adsorption was confirmed by SEM-EDS and XPS analysis. In addition, the reusability of such a column was analysed to establish the economic feasibility of the process.

5.2 Materials and methods

5.2.1 Materials

Spent coffee grounds biochar was produced via pyrolysis at 500°C in an inert environment by purging N_2 gas (3L/min). The detailed production process and characterisation were explained in the previous chapter. Laboratory grade silver nitrate ($AgNO_3$) 99.99%, Ag NPs 99.99% wt/wt, and Nitric acid (HNO_3) 99.99% were purchased from Sigma-Aldrich (lot#S6506-25G, lot#MKCJ2718, and lot#225711-475ML, respectively).

5.2.2 Fixed-bed column system

A glass tube of 11 mm inner diameter and 55cm height was used to prepare the adsorption column. A fine mesh of stainless steel was placed at the bottom of the tube to hold the packing materials. For each experiment, 1 g or 0.5 g of SCGs biochar was mixed well with 54 g of quartz sands (particle size: 1.18 – 2.36 mm). SCGs biochar was comprised of fine particles; for instance, according to the particle size distribution, 90% was <371 µm, 50% was <184 µm, and 10% was <24 µm. Small particle size is generally considered favourable for greater contact between solid and liquid phases and could be advantageous to achieve enhanced adsorption capacity [387]. Sand has been used as an inert media to avoid excessive pressure drops. The packing mixture in the column provided a constant column height of 42 cm. The top and bottom of the column were packed with only quartz sands with 4 cm height on each side to maintain a uniform flow. Finally, the column was fitted with a peristaltic pump to ensure continuous flow at a constant flow rate (Figure 20 (a)). During each experiment, a solution was made to flow continuously from top to bottom by holding a constant solution stock on top of the column, avoiding any air trapped inside the column, and allowing the use of a whole cross-section of the column. Thus, every possible care was taken to avoid any possible changes in the flow rate

or column height. In this experiment, initial silver concentration and quantity of biochar were varied to evaluate the dynamic column performance.

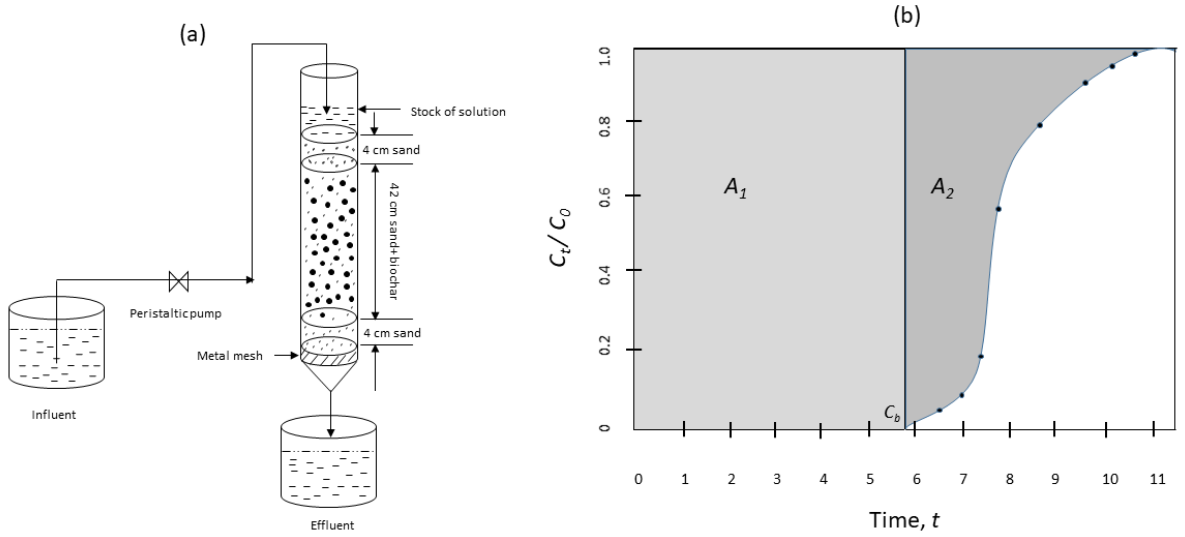

Figure 20: (a) Schematic diagram of the fixed-bed column for continuous silver adsorption, (b) Example of a breakthrough curve.

5.2.3 Fixed-bed column adsorption and regeneration studies

Continuous adsorption studies were carried out with silver nitrate ($AgNO_3$) and Ag NPs solution in double-distilled water at room temperature (22° ± 2°C). 50 mg/L and 100 mg/L Ag^+ solutions were prepared by using $AgNO_3$. These two concentrations were selected based on the literature where a wide range of initial concentrations (50 – 2000 mg/L) were studied. For example, a study demonstrated the application of biochar adsorption of heavy metals (lead, cadmium, copper, zinc and nickel) using the initial concentrations of 20-250 mg/L [424]. Another study demonstrated the removal of cobalt and nickel using an initial concentration of 50-250 mg/L [425]. Ag NPs powder was added into double distilled water to produce 50 mg/L and 100 mg/L of Ag NPs containing solutions that were continuously agitated by a magnetic stirred at 750 rpm overnight. Experiments were carried out maintaining the pH around 6-7. Previous studies have shown that this pH range is highly advantageous to achieve the maximum adsorption, while increasing or decreasing pH reduces the adsorption capacity. For example, a study showed that biochar achieved maximum adsorption for Ni and Co at pH 6, while low and higher pH decreased the adsorption significantly [425]. For each experiment, five litres of the solution was fed into the vertically oriented column using a peristaltic pump (Cole-Parmer,

Masterflex-L/S-07542-01, USA), maintaining a constant flow rate of 10 mL/min. Every half an hour, *ca.* 20 mL of the effluent was collected for ICP-AES analysis. According to Pap and his co-workers, breakthrough and exhaustion time are the two most used parameters when the density of the adsorbate material in the effluent reaches *ca.* 10% and 90% of that in the inlet stream, respectively [426]. Once the column got saturated, 0.05 M HNO_3 was passed through the column at a 7 mL/min flow rate for 2 h. HNO_3 was used to dissolve the adsorbed Ag NPs and to regenerate the column [49]. After the acid treatment, the column was washed with double distilled water until the effluent pH reached 7.5 to 8.5. The adsorption efficiency of the regenerated column was also studied under the same conditions as the initial column. The regeneration rate was obtained from the following Eq. (32) [427]:

$$\%\ of\ Regeneration\ = \frac{amount\ of\ silver\ desorbed}{amount\ of\ silver\ adsorbed} \times 100 \qquad (32)$$

5.2.4 Analytical methods

Silver ions (Ag^+) concentration in influent and effluent solution was measured by the inductively coupled plasma - atomic emission spectroscopy (ICP-AES), makers of Agilent 5100 Varian Liberty Series II (Singapore). For Ag NPs, solutions containing unadsorbed Ag NPs were acidified with 0.05 M HNO_3 to dissolve the Ag NPs into silver ions (Ag^+) before the ICP-AES analysis. A series of silver standards were measured at a wavelength of 338.289 nm maximum for significant figures, and an independent Ag standard solution was measured along with every sample solution for quality control and quantification purpose.

After the adsorption, biochar was collected and dried in an oven at 105°C overnight to analyse the silver morphology and chemistry on biochar by X-ray diffraction (XRD), Scanning Electron Microscopy combined with Energy Dispersive Spectroscopy (SEM-EDS), and X-ray Photoelectron Spectroscopy (XPS). The XRD technique was used to understand the mechanisms of silver adsorption. The Bruker Phaser D2 X-ray Powder Diffractometer, Cu radiation, was used. The XRD spectra were collected from 5° to 65° with a scan step size of 0.02° and a time step of 1 s.

The SEM-EDS was used to get insights into silver distribution on biochar samples before and after the adsorption test. The Jeol JSM5410LVA SEM was used where a beam of high-energy

electrons was scanned across the surface of the biochar samples to get high magnification and high-resolution imaging of the biochar surfaces. For XPS analysis, the Kratos Axis Supra was used to reveal the elemental composition and oxidation states of the biochar surfaces and adsorbed silver.

5.2.5 Column data analysis

The breakthrough (BT) curve expresses the performance of a fixed-bed adsorption column. The time to reach a breakthrough and the shape are vital parameters to determine the operational and dynamic response of a fixed-bed adsorption column [428]. A number of column process parameters, such as the quantity of adsorbent used, initial concentration of adsorbate, flow rate, and fixed-bed column height, have a strong impact on the shape and nature of the BT curve [429]. In these experiments, the quantity of biochar, initial concentration of silver, Ag^+, and Ag NPs were the variables tested. The volume of the treated effluent is obtained by the BT point (t_b) defined as the time where C_t/C_0 becomes 0.1. The exhaustion or saturation point (t_s) is the point when the effluent concentration (C_t) from a column reaches about 90% of the influent concentration (C_0) [430, 431]. A typical BT curve is generally obtained by a C_t/C_0 versus volume of the treated effluent (V) or running time t plot for fixed-bed column height, as shown in Figure 20 (b). The total mass (q_s) of silver adsorbed by the biochar was calculated from the area above the breakthrough curve by using Eq. (33):

$$q_s = \frac{QA}{1000m} = \frac{Q}{1000m}\int_{t=t_0}^{t=t_s} C_{ad}dt = \frac{Q}{1000m}\int_{t=t_0}^{t=t_s}(C_0 - C_t)dt \quad (33)$$

where Q and m are the volumetric flow rate (mL/min) and dry weight of adsorbent (SCGs biochar) (g), respectively.

Adsorption capacity (q_b) at BT time (t_b), was calculated from the area above the breakthrough curve by Eq. (34):

$$q_b = \frac{Q}{1000m}\int_{t=t_0}^{t=t_b}(C_0 - C_t)dt \quad (34)$$

The time equivalent to total capacity is expressed by Eq. (35) [429]:

$$t_t = \int_{t=0}^{t=\infty} \left(1 - \frac{C_t}{C_0}\right) dt = A_1 + A_2 \quad (35)$$

The time equivalent to usable capacity is calculated by Eq. (36):

$$t_u = \int_{t=0}^{t=b} \left(1 - \frac{C_t}{C_0}\right) dt = A_1 \quad (36)$$

The MTZ (Mass Transfer Zone) is the area of a fixed-bed column where the adsorption occurs more intense. Smaller values of MTZ indicate the efficient utilisation of the adsorbents [432]. The MTZ length can be calculated by the Eq. (37)

$$MTZ = H \left(1 - \frac{q_b}{q_s}\right) \quad (37)$$

According to Figure 20 (b), the usable capacity of the bed is area A_1 up to the breakthrough time point t_b, and area A_2 is the unused portion of the column. Considering $t_u \approx t_b$, then equations (35) and (36) can be solved either graphically or by mathematical integration.

All other dynamic column parameters, such as hydraulic retention time (HRT), effluent volume till breakthrough (V_{eff_b}), effluent volume until saturation (V_{eff_s}), the total amount of silver (m_{total}) was passed through the column was calculated from the following equations:

$$V_{eff\_s} = Qt_s \quad (38)$$

$$V_{eff\_b} = Qt_b \quad (39)$$

$$m_{total} = \frac{C_0 Q t_{total}}{1000} \quad (40)$$

where V_c is the volume of the pack-bed (L) and H is the height of the bed (cm).

The total percentage of silver removal was calculated from the following Eq. (41):

$$\%\ of\ silver\ removal\ = \frac{q_{total}}{m_{total}} \times 100 \quad (41)$$

5.2.6 Theoretical models for Breakthrough (BT) curves simulation

Breakthrough (BT) curves were simulated by using different theoretical models, such as Thomas and Yoon-Nelson models. Experimental data were also compared with the model-derived parameters to understand the compliance of silver adsorption by a fixed-bed column and to predict the column parameters to scale up the full process.

Thomas model is the most frequently used model to predict the adsorption capacity and concentration-time profile of the whole breakthrough curves. Thomas' model assumes (1) plug flow in the bed and (2) reversible kinetics reaction with Langmuir isotherms for equilibrium [433]. These model equations are expressed in Table 13.

Yoon-Nelson model is the simplest model that does not include any process parameters [434]. The theoretical model assumes that the rate of adsorption for each adsorbate is proportional to the rate of decrease in adsorption [435]. The model does not require explicit information about the characteristics of adsorbate and its type. In fact, it predicts 50% of the breakthrough time and simulates column data obtained from a single adsorbate system [345].Yoon-Nelson model is expressed in Table 13

Table 13: Equations of kinetic models and their linearised forms to simulate breakthrough curves.

Model	Equation	Linear Equation	Plots	Constants
Thomas model	$\frac{C_t}{C_0} = \frac{1}{1 + e^{\left(\frac{K_T}{Q}\right)q_0 m - K_T C_0 t}}$	$ln\left(\frac{C_0}{C_t} - 1\right) = \left(\frac{K_T}{Q}\right) q_0 m - K_T C_0 t$	$\ln\left(\frac{C_0}{C_t} - 1\right)$ *vs* time, *t*	Kinetic constant K_T and q_0
Yoon-Nelson model	$\frac{C_t}{C_0} = \frac{1}{1 + e^{(K_{YN}(\tau - t))}}$	$\ln\left(\frac{C_t}{C_0 - C_t}\right) = K_{YN} t - K_{YN}\tau$	$\ln\left(\frac{C_t}{C_0 - C_t}\right)$ vs time, *t*	Kinetic constant K_{YN} and q_0

where K_T is the Thomas constant (mL/mg.min), m is the quantity of biochar in the column, q_0 is the maximum adsorption capacity, and t is the time (min) at a given flow rate (Q). K_{YN} is the Yoon-Nelson constant rate (min^{-1}), and τ is the time required to maintain 50% of the initial sorbent in its original form (min) [434].

5.3 Results and Discussion

5.3.1 Effect of fixed-bed adsorption column parameters on BT curves

A summary of experimental parameters of silver (Ag^+ and Ag NPs) adsorption in a fixed-bed column, such as q_s, t_s, m_{total}, and percentage of removal, is presented in Table 14.

5.3.1.1 Effect of initial concentration on BT curves

The effect of the initial concentration of Ag^+ and Ag NPs were investigated using two different concentrations, 50 and 100 mg/L, with the same amount of biochar using a flow rate of 10 ml/min at room temperature 22 ± 2°C.

According to the results reported in Table 14, adsorption capacities at saturation points (q_s) increased with the increase in the initial concentration of silver (Ag^+ and Ag NPs). For instance, 50 mg/L and 100 mg/L of Ag^+ with the loading of 1 g biochar showed an adsorption capacity of 42.78 mg/g and 45.85 mg/g, respectively. Similar results were reported in studies where maximum batch scale adsorption capacity was reported as 49.0 and 46.2 mg/g [48]. Similarly, 50 mg/L and 100 mg/L of Ag NPs with 1 g biochar loading showed an adsorption capacity of 13.72 mg/g and 19.12 mg/g, respectively. Increased adsorption capacities at higher initial concentrations were expected since a higher initial silver concentration offers a higher driving force to overcome the mass transfer resistance for the adsorption process for the specific amount of adsorbent (biochar) [436]. The Ag NPs adsorption using SCGs biochar was significantly low when compared to a recent study reported on vineyard biochar, where a maximum adsorption capacity of 88.9 mg/g was reported for Ag NPs adsorption on the batch scale. However, the study was not conducted in a continuous mode where biochar and Ag NPs got in contact for a short time, and the initial concentration of Ag NPs was 500 mg/L [23].

Ag^+ adsorption capacity (49.0 mg/g) carried out in batch mode in the previous chapter was higher than in this study (45.48 mg/g). A plausible reason could be, in the batch mode, the adsorbates may have a better interaction and higher contact time in the solutions with adsorbents, which is favourable for the external diffusion [430]. These findings are similar to previous studies [434]. However, it can be observed from to Table 14 that an increase in the

initial silver concentration decreased the breakthrough and saturation time (t_b and t_s), resulting in an early saturation of the adsorption column and a low volume of treated effluent.

In addition, at the higher initial concentration of silver, the total amount of silver adsorbed (m_{total}) increased, however, the percentage of silver removal and total volume of treated water decreased. This could be attributed to the fact that the active binding sites of the biochar were occupied by the adsorbates, and biochar got saturated quickly [437]. In this study, breakthrough time (t_b) and saturation time (t_s) were relatively low, which could be attributed to the relatively low adsorption capacity of unmodified SCGs biochar. In addition, at higher initial concentrations (100 mg/L), MTZ values increased a bit. For instance, for the fixed-bed column with 0.5 g biochar, MTZ length increased from 25.02 cm to 31.98 cm when the initial concentration was increased from 50 mg/L to 100 mg/L. This was expected as the column received a higher quantity of silver and thereby reduced the performance [438]. MTZ length is an important parameter to determine the efficiency of the column. It has been suggested that if the ratio of MTZ length and the total bed length is <1.0, the MTZ is fully developed, and the column is considered highly efficient [439]. Besides, the smaller MTZ length indicates that most of the bed has been used at the breakthrough point, and a steep breakthrough curve is generated. In this study, the initial concentration of 50 mg/L showed a smaller MTZ length compared to 100 mg/L, suggesting the former scenario was more efficient and economical. On the other hand, feed flow rate also plays a pivotal role in MTZ. Though the effect of the feed flow rate on MTZ was not examined in this study, it has a significant impact on MTZ. For example, Naja and Volesky [440] demonstrated the effect of the flow rate (2–16 cm/min) on MTZ in a fixed bed column of a length of 60 cm. The results of the study revealed that the higher flow rate of 16 cm/min achieved the maximum MTZ of around 18 cm in a rapid time (nearly 10 min). In comparison, the slowest flow rate of 2 cm/min achieved an MTZ of approximately 16 cm after a long residence time (100 h) [440]. The high flow rates usually do

not allow enough time for metal ions to penetrate the biochar pores and react with functional groups. In contrast, low flow rates allow adequate time for metal ions to immobilize on biochar but might not be desirable in terms of effectiveness. Therefore, a flow rate of 4 cm/min was suggested to achieve desirable results with a column length of up to 60 cm [440]. However, in this study, a flow rate of 10 mL/min was used, which proved to achieve low MTZ with 50 mg/L concentration, indicating an efficient performance of the column.

5.3.1.2 Effect of biochar quantity in the fixed-bed column on BT curves

The effect of biochar quantity on the BT curves and Ag^+ adsorption was investigated by varying the weight of biochar (0.5 g and 1 g), maintaining the other process parameters constant. The other process parameters included bed height, flow rate, and solution temperature, which were maintained at 42 cm, 10 mL/min, and 22° ± 1°C, respectively. According to Table 14, at the breakthrough point (t_b), with the increase in the quantity of biochar, the adsorption capacity (q_b) increased while the maximum adsorption capacity (q_s) decreased. However, by increasing the quantity of biochar from 0.5 g to 1 g in the column, breakthrough time (t_b), saturation time (t_s), and the total percentage of silver removal were increased.

Further, the total volume of treated water increased with an increase in the biochar quantity as more biochar particles into the fixed-bed column resulted in an increase in the number of available active adsorption sites for Ag^+ interaction [429]. Thus, the increase in the adsorbent quantity can be considered favourable in scaling up the fixed-bed adsorption column for industrial operation. Similar findings were reported in the literature [261]. Further, in the fixed-bed column, when the quantity of biochar exceeded 1 g of weight, the aqueous flow was noticed to get blocked. This limited the study to a maximum of 1 g of biochar.

Table 14: Dynamic column parameters of BTC at different experimental conditions.

Parameters	Ag^+ adsorption in 0.5 g of biochar		Ag^+ adsorption in 1 g of biochar		Ag NPs adsorption in 1 g of biochar	
	C_0 = 50 mg/L	C_0 = 100 mg/L	C_0 = 50 mg/L	C_0 = 100 mg/L*	C_0 = 50 mg/L	C_0 = 100 mg/L
q_b (mg/g)	8.51	9.28	6.66	8.54	4.31	5.53
q_s (mg/g)	21.05	38.90	42.78	45.85	13.72	19.12
$V_{eff\ b}$ (L)	50	100	150	100	150	100
$V_{eff\ s}$ (L)	2100	1500	2100	2100	2100	900
MTZ (cm)	25.02	31.98	35.04	35.48	28.81	29.85
t_b (min)	10	5	15	10	10	5
t_s (min)	180	150	210	210	210	90
m_{total} (mg)	93.06	142.35	103.53	199.92	75.53	104.40
% Removal	31%	15%	41%	23%	25%	13%

*This column was regenerated to evaluate the reusability.

Table 15: Simulated BTC analysis by using Thomas and Yoon-Nelson models.

Models	Parameters	Ag^+ adsorption in 0.5 g of biochar		Ag^+ adsorption in 1 g of biochar		Ag NPs adsorption in 1 g of biochar	
		C_0 = 50 mg/L	C_0 = 100 mg/L	C_0 = 50 mg/L	C_0 = 100 mg/L	C_0 = 50 mg/L	C_0 = 100 mg/L
Thomas	K_T *(mL/mg.min)*	0.530	0.426	0.769	0.338	1.176	1.102
	q_0 *(mg/g)*	23.84	47.25	57.91	58.41	11.77	24.67
	R^2	0.958	0.976	0.994	0.996	0.956	0.869
Yoon-Nelson	K_{YN} *(L/mg.min)*	0.0274	0.0493	0.0379	0.0322	0.0637	0.118
	q_{NY} *(mg/g)*	24.14	46.37	56.97	58.78	24.28	11.86
	τ *(min)*	34.87	12.90	52.90	54.05	5.59	17.23
	R^2	0.993	0.962	0.994	0.996	0.9653	0.869

5.3.1.3 Effect of Ag^+ and Ag NPs in the fixed-bed column on BT curves

Silver (either Ag^+ or Ag NPs) adsorption by biochar has not been well explored, and all these investigations were only in batch mode [393]. To the best of our knowledge, this is the first study that reports the adsorption potential of biochar in the removal of Ag^+ and Ag NPs in a continuous mode. Silver ions (Ag^+) and Ag NPs have different degrees of interaction with particular biochar because of their different chemical properties. In this study, Ag NPs had half the adsorption capacity and removal percentage of Ag^+ under the same testing conditions. According to Table 14, the initial concentration of 50 mg/L and 100 mg/L of Ag NPs with 1 g biochar loading recorded the maximum adsorption capacity of 13.72 mg/g and 19.12 mg/g, respectively. However, 50 mg/L and 100 mg/L of Ag^+ with 1 g biochar loading provided the maximum adsorption capacity of 42.78 mg/g and 45.85 mg/g, respectively. The results can be attributed to the ionic state of silver, which is expected to have a direct influence on adsorption [441]. Especially, ionic silver has more affinity to the biochar than elemental silver such as Ag NPs [442]. This could be explained as biochar is negatively charged in the water solution and attached with the positively charged Ag^+. Moreover, Ag NPs were coated with poly vinylpyrrolidone (PVP). This PVP tightly binds with the surface of the nanoparticles and helps to block them sterically from aggregate [443]. The Ag NPs were adsorbed on the biochar surface because of the covalent interaction (less strong than ionic) between oxygen atom present in biochar and the carbonyl, or the tertiary amine group of the pyrrolidone ring of PVP [23, 444].

In the scenario where the concentration of Ag^+ and Ag NPs was set as 100 mg/L, and 1 g biochar was loaded, the fixed-bed column got saturated more quickly for Ag NPs than for Ag^+. Thus, the total treated effluent volume at the saturation point ($V_{eff\,s}$) was 2100 mL and 900 mL, respectively. This saturation time or reduction in the treated volume of effluents for Ag NPs might be due to the short residence time in the column. A shorter residence time-limited the interaction between biochar and Ag NPs and may have led to low adsorption and low volume of treated effluents. It is also worth mentioning that the possibility of batch adsorption study of Ag NPs hindered by technical difficulties cannot be ignored. When it was required to collect the filtrate solution after batch adsorption for ICP analysis, the filtration process was also separating Ag NPs from the solution. Thus, it was not possible to distinguish the effect of adsorption and filtration.

5.3.2 Simulation of BT curves and comparison with experimental BT curves

Thomas and Yoon-Nelson models were used to compare the experimental results with theoretical model-derived values. Table 15 summarizes the obtained theoretical values of silver (Ag^+ and Ag NPs) adsorption in a fixed-bed column. The Thomas model considers all the adsorption parameters such as flow rate, time, and quantity of adsorbent, but Yoon-Nelson uses only time. Thus, the Thomas model seems to be more appropriate than the Yoon-Nelson model. An increase in the initial concentration resulted in a decrease in the Thomas kinetic constant (K_T) under all tested conditions. For instance, when the initial concentration of Ag^+ with 0.5 g of biochar loading was increased from 50 mg/L to 100 mg/L, K_T was noticed to decrease from 0.530 to 0.426 mL/mg-min, respectively. Similar observations for both models were reported in a previous study of Co ions adsorption [427] Evidently, the study showed that increasing the initial concentration of Co from 25 mg/L to 75 mg/L decreased K_T approximately three times from 0.00036 to 0.00012 mL/mg·min and similar results were obtained for Ni ions, the values for K_T reduced from 0.00047 to 0.00013 mL/mg. min when the initial concentration of Ni was increased from 25 mg/L to 75 mg/L [427]. In contrast, other kinetic parameter of the Thomas model, q_0 (predicted adsorption bed capacity), increased approximately two times with an increase in the initial concentration from 50 to 100 mg/L of Ag ions as well as Ag NPs. For instance, the values of q_0 increased from 23.84 to 47.25 mg/g when the concentration of Ag ions was increased from 50 to 100 mg/L, whereas for Ag NPs, q_0 increased from 11.77 to 24.67 mg/g. These results are also consistent with the previous study carried out by [427]. However, opposite trends were noticed for the Yoon-Nelson kinetic constant (K_{YN}) that increased with an increase in the initial concentration of Ag ions and Ag NPs. For example, K_{YN} increased from 0.0274 to 0.0493 L/mg·min when the initial concentration of Ag ions was increased from 50 to 100 mg/L. In addition, τ (min), which represents the time required to complete 50% of breakthrough, decreased from 34.87 to 12.90 min with an increase in the initial concentration. These changes in kinetic parameters indicate the effect of mass transfer or hydrodynamic conditions on the models and thus should be used carefully in pilot-scale studies. .

Additionally, experimental and theoretical adsorption capacities for Ag^+ obtained at the saturation points were close to each other, as well as those calculated from the batch

experiments. For Ag NPs, initial Ag NPs concentration reversely affected the adsorption capacity derived from the Yoon-Nelson model, as reported in Table 15. This could be due to the limitation of the Yoon-Nelson model that assumes time as the only variable that affects BT curves. A good correlation between the Thomas and Yoon-Nelson models was observed from the mid-range of the breakthrough curves, as shown in Figure 21. This might be attributed to the rapid initial adsorption of pore diffusion or internal diffusion taking place at a slower rate depending on the silver particle size and pore size [50]. These silver adsorption kinetics phenomena were the assumption of models that showed better compliance [433]. Furthermore, both models can simulate the behaviour of the fixed bed column for all the experiments. As shown in Table 15, both the Thomas and Yoon-Nelson models had good agreement with the experimental breakthrough curves with a high correlation coefficient (R^2 values >0.90), implying the suitability of these models for the fixed-bed column system. Similar results were reported during the removal of silver ions using vermiculite [433]. However, the experimental BTCs (in Figure 21) showed a drastic rise at the beginning of the BT curves, and after 75-100 min, experimental lines of breakthrough curves were fitted well with the model-derived curves. This might be due to the rapid film diffusion or external diffusion at the beginning, which was described by the pseudo-second-order kinetic model [50].

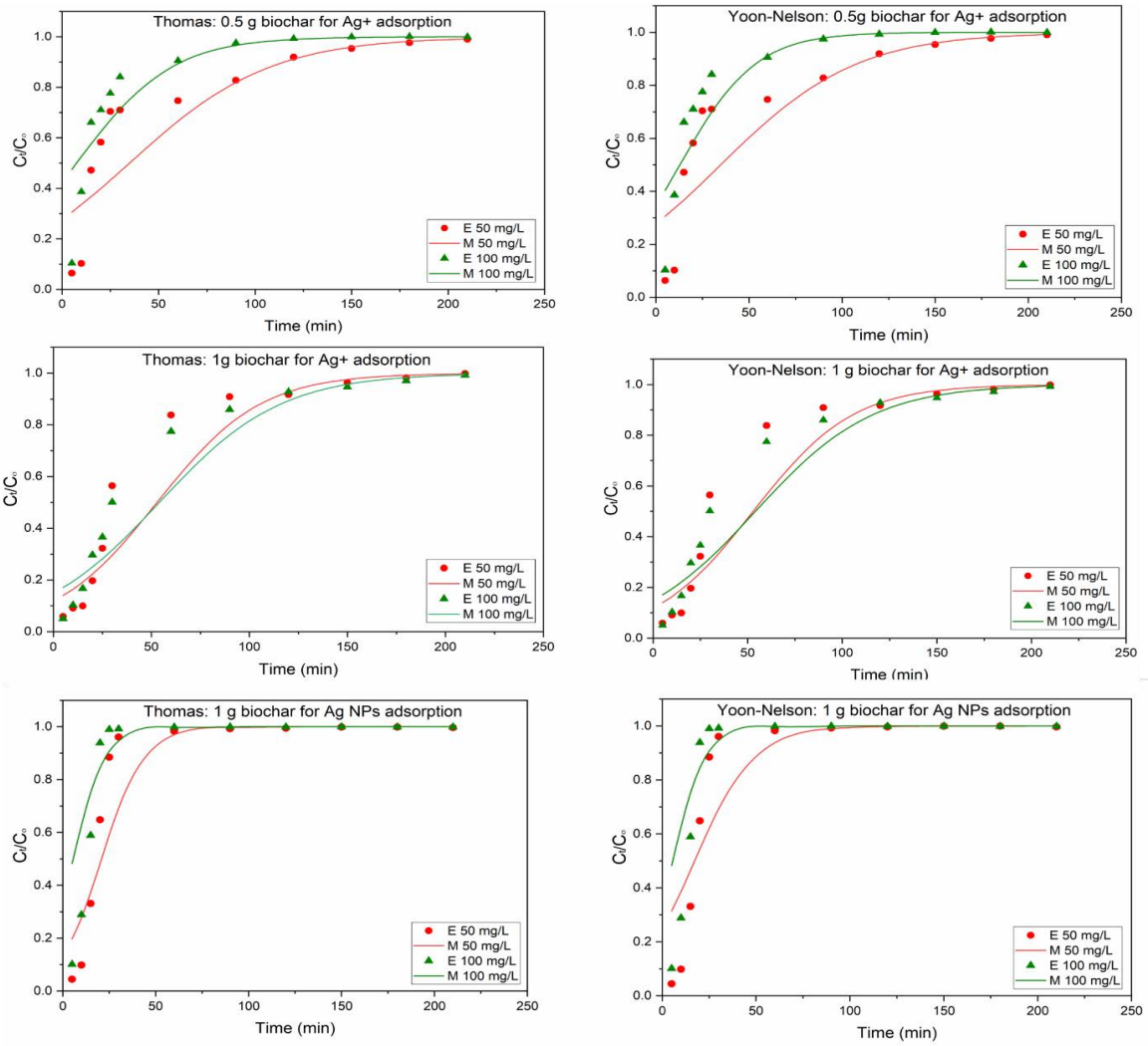

Figure 21: Comparison between Thomas model and Yoon-Nelson model derived breakthrough curves with experimental breakthrough curves.

5.3.3 Column regeneration and reusability

After the first cycle of adsorption with 100 mg/L of Ag^{+} and 1 g of biochar loading, the adsorption column was regenerated by using 0.05 M HNO_3 as eluent and running the second cycle of adsorption under similar conditions. Since, under these conditions, the column adsorbed the maximum quantity of silver, the regeneration performance of this column could be possible to achieve for other column conditions where a lesser quantity of silver was adsorbed. The regeneration process was repeated till the third cycle of adsorption to evaluate the reusability of the fixed-bed column and understand the feasibility at an industrial scale. In order to evaluate the performance, the parameters such

as maximum adsorption capacity (q_s) at the saturation point (t_s), saturation time (t_s), % removal, and % regeneration are reported in Figure 22.

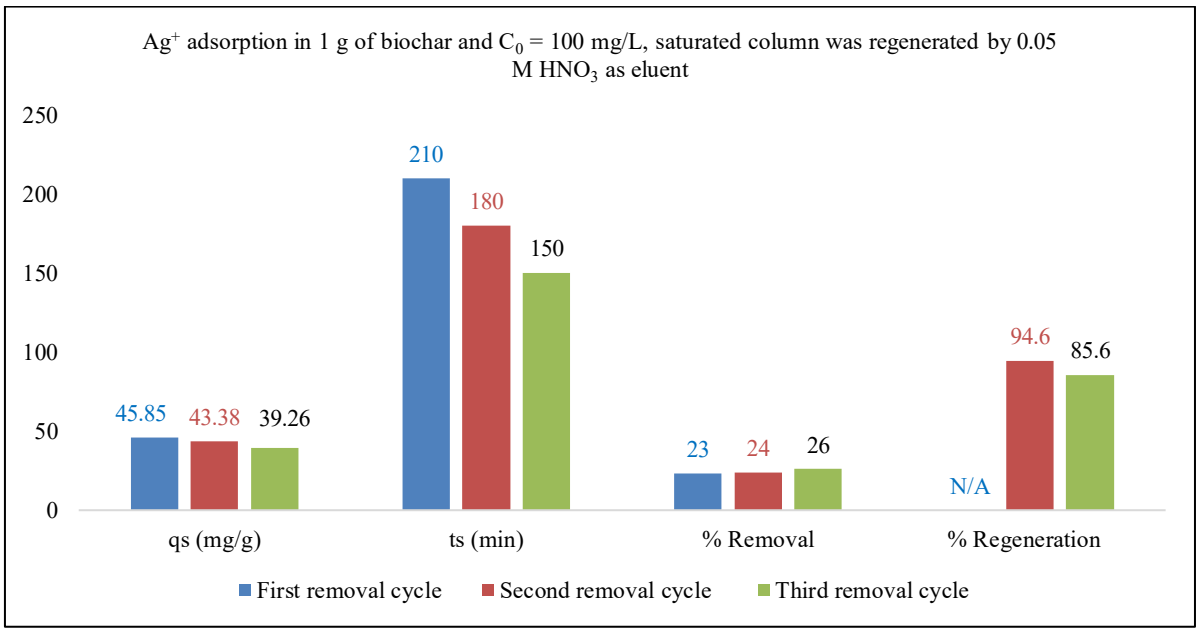

Figure 22. Comparison of column performance after two cycles of regenerations.

According to the results in **Error! Reference source not found.**, maximum adsorption capacities (q_s) at saturation point were 45.85, 43.38, and 39.26 mg/g during the first, second, and third cycles, respectively. After the first adsorption cycle, the regenerated column got saturated after 180 min operation, which was 30 min early than the first cycle. The loss in the adsorption capacity was noticed to be 5.4%. Similarly, after the second regeneration, the column lost 14.4% maximum adsorption capacity compared to the first cycle. Moreover, after each run, the column treated 300 mL solution less than the previous run. This capacity loss might occur due to the physicochemical change in the biochar by HNO_3, while regeneration and/or the HNO_3 solution was unable to reach into some of the micropores to dissolve the adsorbed silver, thus reducing the number of active adsorption sites. Similar capacity loss and lower volume of treated effluent were noticed in other studies which reported the use of a fixed-bed adsorption column for silver ions removal [37]. Therefore, it could be suggested that a setup that has three columns in series might be able to confirm the complete removal of silver for a continuous process. After three cycles of adsorptions, the columns will need replacement with new materials to keep the column performance at an optimum level.

5.3.4 Surface characteristics of silver loaded SCGs biochar

Figure 23 (a) and (b) represent the SEM images of biochar before adsorption, (c) and (d) represent after adsorption of silver ions (Ag^+), and (e) and (f) show the biochar after adsorption of Ag NPs. These SEM images were used to understand the change in surface characteristics and morphology of silver loaded SCGs biochar before and after adsorption. Both forms of silver forms were noticed on the biochar surface as white beads in Figure 23 (c), (d), (e), and (f). As silver backscatter electrons are stronger than light elements (low atomic numbers, such as carbon), they appear brighter in the SEM images [223]. In addition, on the raw biochar, there were no traces of such white beads on the raw biochar (Figure 23 (a) and (b)). This indicates the presence of a significant amount of silver on the biochar [209]. Figure 23 (c) and (d) also indicated that the Ag^+ is oxidised on the biochar surface and forms Ag NPs, which are distributed homogeneously. However, Figure 23 (e) and (f) mainly showed the aggregates of Ag NPs, but the aggregated quantity of Ag NPs was lower in this case, which is expected due to the lower adsorption capacity of biochar contacted with Ag NPs containing solution. From Figure 23 (g) and (h), high peaks in the elemental analysis by energy-dispersive X-ray spectroscopy (EDS) confirmed that the white spots in the SEM images are basically silver [345], implying successful adsorption of silver onto the SCG biochar. The oxygen signals in the EDS spectrum could be attributed to adsorbed water and oxygen molecules to form silver oxide [223]. In contrast, aluminium and silicon peaks could be from sand which was used with SCGs biochar in the fixed-bed column to improve porosity.

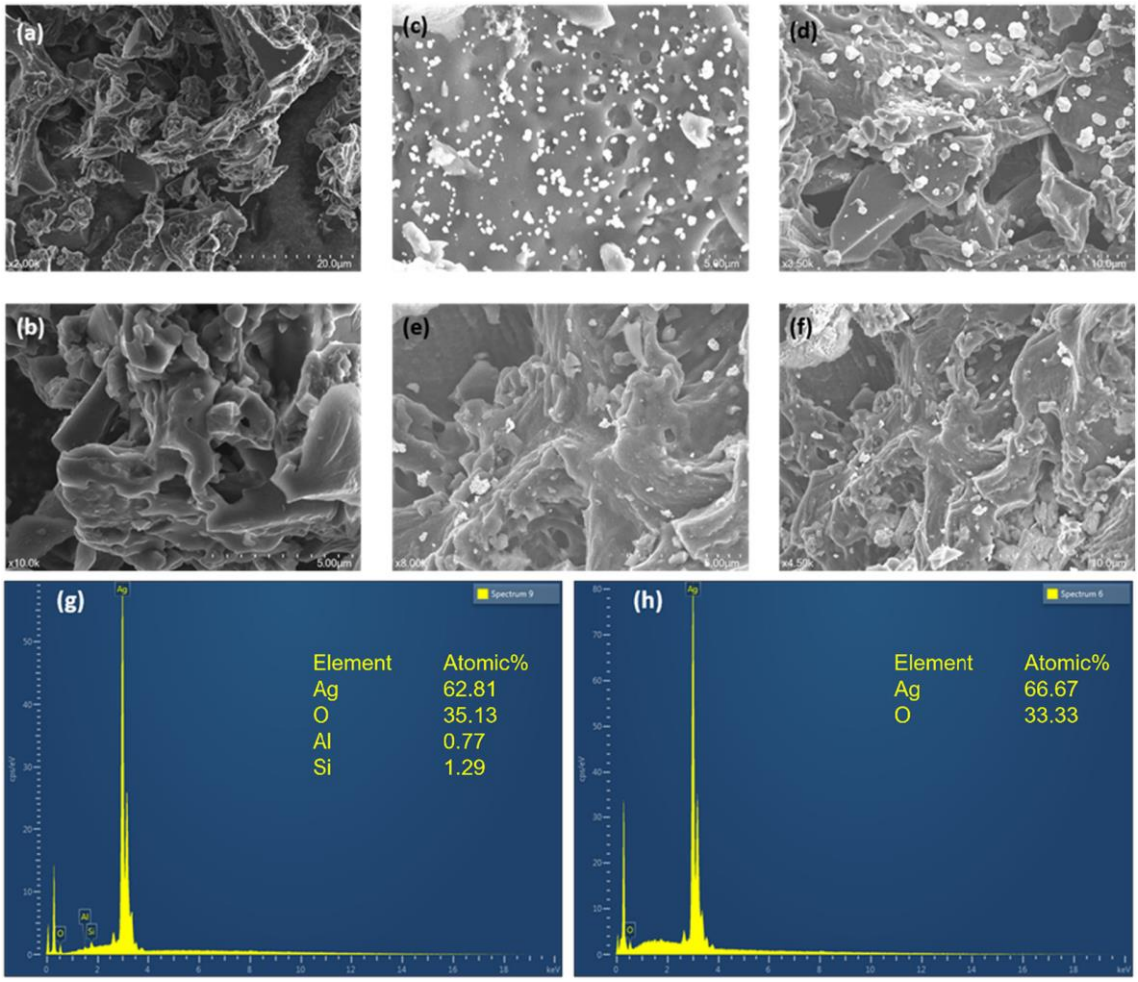

Figure 23: (a) and (b) biochar before adsorption; (c) and (d) biochar after adsorption of silver ions; (e) and (f) biochar after adsorption of Ag NPs; (g) EDS spectra of biochar after adsorption of Ag^{+}; (h) EDS spectra of biochar after adsorption of Ag NPs.

X-ray powder diffraction patterns of biochar before adsorption and after adsorption of Ag ions and Ag NPs are shown in Figure 24 (a). XRD spectrum of biochar before adsorption showed a broad peak with 2θ at around 24°, which confirmed the existence of graphitic structure in the biochar [352]. After the adsorption, both the silver loaded biochar showed sharp peaks with 2θ at around 38.4, 44.6, and 65.1°, implying the presence of crystalline silver having face-centred cubic (FCC) lattice structures (111), (200) and (220), respectively [52, 145]. The XRD results further confirm that the white beads detected by SEM-EDS were silver. In addition, higher intensity of XRD peaks corresponds to a higher degree of crystallinity [445], as noticed for biochar with Ag NPs as compared to biochar with Ag^{+}. Higher crystallinity might be explained as follows; the lesser amount of Ag NPs may get ionised when in contact with the biochar to form silver ions. However, a

few small sharp peaks of quartz were also identified at 2θ of around 20.9, 26.5, and 29.9 [446] as biochar collected after adsorption was contaminated with quartz sand which was used with biochar in the column.

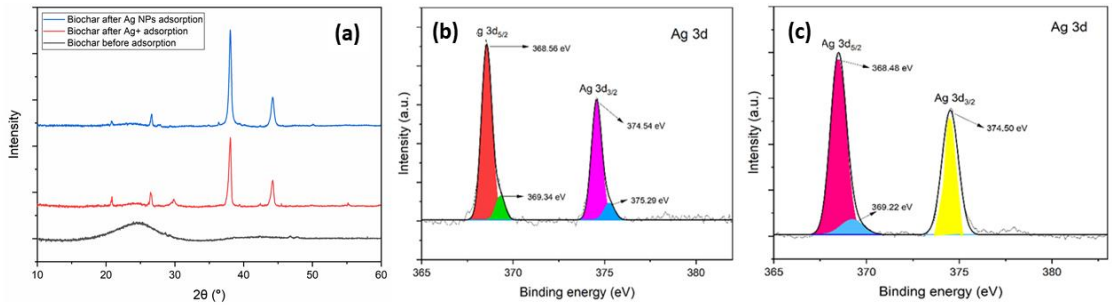

Figure 24: (a) XRD images of biochar before and after adsorption; (b) XPS analysis of SCGs biochar after Ag^{+} adsorption; (c) XPS analysis of SCGs biochar after Ag NPs.

SEM-EDS and XRD analysis revealed the presence of silver in the biochar matrix. Furthermore, XPS analysis of the biochar after adsorption was conducted to determine the oxidation state of silver. Figure 24 (b) and (c) represent the XPS analysis results of the biochar samples that were used to adsorb Ag^{+} and Ag NPs, respectively. A separate data table of XPS analysis is added in Appendix 3 Table A9. Electron binding energy corresponding to Ag $3d_{5/2}$ and Ag $3d_{3/2}$ orbitals were observed. Additionally, in Figure 24 (b), biochar adsorbed Ag^{+} Ag $3d_{5/2}$ and Ag $3d_{3/2}$ could be divided into 368.56/369.34 and 374.54/375.29 eV, respectively. The peaks at the binding energy of 368.56/369.34 eV can confirm the presence of Ag^{+} (atomic concentration of 52.1%), whereas peaks at 374.54/375.29 eV reveal the presence of metallic Ag^{0} (atomic concentration of 34.6%) [52]. On the other hand, peaks at nearly similar binding energies were also observed for the biochar with Ag NPs, confirming the presence of both Ag^{+} (atomic concentration of 58.1%) and Ag^{0} (atomic concentration of 38.6%) [248]. Multifunctional oxygenic groups' presence on the biochar surface might participate in the electrostatic attraction during the adsorption process [447]. Both findings might confirm the chemical transformation of Ag^{+} and Ag NPs in contact with SCGs biochar which was also identified during the adsorption kinetic studies [50]. Previous research on the kinetic analysis showed that the silver adsorption by biochar was dominated by the pseudo-second-order kinetic model which was driven by surface interactions through chemisorption and precipitation [349].

5.3.5 Techno-economic feasibility study

SGCs derived biochar is eco-friendly, low cost, and easily available. In this study, a single fixed-bed column showed a good level of adsorption. Similar three columns in a series can ensure the complete removal of silver. For instance, 1 kg of SCGs biochar will be able to treat 1400 L of wastewater having 50 mg/L of silver solution. It can be noted that 50 mg/L of silver concentration is higher than the realistic concentration, which is <1 mg/L. Therefore, the same quantity of biochar may be able to treat several folds higher than the volume considered in this study. In addition, the same column can be used and regenerated at least three times by backwash with 0.05 M HNO_3, which will cost $2.5 AUD. As the SCGs can be collected free of charge and dried by sunlight, there will be no additional cost for feedstock except the transportation cost. Although the biochar production by pyrolysis of SCGs at 500°C is the most cost-intensive process in the pilot scale, the value-added pyrolysis by-product bio-oil collection and selling can subsidise the energy cost of pyrolysis by around 50% [373, 448]. The previous investigation showed that the production cost of biochar for a pilot-scale pyrolysis plant could be USD 485 [373]. In addition, pyrolytic conversion of the organic food waste, such as SCGs can reduce GHG emissions, which is one of the major issues in view of global warming [449]. However, silver recovery from the spent biochar might also open some possibility of economic feasibility of the overall process. After the silver recovery from biochar (after 3rd cycle), SCGs biochar could be applied for soil remediation and carbon storage to avoid toxic impact and increase environmental benefit [450]. Compared to the environmental footprint and economic feasibility, this fixed-bed column process might be viable to be industrialised. Obviously, it is a preliminary laboratory-scale study where energy, operational, and equipment costs were not considered. However, adsorption capacity can significantly be increased by activation of biochar [451], and flow dynamics can be overcome by pelletising biochar before mixing with the sand [452]. A detailed cost study of the full process using improvised biochar and treating real wastewater can confirm the prospect of this new approach.

5.4 Conclusion

This study investigated the performance of a fixed-bed column study to remove silver from wastewater using SCG biochar in a continuous mode of operation. This study provides the much-needed fundamental understanding to evaluate the feasibility of scaling up this technique. Fixed-bed column using SCGs biochar demonstrated a significant removal efficiency of both Ag^+ and Ag NPs. The initial concentration of silver, biochar quantity, and the form of silver (Ag^+ and Ag NPs) had a direct effect on column performance. 50 mg/L silver ions solution passing through a column with a flow rate of 10 mL/min showed the maximum Ag^+ adsorption capacity of 42.78 mg/g. However, under the same condition, for 100 mg/L of Ag NPs, the maximum adsorption capacity for Ag NPs was 19.12 mg/g. Thomas and Yoon-Nelson models fitted well the breakthrough curves and experimental operational parameters, which could be useful to scale up the process for industrial application. The column was regenerated and reused three times with a total capacity loss of only 14.4% using HNO_3 as eluent. Furthermore, XRD, SEM-EDS, and XPS analysis of silver-loaded biochar revealed the morphology and chemistry of silver (Ag^+ and Ag NPs) after adsorption. Especially, the XPS analysis demonstrated the chemical transformation of both forms of silver (Ag^+ and Ag NPs), which eventually reconfirmed that silver adsorption on SCGs biochar was partially dominant by chemisorption and silver transformation in the environment.

6 CONCLUSION AND RECOMMENDATIONS

Investigation of biomass waste derived biochar to adsorb silver species from aqueous solution has been concluded successfully. The outcome of this research is a significant contribution to mitigate silver ions and silver nanoparticles pollution in order to save the aquatic ecosystem. This chapter combines the overall outcomes of this research. Conclusions are compiled chapter by chapter, followed by implications of the study. Finally, challenges and future research directions are presented as recommendations.

6.1 Impact of biomass feedstocks and pyrolysis kinetics

The quality and yield of biochar mainly depend on the composition of biomass and the pyrolysis conditions. Based on the literature review and the availability in QLD, three biomass wastes were selected from different sources, such as spent coffee grounds (SCGs), algae and sawdust, to produce biochar with varying physicochemical properties. After the initial TGA and DTGA analyses of the three biomasses, 10°C/min was the optimum heating rate for the pyrolysis, and algae showed the most complex decomposition behaviour while producing the highest quantity of biochar. However, the proximate analysis showed that algae contain 23.2% wt/wt ash that ends up in biochar.

Ozawa-Flynn-Wall (OFW) and Kissinger-Akahira-Sunose (KAS) methods were used to obtain pyrolysis kinetic plots. The activation energy fluctuation over the decomposition period demonstrated that the algae had a more complex composition compared to the SCGs and sawdust. The experimental kinetic parameters were very similar to the model-derived values. This finding confirmed good compliance with the models that could be used to simulate the thermochemical decomposition process under a specific condition.

Biochar produced from sawdust provided the highest specific surface area of 345.7 m^2/g at 700°C while SCGs provided 40.1 m^2/g at 500°C pyrolysis. FTIR analyses revealed the maximum presence of –COOH, –OH, –COO groups in the SCGs biochar produced at 500°C compared to all other biochars. These oxygen-containing groups are mainly responsible for the chemisorption of any heavy metal ions and polar substances to increase the overall adsorption. In terms of actual silver adsorption performance, SCGs

were the best among the three biomass wastes. However, algae biochar showed the highest silver removal capacity, 196.2 mg/g, which was mainly due to the precipitation of silver salts in the presence of chlorides in the seaweeds. SCGs biochar produced at 500°C and sawdust derived biochar at 700°C offered adsorption capacities of 25.11 mg/g and 24.68 mg/g, respectively, with 99% silver removal efficiency. Although the adsorption capacities were very similar, SCGs biochar produced at 500°C required less energy and was more advantageous than sawdust biochar for silver adsorption. Overall, biochar production from SCGs can be converted into biochar to be used as an adsorbent while avoiding hazardous consequences from the landfilling of SCGs.

6.2 Impact of pyrolysis conditions and mechanisms of silver adsorption by biochar

After selecting the best biomass for biochar production with a heating rate of 10°C/min, to optimise the pyrolysis temperature, SCGs were pyrolysed at 500° to 1000°C and tested for silver adsorption performance. The results revealed that biochar produced at 500°C provided the highest surface area, 40.1 m^2/g, with a maximum biochar yield of 23.48%, but increasing the pyrolysis temperature significantly decreased the surface area. FTIR analysis also showed that the SCGs biochar produced at 500°C had a significant amount of surface functional groups, such as –COOH, –OH, and –COO. FTIR curves became flat while increasing the pyrolysis temperatures, which indicated that the functional groups were decomposed at higher temperature pyrolysis.

Silver adsorption capacities of the different SCGs biochar were assessed. Results revealed that the biochar produced at 500°C achieved a maximum adsorption capacity of 49.0 mg/g with 99.9% silver removal efficiency. In contrast, SCGs biochar produced at 1000°C showed the lowest adsorption capacity of 23.6 mg/g with 48.1% silver removal efficiency. Biochar produced at higher temperatures achieved low adsorption capacity and thereby low silver removal efficiency. This could be ascribed to their low surface area and pore volume, and the lower number of remaining functional groups at high pyrolysis temperature, which provided a smaller number of adsorption sites resulting in a low adsorption capacity.

Silver loaded biochar were analysed to understand the morphology of silver deposited on biochars by using SEM-EDS and XRD analysis. Results evidenced an even distribution of silver on the biochar surface. Moreover, the XPS analysis confirmed the chemical transformation of Ag^{+} into metallic silver (Ag^{0}) and Ag^{2+} on the biochar surface. According to XPS analysis, 34.60% and 6.54% of atomic concentrations of Ag^{+} were converted to metallic Ag^{0} and Ag^{2+}, respectively.

The kinetic evaluation of silver adsorption showed very good compliance with the pseudo-second-order model, which validated the presence of chemisorption. Additionally, an isothermal study confirmed that the batch process of silver removal was dominated by homogeneous monolayer adsorption.

6.3 Silver removal performance in a fixed-bed adsorption column

After the successful application of SCGs biochar for silver adsorption in the batch mode, a dynamic study of a fixed-bed biochar adsorption column was investigated to understand the possibility of scaling up the batch process to continuous mode. The column demonstrated a significant performance to remove both Ag^{+} and Ag NPs. The study also revealed the impact of the initial concentration of silver, biochar quantity, and the form of silver (Ag^{+} and Ag NPs) on column performance. For instance, the column was able to show the maximum Ag^{+} adsorption capacity of 42.78 mg/g for a 50 mg/L silver ions solution passing through the column with a flow rate of 10 mL/min. This result was very close to the batch scale performance, which was 49.0 mg/g. Nevertheless, using the same column conditions, for an initial concentration of 100 mg/L of Ag NPs, the maximum adsorption capacity for Ag NPs was 19.12 mg/g. These results also confirmed that the adsorption capacity of SCGs biochar for Ag NPs was half that of the Ag^{+}, which could be explained by the PVP coated Ag NPs might be less prone to interact with the negatively charged biochar.

The kinetic evaluation showed that the Thomas and Yoon-Nelson models derived BTC fitted well with the experimental BTC. Models derived operational parameters were very similar to the experimental values, which demonstrated the potential usability of these models to design industrial scale processes for large-scale applications. Moreover, the

column was regenerated by 0.05 M HNO_3 and reused up to three times with a total capacity loss of only 14.4% compared to the initial column performance.

Furthermore, similar XRD, SEM-EDS, and XPS analyses were carried out to better understand the silver adsorption on the SCGs biochar surface. Morphological analysis revealed that both Ag^+ and Ag NPs were homogeneously distributed on the biochar, but the quantity of adsorbed silver for the Ag NPs used column was less than the Ag^+ used column. Furthermore, the XPS analysis showed that both Ag^+ and Ag NPs were partially transformed into Ag^0 and Ag^+, respectively. According to the XPS analysis of biochar before and after adsorption, these chemical transformations were validated by the significant change in atomic concentration between aliphatic and aromatic oxygens. These findings reconfirmed that silver adsorption on SCGs biochar was partly dominated by chemisorption and as well as the transformation of silver in the surrounding environment. Overall, this investigation clearly concluded that the biochar derived from SCGs could successfully adsorb silver species from aqueous solutions, and this safe disposal pathway of SCGs might decrease GHG emissions from landfills.

6.4 Implications of this research

This research brought several economic and environmental implications parallel to reach its main objectives. For instance, this research demonstrated significant progress towards the mitigation of silver pollution from wastewater by using biomass wastes. Pyrolysis of biomass wastes produces biochar, bio-oil and non-condensable pyrolysis gas or syngas. This thermal treatment of biomass has several advantages:

- reduce CO_2 emission load from the landfilling sites
- reduce methane emission load from the landfilling sites
- prevents hazardous chemical release from the SCGs landfilling sites

Although the primary focus was not to recover by-products, such as bio-oil and syngas, these by-products can be a very good source of energy and chemicals compounds. Any potential use of these by-products can offset the pyrolysis cost up to a significant level. In addition, any recovery of chemicals reduces the load on the fossil source. Both approaches can lead to reaching the goal of the circular economy concept.

6.5 Challenges and future research directions

Although this research was able to fill a significant knowledge gap, some challenges were also encountered. The following research directives can be considered for future research:

a) Since the adsorption capacity of SCGs biochar was still lower than other biochars, the activation of biochar can improve the adsorption capacity that can directly improve the overall efficiency of the process. Activation or modification often helps to increase the density of surface functional groups, such as –COOH, $–NH_2$, and –OH, which can significantly increase the adsorption capacity. Generally, chemical modification produces better outcomes, but physical activation can be used with less use of chemicals.
b) The impact of co-existing inorganic pollutants (heavy metals) in wastewater and the selectivity of silver adsorption were not considered in this research scope. Nevertheless, it is very crucial to test the performance of the SCGs biochar in a real-life scenario using wastewater that may contain multiple heavy metals.
c) A further pilot-scale investigation of a continuous adsorption column by using a real wastewater sample can help to better understand the ability to handle actual wastewater.
d) As the SCGs biochar was comprised of fine particles, which were blocking the flow through the fixed-bed column, biochar can be pelletised to overcome this issue. This will help to avoid any extra bulking materials, such as quartz sand, to improve the flow dynamics. However, this approach can compromise some degree of adsorption capacity.
e) The single adsorption column was unable to achieve the complete removal of silver as the quantity of biochar was optimised to keep a constant flow through the column, but not enough for complete adsorption. Activation or modification of biochar can improve this challenge. Otherwise, a multiple (at least three fixed-bed columns in series) stage adsorption setup can ensure the complete removal of silver species from wastewater.
f) This process is also capable to concentrate the precious metal silver onto biochar from which silver can be recycled. A suitable recycling technique can recover the silver and offset the overall process cost.

g) Morphological and size changes of silver nanoparticles before and after adsorption should be investigated to better understand the Ag NPs adsorption phenomena.

h) Finally, an in-depth economic feasibility study needs to be carried out considering multiple issues. For instance, energy efficient biomass pyrolysis process along with the by-products recovery system can significantly reduce the energy cost of pyrolysis. Solar drying of biomass can significantly reduce the energy required to dry the biomass waste, and energy recovery from the pyrolysis gas can be used to pre-heat the biomass before pyrolysis.

References

1. Yurtsever, M. and A. ŞEng▪L, *Adsorption and desorption behavior of silver ions onto valonia tannin resin*. 2012, Elsevier Ltd. p. 2846-2854.

2. Khan, S.S., A. Mukherjee, and N. Chandrasekaran, *Adsorptive removal of silver nanoparticles (SNPs) from aqueous solution by Aeromonas punctata and its adsorption isotherm and kinetics.* Colloids and Surfaces B: Biointerfaces, 2012. **92**: p. 156-160.

3. Massarsky, A., V.L. Trudeau, and T.W. Moon, *Predicting the environmental impact of nanosilver.* Environmental Toxicology and Pharmacology, 2014. **38**(3): p. 861-873.

4. Du, J., et al., *A review on silver nanoparticles-induced ecotoxicity and the underlying toxicity mechanisms.* Regulatory Toxicology and Pharmacology, 2018. **98**: p. 231-239.

5. Syafiuddin, A., et al., *Silver Nanoparticles in the Water Environment in Malaysia: Inspection, characterization, removal, modeling, and future perspective.* Scientific reports, 2018. **8**(1): p. 986-15.

6. Lekamge, S., et al., *The toxicity of silver nanoparticles (AgNPs) to three freshwater invertebrates with different life strategies: Hydra vulgaris, Daphnia carinata, and Paratya australiensis.* Frontiers in Environmental Science, 2018. **6**: p. 152.

7. Azimzada, A., N. Tufenkji, and K.J. Wilkinson, *Transformations of silver nanoparticles in wastewater effluents: links to Ag bioavailability.* Environmental Science: Nano, 2017. **4**(6): p. 1339-1349.

8. Jacobson, A.R., et al., *Environmental factors determining the trace-level sorption of silver and thallium to soils.* Science of the total environment, 2005. **345**(1-3): p. 191-205.

9. Cantuaria, M.L., et al., *Adsorption of silver from aqueous solution onto pre-treated bentonite clay: complete batch system evaluation.* Journal of cleaner production, 2016. **112**: p. 1112-1121.

10. Schluesener, J.K. and H.J. Schluesener, *Nanosilver: application and novel aspects of toxicology.* Archives of Toxicology, 2013. **87**(4): p. 569-576.

11. Sohn, E.K., et al., *Aquatic toxicity comparison of silver nanoparticles and silver nanowires.* BioMed research international, 2015. **2015**.

12. Syafiuddin, A., et al., *A Review of Silver Nanoparticles: Research Trends, Global Consumption, Synthesis, Properties, and Future Challenges: A Review of Silver Nanoparticles.* Journal of the Chinese Chemical Society, 2017. **64**(7): p. 732-756.

13. Zhou, Y., et al., *Biochar-supported zerovalent iron reclaims silver from aqueous solution to form antimicrobial nanocomposite.* Chemosphere, 2014. **117**: p. 801-805.

14. Fewtrell, L., *Silver: water disinfection and toxicity.* Aberystwyth University, Aberystwyth, 2014.

15. NHMRC, N., *Australian drinking water guidelines.* Commonwealth of Australia, 2011.

16. Hamilton, R.F., et al., *Modification of nano-silver bioactivity by adsorption on carbon nanotubes and graphene oxide.* Inhalation Toxicology, 2018. **30**(11-12): p. 429-438.

17. Voelker, D., et al., *Approach on environmental risk assessment of nanosilver released from textiles.* Environmental Research, 2015. **140**: p. 661-672.

18. Zhang, W., B. Xiao, and T. Fang, *Chemical transformation of silver nanoparticles in aquatic environments: Mechanism, morphology and toxicity.* Chemosphere, 2018. **191**: p. 324-334.

19. Ghassabzadeh, H., et al., *Adsorption of Ag, Cu and Hg from aqueous solutions using expanded perlite.* Journal of Hazardous Materials, 2010. **177**(1): p. 950-955.

20. Wang, Y., P. Westerhoff, and K.D. Hristovski, *Fate and biological effects of silver, titanium dioxide, and C 60 (fullerene) nanomaterials during simulated wastewater treatment processes.* Journal of Hazardous Materials, 2012. **201**: p. 16-22.

21. Zhang, W., et al., *Fate and toxicity of silver nanoparticles in freshwater from laboratory to realistic environments: a review.* Environmental Science and Pollution Research, 2019. **26**(8): p. 7390-7404.

22. Islam, M.A., M.V. Jacob, and E. Antunes, *A critical review on silver nanoparticles: From synthesis and applications to its mitigation through low-cost adsorption by biochar.* Journal of Environmental Management, 2021. **281**: p. 111918.

23. Tomczyk, A., et al., *Purification of Aqueous Media by Biochars: Feedstock Type Effect on Silver Nanoparticles Removal.* Molecules (Basel, Switzerland), 2020. **25**(12): p. 2930.

24. Liu, W.-J., H. Jiang, and H.-Q. Yu, *Development of Biochar-Based Functional Materials: Toward a Sustainable Platform Carbon Material.* Chemical Reviews, 2015. **115**(22): p. 12251-12285.

25. Guedes, R.E., A.S. Luna, and A.R. Torres, *Operating parameters for bio-oil production in biomass pyrolysis: A review.* Journal of Analytical and Applied Pyrolysis, 2018. **129**: p. 134-149.

26. Dada, T.K., et al., *A review on catalytic pyrolysis for high-quality bio-oil production from biomass.* Biomass Conversion and Biorefinery, 2021: p. 1-20.

27. Song, C., et al., *Thermochemical liquefaction of agricultural and forestry wastes into biofuels and chemicals from circular economy perspectives.* Science of The Total Environment, 2020: p. 141972.

28. Bioenergy, I., *Waste to Energy: Summary and Conclusions from the IEA Bioenergy ExCo71 Workshop.* 2014. **IEA Bioenergy: ExCo:2014:03**(IEA Bioenergy: ExCo:2014:03).

29. Oćwieja, M., et al., *Silver particle monolayers — Formation, stability, applications.* Advances in Colloid and Interface Science, 2015. **222**: p. 530-563.

30. Pulit-Prociak, J., et al., *Nanosilver products and toxicity.* Environmental Chemistry Letters, 2015. **13**(1): p. 59-68.

31. Suresh, A.K., et al., *Cytotoxicity Induced by Engineered Silver Nanocrystallites Is Dependent on Surface Coatings and Cell Types.* Langmuir, 2012. **28**(5): p. 2727-2735.

32. Calderón-Jiménez, B., et al., *Silver Nanoparticles: Technological Advances, Societal Impacts, and Metrological Challenges.* Frontiers in chemistry, 2017. **5**: p. 6.

33. Wang, S., et al., *Pyrogenic temperature affects the particle size of biochar-supported nanoscaled zero valent iron (nZVI) and its silver removal capacity.* Chemical Speciation & Bioavailability, 2017. **29**(1): p. 179-185.

34. Marambio-Jones, C. and E.M.V. Hoek, *A review of the antibacterial effects of silver nanomaterials and potential implications for human health and the environment.* Journal of Nanoparticle Research, 2010. **12**(5): p. 1531-1551.

35. Dumont, E., et al., *Nano silver and nano zinc-oxide in surface waters – Exposure estimation for Europe at high spatial and temporal resolution.* Environmental Pollution, 2015. **196**: p. 341-349.

36. Wimmer, A., et al., *Sampling and pre-treatment effects on the quantification of (nano)silver and selected trace elements in surface water - Application in a Dutch case study.* Science of the Total Environment, 2019. **663**: p. 154-161.

37. Jeon, C., *Adsorption behavior of silver ions from industrial wastewater onto immobilized crab shell beads.* Journal of Industrial and Engineering Chemistry, 2015. **32**: p. 195-200.

38. Hoque, M.E., et al., *Detection and characterization of silver nanoparticles in aqueous matrices using asymmetric-flow field flow fractionation with inductively coupled plasma mass spectrometry.* Journal of Chromatography A, 2012. **1233**: p. 109-115.

39. Li, L., et al., *Quantification of nanoscale silver particles removal and release from municipal wastewater treatment plants in Germany.* Environmental science & technology, 2013. **47**(13): p. 7317-7323.

40. Ma, R., et al., *Fate of zinc oxide and silver nanoparticles in a pilot wastewater treatment plant and in processed biosolids.* Environmental science & technology, 2014. **48**(1): p. 104-112.

41. Zhang, C., et al., *Governing factors affecting the impacts of silver nanoparticles on wastewater treatment.* Science of the Total Environment, 2016. **572**: p. 852-873.

42. Alizadeh, S., S. Ghoshal, and Y. Comeau, *Fate and inhibitory effect of silver nanoparticles in high rate moving bed biofilm reactors.* Science of the Total Environment, 2019. **647**: p. 1199-1210.

43. Syafiuddin, A., et al., *Removal of Silver Nanoparticles from Water Environment: Experimental, Mathematical Formulation, and Cost Analysis.* Water, Air, & Soil Pollution, 2019. **230**(5): p. 1-15.

44. Wang, S., et al., *Fate and transformation of nanoparticles (NPs) in municipal wastewater treatment systems and effects of NPs on the biological treatment of wastewater: a review.* 2017. **7**(59): p. 3765-3775.

45. Barker, L., et al., *Effects of short-and long-term exposure of silver nanoparticles and silver ions to Nitrosomonas europaea biofilms and planktonic cells.* Chemosphere, 2018. **206**: p. 606-614.

46. Sim, J.H., et al., *Comparison of adsorptive features between silver ion and silver nanoparticles on nanoporous materials.* Journal of Industrial and Engineering Chemistry, 2014. **20**(5): p. 2864-2869.

47. Mohan, D., et al., *Organic and inorganic contaminants removal from water with biochar, a renewable, low cost and sustainable adsorbent – A critical review.* Bioresource Technology, 2014. **160**: p. 191-202.

48. Jeon, C., *Adsorption of silver ions from industrial wastewater using waste coffee grounds.* Korean Journal of Chemical Engineering, 2017. **34**(2): p. 384-391.

49. Song, X., et al., *Surface activated carbon nanospheres for fast adsorption of silver ions from aqueous solutions.* Journal of Hazardous Materials, 2011. **194**: p. 162-168.

50. Antunes, E., et al., *Silver removal from aqueous solution by biochar produced from biosolids via microwave pyrolysis.* Journal of Environmental Management, 2017. **203**(Pt 1): p. 264-272.

51. Alandis, N.M., et al., *Adsorptive Applications of Montmorillonite Clay for the Removal of Ag(I) and Cu(II) from Aqueous Medium.* Journal of Chemistry, 2019. **2019**: p. 1-7.

52. Yao, Y., et al., *Engineered biochar from biofuel residue: characterization and its silver removal potential.* ACS applied materials & interfaces, 2015. **7**(19): p. 10634-10640.

53. Chen, H., A. Xie, and S. You, *A Review: Advances on Absorption of Heavy Metals in the Waste Water by Biochar.* IOP Conference Series: Materials Science and Engineering, 2018. **301**: p. 12160.

54. Wijnhoven, S.W.P., et al., *Nano-silver - a review of available data and knowledge gaps in human and environmental risk assessment.* Nanotoxicology, 2009. **3**(2): p. 109-138.

55. Lansdown, A.B.G., *A Pharmacological and Toxicological Profile of Silver as an Antimicrobial Agent in Medical Devices.* Advances in pharmacological sciences, 2010. **2010**: p. 910686-16.

56. Liu, J. and G. Jiang, *Silver nanoparticles in the environment*. 2015 ed. 2015, S.l.: Springer.

57. León-Silva, S., F. Fernández-Luqueño, and F. López-Valdez, *Silver Nanoparticles (AgNP) in the Environment: a Review of Potential Risks on Human and Environmental Health.* Water, Air, & Soil Pollution, 2016. **227**(9): p. 1-20.

58. Dell'Aglio, M., et al., *Collinear double pulse laser ablation in water for the production of silver nanoparticles.* Physical chemistry chemical physics : PCCP, 2013. **15**(48): p. 2868-2875.

59. Haider, A. and I.-K. Kang, *Preparation of Silver Nanoparticles and Their Industrial and Biomedical Applications: A Comprehensive Review.* Advances in Materials Science and Engineering, 2015. **2015**: p. 1-16.

60. Natsuki, J., T. Natsuki, and Y. Hashimoto, *A review of silver nanoparticles: synthesis methods, properties and applications.* Int. J. Mater. Sci. Appl, 2015. **4**(5): p. 325-332.

61. Mafuné, F., et al., *Formation and Size Control of Silver Nanoparticles by Laser Ablation in Aqueous Solution.* The Journal of Physical Chemistry B, 2000. **104**(39): p. 9111-9117.

62. Shenashen, M.A., S.A. El-Safty, and E.A. Elshehy, *Synthesis, Morphological Control, and Properties of Silver Nanoparticles in Potential Applications.* Particle & Particle Systems Characterization, 2014. **31**(3): p. 293-316.

63. Lee, K.H., S.C. Rah, and S.-G. Kim, *Formation of monodisperse silver nanoparticles in poly(vinylpyrrollidone) matrix using spray pyrolysis.* Journal of Sol-Gel Science and Technology, 2008. **45**(2): p. 187-193.

64. Kim, H.-S., K.-H. Lee, and S.-G. Kim, *Growth of Monodisperse Silver Nanoparticles in Polymer Matrix by Spray Pyrolysis.* Aerosol science and technology, 2006. **40**(7): p. 536-544.

65. Pingali, K.C., D.A. Rockstraw, and S. Deng, *Silver Nanoparticles from Ultrasonic Spray Pyrolysis of Aqueous Silver Nitrate.* Aerosol science and technology, 2005. **39**(10): p. 1010-1014.

66. Hannemann, S., et al., *Electron microscopy and EXAFS studies on oxide-supported gold–silver nanoparticles prepared by flame spray pyrolysis.* Applied surface science, 2006. **252**(22): p. 7862-7873.

67. Siegel, J., et al., *Progressive approach for metal nanoparticle synthesis.* Materials Letters, 2012. **89**: p. 47-50.

68. Antunes, E.M.D.S., J.M.C. Da Silva, and A.L.C. Lagoa, *Process for nanomaterial synthesis from the preparation and detonation of an emulsion, products and emulsions thereof*. 2015, Google Patents.

69. Lee, S. and B.-H. Jun, *Silver Nanoparticles: Synthesis and Application for Nanomedicine.* International journal of molecular sciences, 2019. **20**(4): p. 865.

70. Verma, P. and S.K. Maheshwari, *Applications of Silver nanoparticles in diverse sectors.* International Journal of Nano Dimension, 2019. **10**(1): p. 18-36.

71. Patil, R.S., et al., *One-pot synthesis of PVA-capped silver nanoparticles their characterization and biomedical application.* Advances in natural sciences. Nanoscience and nanotechnology, 2012. **3**(1): p. 015013.

72. McGillicuddy, E., et al., *Silver nanoparticles in the environment: Sources, detection and ecotoxicology.* Science of the Total Environment, 2017. **575**: p. 231-246.

73. Janardhanan, R., et al., *Synthesis and surface chemistry of nano silver particles.* Polyhedron, 2009. **28**(12): p. 2522-2530.

74. Kharissova, O.V., et al., *The greener synthesis of nanoparticles.* Trends in biotechnology (Regular ed.), 2013. **31**(4): p. 240-248.

75. Gamboa, S., E. Rojas, and V. Martínez, *Synthesis and characterization of silver nanoparticles and their application as an antibacterial agent.* Int J Biosen Bioelectron, 2019. **5**(5): p. 166-173.

76. Sampaio, S. and J.C. Viana, *Production of silver nanoparticles by green synthesis using artichoke (Cynara scolymus L.) aqueous extract and measurement of their electrical conductivity.* Advances in natural sciences. Nanoscience and nanotechnology, 2018. **9**(4): p. 45002.

77. Panáček, A., et al., *Silver Colloid Nanoparticles: Synthesis, Characterization, and Their Antibacterial Activity.* The Journal of Physical Chemistry B, 2006. **110**(33): p. 16248-16253.

78. Zhang, X.-F., et al., *Silver Nanoparticles: Synthesis, Characterization, Properties, Applications, and Therapeutic Approaches.* International journal of molecular sciences, 2016. **17**(9): p. 1534.

79. Beyene, H.D., et al., *Synthesis paradigm and applications of silver nanoparticles (AgNPs), a review.* Sustainable Materials and Technologies, 2017. **13**: p. 18-23.

80. Bélteky, P., et al., *Silver nanoparticles: aggregation behavior in biorelevant conditions and its impact on biological activity.* International journal of nanomedicine, 2019. **14**: p. 667-687.

81. Hu, M.Z., et al., *A novel thermal electrochemical synthesis method for production of stable colloids of "naked" metal (Ag) nanocrystals.* Materials Science & Engineering C, 2009. **29**(3): p. 726-736.

82. Yin, B., et al., *Electrochemical Synthesis of Silver Nanoparticles under Protection of Poly(N-vinylpyrrolidone).* The Journal of Physical Chemistry B, 2003. **107**(34): p. 8898-8904.

83. Courrol, L.C., F.R. de Oliveira Silva, and L. Gomes, *A simple method to synthesize silver nanoparticles by photo-reduction.* Colloids and Surfaces A: Physicochemical and Engineering Aspects, 2007. **305**(1): p. 54-57.

84. Purushotham, E., et al., *Preparation and characterization of silver nano particles.* Indian Journal of Physics, 2014. **88**(2): p. 157-163.

85. Rak, M.J., T. Friščić, and A. Moores, *One-step, solvent-free mechanosynthesis of silver nanoparticle-infused lignin composites for use as highly active multidrug resistant antibacterial filters.* RSC advances, 2016. **6**(63): p. 58365-58370.

86. Baláž, M., et al., *Bio-mechanochemical synthesis of silver nanoparticles with antibacterial activity.* Advanced powder technology : the international journal of the Society of Powder Technology, Japan, 2017. **28**(12): p. 3307-3312.

87. Tsuji, T., et al., *Preparation of silver nanoparticles by laser ablation in solution: influence of laser wavelength on particle size.* Applied surface science, 2002. **202**(1-2): p. 80-85.

88. Pyatenko, A., et al., *Synthesis of silver nanoparticles by laser ablation in pure water.* Applied physics. A, Materials science & processing, 2004. **79**(4-6): p. 803-806.

89. Xue, B., et al., *Towards high quality triangular silver nanoprisms: improved synthesis, six-tip based hot spots and ultra-high local surface plasmon resonance sensitivity.* Nanoscale, 2015. **7**(17): p. 8048-8057.

90. Elfassy, E., Y. Mastai, and A. Salomon, *Cysteine sensing by plasmons of silver nanocubes.* Journal of solid state chemistry, 2016. **241**: p. 110-114.

91. Hu, Z.-S., et al., *Align Ag Nanorods via Oxidation Reduction Growth Using RF-Sputtering.* Journal of nanomaterials, 2012. **2012**: p. 1-6.

92. Yin, H., et al., *Large-scale and size-controlled synthesis of silver nanoparticles under microwave irradiation.* Materials chemistry and Physics, 2004. **83**(1): p. 66-70.

93. Roy, E., et al., *Shape effect on the fabrication of imprinted nanoparticles: Comparison between spherical-, rod-, hexagonal-, and flower-shaped nanoparticles.* Chemical engineering journal (Lausanne, Switzerland : 1996), 2017. **321**: p. 195-206.

94. Murphy, C.J. and N.R. Jana, *Controlling the Aspect Ratio of Inorganic Nanorods and Nanowires.* Advanced materials (Weinheim), 2002. **14**(1): p. 80-82.

95. Alsammarraie, F.K., et al., *Green synthesis of silver nanoparticles using turmeric extracts and investigation of their antibacterial activities.* Colloids and surfaces, B, Biointerfaces, 2018. **171**: p. 398-405.

96. Pilaquinga, F., et al., *Green synthesis of silver nanoparticles using Solanum mammosum L. (Solanaceae) fruit extract and their larvicidal activity against Aedes aegypti L. (Diptera: Culicidae).* PloS one, 2019. **14**(10): p. e0224109.

97. Bollella, P., et al., *Green synthesis and characterization of gold and silver nanoparticles and their application for development of a third generation lactose biosensor*. Electroanalysis, 2017. **29**(1): p. 77-86.

98. Kahrilas, G.A., et al., *Microwave-assisted green synthesis of silver nanoparticles using orange peel extract.* ACS Sustainable Chemistry & Engineering, 2014. **2**(3): p. 367-376.

99. Bagherzade, G., M.M. Tavakoli, and M.H. Namaei, *Green synthesis of silver nanoparticles using aqueous extract of saffron (Crocus sativus L.) wastages and its antibacterial activity against six bacteria.* Asian Pacific journal of tropical biomedicine, 2017. **7**(3): p. 227-233.

100. Pugazhenthiran, N., et al., *Microbial synthesis of silver nanoparticles by Bacillus sp.* Journal of Nanoparticle Research, 2009. **11**(7): p. 1811.

101. Balaji, D., et al., *Extracellular biosynthesis of functionalized silver nanoparticles by strains of Cladosporium cladosporioides fungus.* Colloids and surfaces B: biointerfaces, 2009. **68**(1): p. 88-92.

102. Vaidyanathan, R., et al., *Enhanced silver nanoparticle synthesis by optimization of nitrate reductase activity.* Colloids and surfaces B: Biointerfaces, 2010. **75**(1): p. 335-341.

103. Loiseau, A., et al., *Silver-Based Plasmonic Nanoparticles for and Their Use in Biosensing.* Biosensors (Basel), 2019. **9**(2): p. 78.

104. Toropov, N.A., N.B. Leonov, and T.A. Vartanyan, *Influence of Silver Nanoparticles Crystallinity on Localized Surface Plasmons Dephasing Times.* physica status solidi (b), 2018. **255**(3): p. 1700174-n/a.

105. Tanvi, et al., *Effect of the crystallinity of silver nanoparticles on surface plasmon resonance induced enhancement of effective absorption cross-section of dyes.* Journal of applied physics, 2015. **117**(8): p. 083111.

106. Harjono and Y. Yulizar, *Morphological and Dimensional Properties of Colloidal Silver Nanoparticles Prepared under Microwave Irradiation.* Advanced materials research, 2015. **1101**: p. 138-143.

107. Varadavenkatesan, T., R. Vinayagam, and R. Selvaraj, *Structural characterization of silver nanoparticles phyto-mediated by a plant waste, seed hull of Vigna mungo and their biological applications.* Journal of molecular structure, 2017. **1147**: p. 629-635.

108. Jang, E.-Y., et al., *Improved biosynthesis of silver nanoparticles using keratinase from Stenotrophomonas maltophilia R13: reaction optimization, structural characterization, and biomedical activity.* Bioprocess and biosystems engineering, 2018. **41**(3): p. 381-393.

109. Khan, S.S., A. Mukherjee, and N. Chandrasekaran, *Studies on interaction of colloidal silver nanoparticles (SNPs) with five different bacterial species.* Colloids and surfaces, B, Biointerfaces, 2011. **87**(1): p. 129-138.

110. Singh, S., A. Bharti, and V.K. Meena, *Structural, thermal, zeta potential and electrical properties of disaccharide reduced silver nanoparticles.* Journal of materials science. Materials in electronics, 2014. **25**(9): p. 3747-3752.

111. Shameli, K., et al., *Synthesis and characterization of polyethylene glycol mediated silver nanoparticles by the green method.* International journal of molecular sciences, 2012. **13**(6): p. 6639-6650.

112. Ajitha, B., et al., *Role of capping agents in controlling silver nanoparticles size, antibacterial activity and potential application as optical hydrogen peroxide sensor.* RSC advances, 2016. **6**(42): p. 36171-36179.

113. Pourzahedi, L. and M.J. Eckelman, *Comparative life cycle assessment of silver nanoparticle synthesis routes.* Environmental Science: Nano, 2015. **2**(4): p. 361-369.

114. Sintubin, L., W. Verstraete, and N. Boon, *Biologically produced nanosilver: Current state and future perspectives.* Biotechnology and Bioengineering, 2012. **109**(10): p. 2422-2436.

115. Singh, R., et al., *Bacteriagenic silver nanoparticles: synthesis, mechanism, and applications.* Applied Microbiology and Biotechnology, 2015. **99**(11): p. 4579-4593.

116. Galdiero, S., et al., *Silver Nanoparticles as Potential Antiviral Agents.* Molecules (Basel, Switzerland), 2011. **16**(10): p. 8894-8918.

117. Castellano, J.J., et al., *Comparative evaluation of silver-containing antimicrobial dressings and drugs.* International Wound Journal, 2007. **4**(2): p. 114-122.

118. Lara, H.H., et al., *Silver nanoparticles are broad-spectrum bactericidal and virucidal compounds.* Journal of nanobiotechnology, 2011. **9**(1): p. 30-30.

119. Xing, M., et al., *Nanosilver particles in medical applications: synthesis, performance, and toxicity.* International journal of nanomedicine, 2014. **9**: p. 2399.

120. Riau, A.K., et al., *Surface Immobilization of Nano-Silver on Polymeric Medical Devices to Prevent Bacterial Biofilm Formation.* Pathogens (Basel), 2019. **8**(3): p. 93.

121. Sardella, E., et al., *Non-Equilibrium Plasma Processing for the Preparation of Antibacterial Surfaces.* Materials, 2016. **9**(7): p. 515.

122. Shivaram, A., S. Bose, and A. Bandyopadhyay, *Understanding long-term silver release from surface modified porous titanium implants.* Acta biomaterialia, 2017. **58**: p. 550-560.

123. Qureshi, A.T., et al., *Can a novel silver nano coating reduce infections and maintain cell viability in vitro?* Journal of biomaterials applications, 2014. **28**(7): p. 1028-1038.

124. Pokrowiecki, R., et al., *In vitro studies of nanosilver-doped titanium implants for oral and maxillofacial surgery.* International journal of nanomedicine, 2017. **12**: p. 4285-4297.

125. Zhou, G. and W. Wang, *Synthesis of Silver Nanoparticles and their Antiproliferation against Human Lung Cancer Cells In vitro.* Oriental journal of chemistry, 2012. **28**(2): p. 651-655.

126. Blanco, J., et al., *Polyvinyl pyrrolidone-coated silver nanoparticles in a human lung cancer cells: time- and dose-dependent influence over p53 and caspase-3 protein expression and epigenetic effects.* Archives of toxicology, 2016. **91**(2): p. 651-666.

127. Lara, H.H., et al., *PVP-coated silver nanoparticles block the transmission of cell-free and cell-associated HIV-1 in human cervical culture.* Journal of nanobiotechnology, 2010. **8**(1): p. 15.

128. Elechiguerra, J.L., et al., *Interaction of silver nanoparticles with HIV-1.* Journal of nanobiotechnology, 2005. **3**(1): p. 1-10.

129. Lara, H.H., et al., *Use of silver nanoparticles increased inhibition of cell-associated HIV-1 infection by neutralizing antibodies developed against HIV-1 envelope proteins.* Journal of Nanobiotechnology, 2011. **9**(1): p. 1-9.

130. Piddock, L.J.V.P., *The crisis of no new antibiotics—what is the way forward?* Lancet Infectious Diseases, The, 2012. **12**(3): p. 249-253.

131. Levy, S.B. and B. Marshall, *Antibacterial resistance worldwide: causes, challenges and responses.* Nature medicine, 2004. **10**(12 Suppl): p. S122-S129.

132. Davies, J. and D. Davies, *Origins and Evolution of Antibiotic Resistance.* Microbiology and Molecular Biology Reviews, 2010. **74**(3): p. 417-433.

133. Edwards-Jones, V., *The benefits of silver in hygiene, personal care and healthcare.* Letters in applied microbiology, 2009. **49**(2): p. 147-152.

134. Anjum, S. and B. Gupta, *Bioengineering of functional nanosilver nanogels for smart healthcare systems.* Global Challenges, 2018. **2**(10): p. 1800044.

135. Zheng, K., et al., *Antimicrobial silver nanomaterials.* Coordination Chemistry Reviews, 2018. **357**: p. 1-17.

136. Rai, M.K., et al., *Silver nanoparticles: the powerful nanoweapon against multidrug-resistant bacteria.* Journal of applied microbiology, 2012. **112**(5): p. 841-852.

137. S, N.T., et al., *Environmentally benign synthesis of silver nano particles with applications in pollution monitoring.* AIP Conference Proceedings, 2019. **2087**(1).

138. Ravindran, A., P. Chandran, and S.S. Khan, *Biofunctionalized silver nanoparticles: advances and prospects.* Colloids and Surfaces B: Biointerfaces, 2013. **105**: p. 342-352.

139. Li, Y., Y. Wu, and B.S. Ong, *Facile synthesis of silver nanoparticles useful for fabrication of high-conductivity elements for printed electronics.* Journal of the American Chemical Society, 2005. **127**(10): p. 3266-3267.

140. Istiqola, A. and A. Syafiuddin, *A review of silver nanoparticles in food packaging technologies: Regulation, methods, properties, migration, and future challenges.* Journal of the Chinese Chemical Society, 2020. **67**(11): p. 1942-1956.

141. Gaillet, S. and J.-M. Rouanet, *Silver nanoparticles: their potential toxic effects after oral exposure and underlying mechanisms–a review.* Food and Chemical Toxicology, 2015. **77**: p. 58-63.

142. Lin, S., et al., *Silver nanoparticle-alginate composite beads for point-of-use drinking water disinfection.* Water research (Oxford), 2013. **47**(12): p. 3959-3965.

143. Rus, A., V.-D. Leordean, and P. Berce, *Silver Nanoparticles (AgNP) impregnated filters in drinking water disinfection.* MATEC web of conferences, 2017. **137**: p. 7007.

144. Balagna, C., et al., *Antipathogen nanostructured coating for air filters.* Applied Surface Science, 2020. **508**: p. 145283.

145. Edison, T.N.J.I., et al., *Catalytic degradation of organic dyes using green synthesized N-doped carbon supported silver nanoparticles.* Fuel, 2020. **280**: p. 118682.

146. Steffan, M., et al., *Silica supported silver nanoparticles from a silver (I) carboxylate: Highly active catalyst for regioselective hydrogenation.* Catalysis Communications, 2009. **10**(5): p. 437-441.

147. Farkas, J., et al., *Characterization of the effluent from a nanosilver producing washing machine.* Environment International, 2011. **37**(6): p. 1057-1062.

148. Reidy, B., et al., *Mechanisms of Silver Nanoparticle Release, Transformation and Toxicity: A Critical Review of Current Knowledge and Recommendations for Future Studies and Applications.* Materials (Basel, Switzerland), 2013. **6**(6): p. 2295-2350.

149. Geranio, L., M. Heuberger, and B. Nowack, *The Behavior of Silver Nanotextiles during Washing.* Environmental Science & Technology, 2009. **43**(21): p. 8113-8118.

150. Sikder, M., et al., *A rapid approach for measuring silver nanoparticle concentration and dissolution in seawater by UV–Vis.* Science of the Total Environment, 2018. **618**: p. 597-607.

151. Keller, A.A., et al., *Global life cycle releases of engineered nanomaterials.* Journal of Nanoparticle Research, 2013. **15**(6): p. 1-17.

152. Conde-González, J.E., et al., *Adsorption of silver nanoparticles from aqueous solution on copper-based metal organic frameworks (HKUST-1).* Chemosphere, 2016. **150**: p. 659-666.

153. Lowry, G.V., et al., *Transformations of Nanomaterials in the Environment.* Environmental science & technology, 2012. **46**(13): p. 6893-6899.

154. Durán, N., et al., *Silver nanoparticle protein corona and toxicity: a mini-review.* Journal of nanobiotechnology, 2015. **13**(1): p. 55.

155. Bi, Y., et al., *The complex puzzle of dietary silver nanoparticles, mucus and microbiota in the gut.* Journal of Toxicology and Environmental Health, Part B, 2020. **23**(2): p. 69-89.

156. Cedervall, T., et al., *Understanding the nanoparticle–protein corona using methods to quantify exchange rates and affinities of proteins for nanoparticles.* Proceedings of the National Academy of Sciences, 2007. **104**(7): p. 2050-2055.

157. Jiménez-Lamana, J. and V.I. Slaveykova, *Silver nanoparticle behaviour in lake water depends on their surface coating.* Science of the Total Environment, 2016. **573**: p. 946-953.

158. Yongguang Yin Xiaoya Yang Xiaoxia Zhou Weidong Wang Sujuan Yu Jingfu Liu Guibin, J., *Water chemistry controlled aggregation and photo-transformation of silver nanoparticles in environmental waters.* 环境科学学报：英文版, 2015. **34**(8): p. 116-125.

159. Zhang, W., et al., *Influence of dissolved oxygen on aggregation kinetics of citrate-coated silver nanoparticles.* Environmental pollution (1987), 2011. **159**(12): p. 3757-3762.

160. Hou, W.-C., et al., *Sunlight-Driven Reduction of Silver Ions by Natural Organic Matter: Formation and Transformation of Silver Nanoparticles.* Environmental science & technology, 2013. **47**(14): p. 7713-7721.

161. Chen, S.-F. and H. Zhang, *Aggregation kinetics of nanosilver in different water conditions.* Advances in natural sciences. Nanoscience and nanotechnology, 2012. **3**(3): p. 35006.

162. Bae, S., et al., *Effects of water chemistry on aggregation and soil adsorption of silver nanoparticles.* Environmental health and toxicology, 2013. **28**: p. e2013006.

163. Zook, J.M., et al., *Stable nanoparticle aggregates/agglomerates of different sizes and the effect of their size on hemolytic cytotoxicity.* Nanotoxicology, 2010. **5**(4): p. 517-530.

164. Gao, J., et al., *Dispersion and Toxicity of Selected Manufactured Nanomaterials in Natural River Water Samples: Effects of Water Chemical Composition.* Environmental science & technology, 2009. **43**(9): p. 3322-3328.

165. Helmlinger, J., et al., *Silver nanoparticles with different size and shape: equal cytotoxicity, but different antibacterial effects.* RSC advances, 2016. **6**(22): p. 18490-18501.

166. Pal, S., Y.K. Tak, and J.M. Song, *Does the Antibacterial Activity of Silver Nanoparticles Depend on the Shape of the Nanoparticle? A Study of the Gram-Negative Bacterium Escherichia coli.* Applied and environmental microbiology, 2007. **73**(6): p. 1712-1720.

167. Stoehr, L.C., et al., *Shape matters: effects of silver nanospheres and wires on human alveolar epithelial cells.* Particle and fibre toxicology, 2011. **8**(1): p. 36.

168. Kawata, K., M. Osawa, and S. Okabe, *In Vitro Toxicity of Silver Nanoparticles at Noncytotoxic Doses to HepG2 Human Hepatoma Cells.* Environmental Science & Technology, 2009. **43**(15): p. 6046-6051.

169. Lombi, E., et al., *Transformation of four silver/silver chloride nanoparticles during anaerobic treatment of wastewater and post-processing of sewage sludge.* Environmental Pollution, 2013. **176**: p. 193-197.

170. Kent, R.D., J.G. Oser, and P.J. Vikesland, *Controlled Evaluation of Silver Nanoparticle Sulfidation in a Full-Scale Wastewater Treatment Plant.* Environmental Science & Technology, 2014. **48**(15): p. 8564-8572.

171. Liu, J., K.G. Pennell, and R.H. Hurt, *Kinetics and Mechanisms of Nanosilver Oxysulfidation.* Environmental Science & Technology, 2011. **45**(17): p. 7345-7353.

172. Wang, P., et al., *Silver Nanoparticles Entering Soils via the Wastewater–Sludge–Soil Pathway Pose Low Risk to Plants but Elevated Cl Concentrations Increase Ag Bioavailability.* Environmental Science & Technology, 2016. **50**(15): p. 8274-8281.

173. Pradas del Real, A.E., et al., *Fate of Ag-NPs in Sewage Sludge after Application on Agricultural Soils.* Environmental Science & Technology, 2016. **50**(4): p. 1759-1768.

174. Gagné, F., et al., *Toxicity of silver nanoparticles to rainbow trout: A toxicogenomic approach.* Chemosphere, 2012. **89**(5): p. 615-622.

175. Chae, Y.J., et al., *Evaluation of the toxic impact of silver nanoparticles on Japanese medaka (Oryzias latipes).* Aquatic Toxicology, 2009. **94**(4): p. 320-327.

176. Misra, S.K., et al., *The complexity of nanoparticle dissolution and its importance in nanotoxicological studies.* Science of the total environment, 2012. **438**: p. 225-232.

177. Travan, A., et al., *Non-cytotoxic Silver Nanoparticle-Polysaccharide Nanocomposites with Antimicrobial Activity.* Biomacromolecules, 2009. **10**(6): p. 1429-1435.

178. Gonçalves, S.P.c.C., M. Strauss, and D.S.f.T. Martinez, *The Positive Fate of Biochar Addition to Soil in the Degradation of PHBV-Silver Nanoparticle Composites.* Environmental science & technology, 2018. **52**(23): p. 13845-13853.

179. Liu, C., W. Leng, and P.J. Vikesland, *Controlled Evaluation of the Impacts of Surface Coatings on Silver Nanoparticle Dissolution Rates.* Environmental science & technology, 2018. **52**(5): p. 2726-2734.

180. Vazquez-Muñoz, R., et al., *Toxicity of silver nanoparticles in biological systems: Does the complexity of biological systems matter?* Toxicology letters, 2017. **276**: p. 11-20.

181. Taylor, C., et al., *Toxic interactions of different silver forms with freshwater green algae and cyanobacteria and their effects on mechanistic endpoints and the production of extracellular polymeric substances.* Environmental Science: Nano, 2016. **3**(2): p. 396-408.

182. Navarro, E., et al., *Toxicity of Silver Nanoparticles to Chlamydomonas reinhardtii.* Environmental Science & Technology, 2008. **42**(23): p. 8959-8964.

183. Eckelman, M.J. and T.E. Graedel, *Silver Emissions and their Environmental Impacts: A Multilevel Assessment.* Environmental Science & Technology, 2007. **41**(17): p. 6283-6289.

184. Ray, P.C., H. Yu, and P.P. Fu, *Toxicity and Environmental Risks of Nanomaterials: Challenges and Future Needs.* Journal of Environmental Science and Health, Part C, 2009. **27**(1): p. 1-35.

185. Jorge de Souza, T.A., L.R. Rosa Souza, and L.P. Franchi, *Silver nanoparticles: An integrated view of green synthesis methods, transformation in the environment, and toxicity.* Ecotoxicology and environmental safety, 2019. **171**: p. 691-700.

186. Park, M.V.D.Z., et al., *The effect of particle size on the cytotoxicity, inflammation, developmental toxicity and genotoxicity of silver nanoparticles.* Biomaterials, 2011. **32**(36): p. 9810-9817.

187. Sosenkova, L.S. and E.M. Egorova, *The effect of particle size on the toxic action of silver nanoparticles.* Journal of physics. Conference series, 2011. **291**: p. 012027.

188. Luoma, S., *Silver nanotechnologies and the environment: Old problems or new challenges? Washington: 2008.* There is no corresponding record for this reference.[Google Scholar], 2016.

189. Fiorati, A., et al., *Silver Nanoparticles for Water Pollution Monitoring and Treatments: Ecosafety Challenge and Cellulose-Based Hybrids Solution.* Polymers, 2020. **12**(8): p. 1635.

190. Faunce, T. and A. Watal, *Nanosilver and global public health: international regulatory issues.* Nanomedicine, 2010. **5**(4): p. 617-632.

191. Zhang, C., Z. Hu, and B. Deng, *Silver nanoparticles in aquatic environments: Physiochemical behavior and antimicrobial mechanisms.* Water Research, 2016. **88**: p. 403-427.

192. (ANZECC), A.a.N.Z.E.a.C.C., *Australian Water Quality Guidelines for Fresh and Marine Waters*, C. Australian and New Zealand Environment and Conservation Council, Editor. November 1992, Australian and New Zealand Environment and Conservation Council, Canberra.

193. Environment, C.C.o.M.o.t., *Canadian Water Quality Guidelines for the Protection of Aquatic Life*. 2015.

194. Organization, W.H., *Alternative drinking-water disinfectants: bromine, iodine and silver.* 2018.

195. China, M.o.h.o.t.P.s.R.o., *Standards for Drinking Water Quality.* 1985.

196. Organization, W.H., *Guidelines for drinking-water quality by WHO*. 1996.

197. National Institute for Occupational Safety and Health (NIOSH), C.f.D.C.a.P.C., *Health Effects of Occupational Exposure to Silver Nanomaterials*. 2018.

198. Drake, P.L., K.J. Hazelwood, and unav, *Exposure-Related Health Effects of Silver and Silver Compounds: A Review.* The Annals of occupational hygiene, 2005. **49**(7): p. 575.

199. Sass, J., L. Heine, and N. Hwang, *Use of a modified GreenScreen tool to conduct a screening-level comparative hazard assessment of conventional silver and two forms of nanosilver.* Environmental health, 2016. **15**(1): p. 105-105.

200. Agency, U.S.E.P., *State of the Science Literature Review: Everything Nanosilver and More*. 2010.

201. Hardy, A., et al., *Guidance on risk assessment of the application of nanoscience and nanotechnologies in the food and feed chain: Part 1, human and animal health.* EFSA journal, 2018. **16**(7): p. e05327-n/a.

202. (JRC), S.f.P.r.b.t.J.R.C., *NANoREG framework for the safety assessment of nanomaterials*. 2017.

203. Commission, E., *Are silver nanoparticles safe? Implications for health, the environment and microbial resistance.* 2014.

204. Commission, E., *Scientific Committee on Consumer Safety (SCCS) OPINION ON Colloidal Silver (nano) 2018*

205. Australia, F.o.t.E., *Way too little: Our government's failure to regulate nanomaterials in food and agriculture*. 2014.

206. Hou, L., et al., *Removal of silver nanoparticles in simulated wastewater treatment processes and its impact on COD and NH4 reduction.* Chemosphere, 2012. **87**(3): p. 248-252.

207. Kaegi, R., et al., *Fate and transformation of silver nanoparticles in urban wastewater systems.* Water Research, 2013. **47**(12): p. 3866-3877.

208. Carmona, D., et al., *Al-promoted increase of surface area and adsorption capacity in ordered mesoporous silica materials with a cubic structureElectronic supplementary information (ESI) available: XRD, N2 adsorption, STEM analysis and 27Al NMR spectra. See DOI: 10.1039/c1cc15899f.* 2011. **47**(45): p. 12337-12339.

209. Trinh, V.T., et al., *Phosphate Adsorption by Silver Nanoparticles-Loaded Activated Carbon derived from Tea Residue.* Scientific reports, 2020. **10**(1): p. 3634-3634.

210. Akçakal, Ö., M. Şahin, and M. Erdem, *Synthesis and characterization of high-quality activated carbons from hard-shelled agricultural wastes mixture by zinc chloride activation.* Chemical Engineering Communications, 2019. **206**(7): p. 888-897.

211. Rodriguez Correa, C., T. Otto, and A. Kruse, *Influence of the biomass components on the pore formation of activated carbon.* Biomass and Bioenergy, 2017. **97**: p. 53-64.

212. González-García, P., *Activated carbon from lignocellulosics precursors: A review of the synthesis methods, characterization techniques and applications.* Renewable and Sustainable Energy Reviews, 2018. **82**: p. 1393-1414.

213. Yahya, M.A., Z. Al-Qodah, and C.W.Z. Ngah, *Agricultural bio-waste materials as potential sustainable precursors used for activated carbon production: A review.* Renewable and Sustainable Energy Reviews, 2015. **46**: p. 218-235.

214. Rashidi, N.A. and S. Yusup, *A review on recent technological advancement in the activated carbon production from oil palm wastes.* Chemical Engineering Journal, 2017. **314**: p. 277-290.

215. Ioannidou, O. and A. Zabaniotou, *Agricultural residues as precursors for activated carbon production—A review.* Renewable and Sustainable Energy Reviews, 2007. **11**(9): p. 1966-2005.

216. Danish, M. and T. Ahmad, *A review on utilization of wood biomass as a sustainable precursor for activated carbon production and application.* Renewable and Sustainable Energy Reviews, 2018. **87**: p. 1-21.

217. Jain, A., R. Balasubramanian, and M.P. Srinivasan, *Production of high surface area mesoporous activated carbons from waste biomass using hydrogen peroxide-mediated hydrothermal treatment for adsorption applications.* Chemical Engineering Journal, 2015. **273**: p. 622-629.

218. Ahmed, M.B., et al., *Activated carbon preparation from biomass feedstock: Clean production and carbon dioxide adsorption.* Journal of Cleaner Production, 2019. **225**: p. 405-413.

219. Alslaibi, T.M., et al., *A review: production of activated carbon from agricultural byproducts via conventional and microwave heating.* Journal of Chemical Technology & Biotechnology, 2013. **88**(7): p. 1183-1190.

220. Jia, Y. and G.P. Demopoulos, *Adsorption of Silver onto Activated Carbon from Acidic Media: Nitrate and Sulfate Media.* Industrial & Engineering Chemistry Research, 2003. **42**(1): p. 72-79.

221. Seyedhakimi, A., et al., *Exploring relationships between various activations of granular activated carbon on silver and gold adsorption: A kinetic and equilibrium study.* Separation Science and Technology, 2019. **54**(11): p. 1710-1721.

222. Adani, K.G., R.W. Barley, and R.D. Pascoe, *Silver recovery from synthetic photographic and medical X-ray process effluents using activated carbon.* Minerals Engineering, 2005. **18**(13): p. 1269-1276.

223. Gicheva, G. and G. Yordanov, *Removal of citrate-coated silver nanoparticles from aqueous dispersions by using activated carbon.* Colloids and Surfaces A: Physicochemical and Engineering Aspects, 2013. **431**: p. 51-59.

224. Kumar, A. and H. Mohan Jena, *High surface area microporous activated carbons prepared from Fox nut (Euryale ferox) shell by zinc chloride activation.* Applied surface science, 2015. **356**: p. 753-761.

225. Gao, Y., et al., *Preparation of high surface area-activated carbon from lignin of papermaking black liquor by KOH activation for Ni(II) adsorption.* Chemical engineering journal (Lausanne, Switzerland : 1996), 2013. **217**: p. 345-353.

226. Wu, Q.-F. and F.-S. Zhang, *A clean process for activator recovery during activated carbon production from waste biomass.* Fuel, 2012. **94**: p. 426-432.

227. Aniyikaiye, T.E., et al., *Physico-Chemical Analysis of Wastewater Discharge from Selected Paint Industries in Lagos, Nigeria.* International journal of environmental research and public health, 2019. **16**(7): p. 1235.

228. Igbinosa, E.O. and A.I. Okoh, *Impact of discharge wastewater effluents on the physico-chemical qualities of a receiving watershed in a typical rural community.* International Journal of Environment Science and Technology, 2009. **6**(2): p. 175-182.

229. Fito, J., et al., *Physicochemical Properties of the Sugar Industry and Ethanol Distillery Wastewater and Their Impact on the Environment.* Sugar Tech, 2019. **21**(2): p. 265-277.

230. Romero-Cano, L.A., et al., *Amino-functionalized material from a bio-template for silver adsorption: process evaluation in batch and fixed bed.* Journal of Chemical Technology & Biotechnology, 2019. **94**(2): p. 590-599.

231. Lee, S.U., et al., *Selective silver ion adsorption onto mesoporous graphitic carbon nitride.* Carbon, 2015. **95**: p. 58-64.

232. Silva-Medeiros, F.V., et al., *Kinetics and thermodynamics studies of silver ions adsorption onto coconut shell activated carbon.* Environmental Technology, 2016. **37**(24): p. 3087-3093.

233. Shiming Wang Hongling Li Xiaoya Chen Min Yang Yanxing, Q., *Selective adsorption of silver ions from aqueous solution using polystyrene-supported trimercaptotriazine resin*. 2012, Elsevier B.V: Netherlands. p. 2166-2172.

234. Iglesias, M., E. Anticó, and V. Salvadó, *THE CHARACTERISATION OF SILVER SORPTION BY CHELATING RESINS CONTAINING THIOL AND AMINE GROUPS.* Solvent Extraction and Ion Exchange, 2001. **19**(2): p. 315-327.

235. Wang, L., et al., *Recovery of silver (I) using a thiourea-modified chitosan resin*. 2010, Elsevier B.V: Netherlands. p. 577-582.

236. Bhatnagar, A. and M. Sillanpää, *Applications of chitin- and chitosan-derivatives for the detoxification of water and wastewater — A short review.* Advances in Colloid and Interface Science, 2009. **152**(1): p. 26-38.

237. Wang, Z.N., S. Wang, and H. Zhong, *Synthesis of a Novel Hexanedioyl Thiourea Resin and its Adsorption Properties for Ag(I)*. 2012, Trans Tech Publications Ltd: Zurich. p. 1213-1217.

238. Zhang, M., R. Helleur, and Y. Zhang, *Ion-imprinted chitosan gel beads for selective adsorption of Ag+ from aqueous solutions.* Carbohydrate Polymers, 2015. **130**: p. 206-212.

239. Beyki, M.H., et al., *Synthesis, Characterization, and Silver Adsorption Property of Magnetic Cellulose Xanthate from Acidic Solution: Prepared by One Step and Biogenic Approach.* Industrial & Engineering Chemistry Research, 2014. **53**(39): p. 14904-14912.

240. Dong, Z., et al., *Performance and mechanism of selective adsorption of silver to L-cysteine functionalized cellulose microsphere.* Cellulose, 2020. **27**(6): p. 3249-3261.

241. Saman, N., et al., *Silver Adsorption Enhancement from Aqueous and Photographic Waste Solutions by Mercerized Coconut Fiber.* Separation Science and Technology, 2015. **50**(7): p. 937-946.

242. Liu, P., et al., *Cellulose and chitin nanomaterials for capturing silver ions (Ag+) from water via surface adsorption.* Cellulose, 2014. **21**(1): p. 449-461.

243. Sarı, A. and M. Tüzen, *Adsorption of silver from aqueous solution onto raw vermiculite and manganese oxide-modified vermiculite.* Microporous and Mesoporous Materials, 2013. **170**: p. 155-163.

244. Cantuaria, M.L., et al., *Adsorption of silver from aqueous solution onto pre-treated bentonite clay: complete batch system evaluation.* Journal of Cleaner Production, 2016. **112**: p. 1112-1121.

245. Phothitontimongkol, T., et al., *Functionalized hectorite clay mineral for Ag(I) ions extraction from wastewater and preparation of silver nanoparticles supported clay.* Applied Clay Science, 2013. **80-81**: p. 346-350.

246. Sprynskyy, M., et al., *Preparation of AgNPs/saponite nanocomposites without reduction agents and study of its antibacterial activity.* Colloids and Surfaces B: Biointerfaces, 2019. **180**: p. 457-465.

247. Wajima, T., *Synthesis of zeolitic material from green tuff stone cake and its adsorption properties of silver (I) from aqueous solution.* Microporous and Mesoporous Materials, 2016. **233**: p. 154-162.

248. Kwon, G.-J., et al., *Adsorption Characteristics of Ag Nanoparticles on Cellulose Nanofibrils with Different Chemical Compositions.* Polymers, 2020. **12**(1): p. 164.

249. Han, X., et al., *Catalytic conversion of lignocellulosic biomass into hydrocarbons: A mini review.* Catalysis Today, 2019. **319**: p. 2-13.

250. Yaman, S., *Pyrolysis of biomass to produce fuels and chemical feedstocks.* Energy Conversion and Management, 2004. **45**(5): p. 651-671.

251. Zhu, C., et al., *Adsorption Behavior of Cellulose and Its Derivatives toward Ag(I) in Aqueous Medium: An AFM, Spectroscopic, and DFT Study.* Langmuir, 2015. **31**(45): p. 12390-12400.

252. Sun, Y., et al., *Multifunctional iron-biochar composites for the removal of potentially toxic elements, inherent cations, and hetero-chloride from hydraulic fracturing wastewater.* Environment International, 2019. **124**: p. 521-532.

253. Wang, S. and Y. Peng, *Natural zeolites as effective adsorbents in water and wastewater treatment.* Chemical Engineering Journal, 2010. **156**(1): p. 11-24.

254. Iijima, A., *Geology of natural zeolites and zeolitic rocks.* Pure and Applied Chemistry, 1980. **52**(9): p. 2115-2130.

255. Król, M., *Natural vs. Synthetic Zeolites*. 2020, Multidisciplinary Digital Publishing Institute.

256. Ruíz-Baltazar, A. and R. Pérez, *Kinetic Adsorption Study of Silver Nanoparticles on Natural Zeolite: Experimental and Theoretical Models.* Applied Sciences, 2015. **5**(4): p. 1869-1881.

257. Akgül, M., et al., *Removal of silver (I) from aqueous solutions with clinoptilolite.* Microporous and Mesoporous Materials, 2006. **94**(1): p. 99-104.

258. Zhanpeisov, N.U., et al., *Interaction of N2O with Ag+ ion-exchanged zeolites: an FT-IR spectroscopy and quantum chemical ab initio and DFT studies.* Journal of Molecular Catalysis A: Chemical, 2003. **201**(1-2): p. 237-246.

259. Cantuaria, M.L., et al., *Removal and Recovery of Silver by Dynamic Adsorption on Bentonite Clay Using a Fixed-Bed Column System.* Adsorption Science & Technology, 2015. **33**(2): p. 91-103.

260. Uddin, M.K., *A review on the adsorption of heavy metals by clay minerals, with special focus on the past decade.* Chemical Engineering Journal, 2017. **308**: p. 438-462.

261. de Freitas, E.D., et al., *Continuous adsorption of silver and copper by Verde-lodo bentonite in a fixed bed flow-through column.* Journal of Cleaner Production, 2018. **171**: p. 613-621.

262. Srinivasan, R., *Advances in Application of Natural Clay and Its Composites in Removal of Biological, Organic, and Inorganic Contaminants from Drinking Water.* Advances in Materials Science and Engineering, 2011. **2011**: p. 1-17.

263. Lim, S.T., et al., *Mesoporous graphene adsorbents for the removal of toluene and xylene at various concentrations and its reusability.* Scientific reports, 2019. **9**(1): p. 10922-12.

264. Leng, Y., et al., *Removal of antimony(III) from aqueous solution by graphene as an adsorbent.* Chemical Engineering Journal, 2012. **211-212**: p. 406-411.

265. Stoller, M.D., et al., *Graphene-Based Ultracapacitors.* Nano Letters, 2008. **8**(10): p. 3498-3502.

266. Liu, Y., et al., *Understanding the high adsorption-reduction performance of triethanolamine modified graphene oxide for silver ions.* Colloids and Surfaces A: Physicochemical and Engineering Aspects, 2019. **567**: p. 96-103.

267. Ali, I., et al., *Graphene based adsorbents for remediation of noxious pollutants from wastewater.* Environment International, 2019. **127**: p. 160-180.

268. Fang, Z., et al., *Conversion of biological solid waste to graphene-containing biochar for water remediation: A critical review.* Chemical Engineering Journal, 2020: p. 124611.

269. El-Naggar, A., et al., *Biochar application to low fertility soils: A review of current status, and future prospects.* Geoderma, 2019. **337**: p. 536-554.

270. Kan, T., V. Strezov, and T.J. Evans, *Lignocellulosic biomass pyrolysis: A review of product properties and effects of pyrolysis parameters.* Renewable and Sustainable Energy Reviews, 2016. **57**: p. 1126-1140.

271. Hu, X. and M. Gholizadeh, *Biomass pyrolysis: A review of the process development and challenges from initial researches up to the commercialisation stage.* Journal of Energy Chemistry, 2019. **39**: p. 109-143.

272. Wang, S. and J. Wang, *Preparation, modification and environmental application of biochar: A review.* Journal of Cleaner Production, 2019. **227**: p. 1002-1022.

273. Schaffer, S., et al., *A mass- and energy balance-based process modelling study for the pyrolysis of cotton stalks with char utilization for sustainable soil enhancement and carbon storage.* Biomass and Bioenergy, 2019. **120**: p. 281-290.

274. O'Connor, D., et al., *Biochar application for the remediation of heavy metal polluted land: A review of in situ field trials.* Science of the Total Environment, 2018. **619-620**: p. 815-826.

275. Sun, X., et al., *Characterization of 60 types of Chinese biomass waste and resultant biochars in terms of their candidacy for soil application.* GCB Bioenergy, 2017. **9**(9): p. 1423-1435.

276. Pröll, T., et al., *Reduced Local Emissions and Long-term Carbon Storage through Pyrolysis of Agricultural Waste and Application of Pyrolysis Char for Soil Improvement.* Energy Procedia, 2017. **114**: p. 6057-6066.

277. Uras, Ü., et al., *Physico-chemical characterization of biochars from vacuum pyrolysis of South African agricultural wastes for application as soil amendments.* Journal of Analytical and Applied Pyrolysis, 2012. **98**: p. 207-213.

278. Qambrani, N.A., et al., *Biochar properties and eco-friendly applications for climate change mitigation, waste management, and wastewater treatment: A review.* Renewable and Sustainable Energy Reviews, 2017. **79**: p. 255-273.

279. Oliveira, F.R., et al., *Environmental application of biochar: Current status and perspectives.* Bioresource Technology, 2017. **246**: p. 110-122.

280. Antunes, E., et al., *Isotherms, kinetics and mechanism analysis of phosphorus recovery from aqueous solution by calcium-rich biochar produced from biosolids via microwave pyrolysis.* Journal of Environmental Chemical Engineering, 2018. **6**(1): p. 395-403.

281. Shang, G., et al., *Adsorption of hydrogen sulfide by biochars derived from pyrolysis of different agricultural/forestry wastes.* Journal of the Air & Waste Management Association, 2016. **66**(1): p. 8-16.

282. Xie, T., et al., *Characteristics and Applications of Biochar for Environmental Remediation: A Review.* Critical Reviews in Environmental Science and Technology, 2015. **45**(9): p. 939-969.

283. Tan, X., et al., *Application of biochar for the removal of pollutants from aqueous solutions.* Chemosphere, 2015. **125**: p. 70-85.

284. Qian, K., et al., *Recent advances in utilization of biochar.* Renewable and Sustainable Energy Reviews, 2015. **42**: p. 1055-1064.

285. Varjani, S., G. Kumar, and E.R. Rene, *Developments in biochar application for pesticide remediation: Current knowledge and future research directions.* Journal of Environmental Management, 2019. **232**: p. 505-513.

286. Waqas, M., et al., *Development of biochar as fuel and catalyst in energy recovery technologies.* Journal of Cleaner Production, 2018. **188**: p. 477-488.

287. Amin, F.R., et al., *Biochar applications and modern techniques for characterization.* Clean Technologies and Environmental Policy, 2016. **18**(5): p. 1457-1473.

288. Alaya, M.N., B.S. Girgis, and W.E. Mourad, *Activated Carbon from Some Agricultural Wastes Under Action of One-Step Steam Pyrolysis.* Journal of Porous Materials, 2000. **7**(4): p. 509-517.

289. Hu, X. and M. Gholizadeh, *Biomass pyrolysis: A review of the process development and challenges from initial researches up to the commercialisation stage.* Journal of Energy Chemistry, 2019.

290. Li, H., et al., *Mechanisms of metal sorption by biochars: Biochar characteristics and modifications.* Chemosphere, 2017. **178**: p. 466-478.

291. Li, B., et al., *Adsorption of Cd(II) from aqueous solutions by rape straw biochar derived from different modification processes.* Chemosphere, 2017. **175**: p. 332-340.

292. Kołodyńska, D., et al., *Kinetic and adsorptive characterization of biochar in metal ions removal.* Chemical Engineering Journal, 2012. **197**: p. 295-305.

293. Hameed, S., et al., *A review on biomass pyrolysis models: Kinetic, network and mechanistic models.* Biomass and Bioenergy, 2019. **123**: p. 104-122.

294. Babu, B.V., *Biomass pyrolysis: a state-of-the-art review.* Biofuels, Bioproducts and Biorefining, 2008. **2**(5): p. 393-414.

295. Dada, T.K., et al., *Thermo-catalytic co-pyrolysis of ironbark sawdust and plastic waste over strontium loaded hierarchical Y-zeolite.* Journal of Environmental Management, 2021. **299**: p. 113610.

296. Mutsengerere, S., et al., *A review of operating parameters affecting bio-oil yield in microwave pyrolysis of lignocellulosic biomass.* Renewable and Sustainable Energy Reviews, 2019. **104**: p. 328-336.

297. Mattos, C., et al., *Biocidal applications trends of bio-oils from pyrolysis: Characterization of several conditions and biomass, a review.* Journal of Analytical and Applied Pyrolysis, 2019. **139**: p. 1-12.

298. Hassan, H., J. Lim, and B. Hameed, *Recent progress on biomass co-pyrolysis conversion into high-quality bio-oil.* Bioresource technology, 2016. **221**: p. 645-655.

299. Bridgwater, T., *Challenges and opportunities in fast pyrolysis of biomass: Part I.* Johnson Matthey Technology Review, 2018. **62**(1): p. 118-130.

300. Chhiti, Y. and M. Kemiha, *Thermal conversion of biomass, pyrolysis and gasification.* International Journal of Engineering and Science (IJES), 2013. **2**(3): p. 75-85.

301. Antunes, E., et al., *Biochar produced from biosolids using a single-mode microwave: Characterisation and its potential for phosphorus removal.* Journal of environmental management, 2017. **196**: p. 119-126.

302. Bridgwater, A.V. and G.V.C. Peacocke, *Fast pyrolysis processes for biomass.* Renewable and Sustainable Energy Reviews, 2000. **4**(1): p. 1-73.

303. Cheng, X. and B. Wang, *Influence of organic composition of biomass waste on biochar yield, calorific value, and specific surface area.* Journal of renewable and sustainable energy, 2018. **10**(1): p. 013109.

304. Antunes, E., et al., *Application of biochar for emerging contaminant mitigation*. 2021, Elsevier.

305. Antunes, E., et al., *Silver removal from aqueous solution by biochar produced from biosolids via microwave pyrolysis.* J Environ Manage, 2017. **203**(Pt 1): p. 264-272.

306. Ronsse, F., et al., *Production and characterization of slow pyrolysis biochar: influence of feedstock type and pyrolysis conditions.* GCB Bioenergy, 2013. **5**(2): p. 104-115.

307. Varsha, S., et al., *Co-pyrolysis of microalgae and municipal solid waste: A thermogravimetric study to discern synergy during co-pyrolysis process.* Journal of the Energy Institute, 2021. **94**: p. 29-38.

308. Chaiwong, K., et al., *Biochar production from freshwater algae by slow pyrolysis.* Maejo international journal of science and technology, 2012. **6**(2): p. 186-195.

309. Cho, D.-W., et al., *Fabrication of magnetic biochar as a treatment medium for As(V) via pyrolysis of FeCl 3 -pretreated spent coffee ground.* Environmental pollution (1987), 2017. **229**: p. 942-949.

310. Vuppaladadiyam, A.K., et al., *Influence of microalgae on synergism during co-pyrolysis with organic waste biomass: A thermogravimetric and kinetic analysis.* Renewable energy, 2021. **167**: p. 42-55.

311. Gupta, G.K. and M.K. Mondal, *Kinetics and thermodynamic analysis of maize cob pyrolysis for its bioenergy potential using thermogravimetric analyzer.* Journal of Thermal Analysis and Calorimetry, 2019. **137**(4): p. 1431-1441.

312. Doyle, C., *Estimating isothermal life from thermogravimetric data.* Journal of Applied Polymer Science, 1962. **6**(24): p. 639-642.

313. Yuan, X., et al., *Cattle manure pyrolysis process: kinetic and thermodynamic analysis with isoconversional methods.* Renewable Energy, 2017. **107**: p. 489-496.

314. Bardestani, R., G.S. Patience, and S. Kaliaguine, *Experimental methods in chemical engineering: specific surface area and pore size distribution measurements—BET, BJH, and DFT.* The Canadian Journal of Chemical Engineering, 2019. **97**(11): p. 2781-2791.

315. Meng, F., et al., *The contribution of oxygen-containing functional groups to the gas-phase adsorption of volatile organic compounds with different polarities onto lignin-derived activated carbon fibers.* Environmental Science and Pollution Research, 2019. **26**(7): p. 7195-7204.

316. Kumar, R., et al., *Bio-oil upgrading with catalytic pyrolysis of biomass using Copper/zeolite-Nickel/zeolite and Copper-Nickel/zeolite catalysts.* Bioresour Technol, 2019. **279**: p. 404-409.

317. Wang, S., et al., *Lignocellulosic biomass pyrolysis mechanism: a state-of-the-art review.* Progress in Energy and Combustion Science, 2017. **62**: p. 33-86.

318. Roberts, D.A., et al., *Biochar from commercially cultivated seaweed for soil amelioration.* Scientific Reports, 2015. **5**(1): p. 1-6.

319. Liu, W.-J., et al., *Fates of chemical elements in biomass during its pyrolysis.* Chemical reviews, 2017. **117**(9): p. 6367-6398.

320. Kabir, G. and B. Hameed, *Recent progress on catalytic pyrolysis of lignocellulosic biomass to high-grade bio-oil and bio-chemicals.* Renewable and Sustainable Energy Reviews, 2017. **70**: p. 945-967.

321. Kebelmann, K., et al., *Thermo-chemical behaviour and chemical product formation from Polar seaweeds during intermediate pyrolysis.* Journal of analytical and applied pyrolysis, 2013. **104**: p. 131-138.

322. Li, X., V. Strezov, and T. Kan, *Energy recovery potential analysis of spent coffee grounds pyrolysis products.* Journal of Analytical and Applied Pyrolysis, 2014. **110**: p. 79-87.

323. Bach, Q.V. and W.H. Chen, *Pyrolysis characteristics and kinetics of microalgae via thermogravimetric analysis (TGA): A state-of-the-art review.* Bioresour Technol, 2017. **246**: p. 88-100.

324. Campos-Vega, R., et al., *Spent coffee grounds: A review on current research and future prospects.* Trends in Food Science & Technology, 2015. **45**(1): p. 24-36.

325. Yang, W., et al., *Investigation of holocellulose-lignin interactions during pyrolysis of wood meal by TGA-FTIR.* Biomass Conversion and Biorefinery, 2021: p. 1-10.

326. Rodriguez, C. and G. Gordillo, *Adiabatic gasification and pyrolysis of coffee husk using air-steam for partial oxidation.* Journal of Combustion, 2011.

327. Pujol, D., et al., *The chemical composition of exhausted coffee waste.* Industrial Crops and Products, 2013. **50**: p. 423-429.

328. Bu, Q., et al., *Renewable phenols production by catalytic microwave pyrolysis of Douglas fir sawdust pellets with activated carbon catalysts.* Bioresource technology, 2013. **142**: p. 546-552.

329. Izhar, S., et al., *Hydrodenitrogenation of fast pyrolysis bio-oil derived from sewage sludge on NiMo/Al2O3 sulfide catalyst.* Fuel processing technology, 2012. **101**: p. 10-15.

330. Verma, R., et al., *Catalytic pyrolysis of ulva lactuca macroalgae: Effects of mono and bimetallic catalysts and reaction parameters on bio-oil up-gradation.* Bioresource Technology, 2021. **324**: p. 124594.

331. Milosavljevic, I. and E.M. Suuberg, *Cellulose thermal decomposition kinetics: global mass loss kinetics.* Industrial & Engineering Chemistry Research, 1995. **34**(4): p. 1081-1091.

332. Khan, M.I., et al., *The pyrolysis kinetics of the conversion of Malaysian kaolin to metakaolin.* Applied Clay Science, 2017. **146**: p. 152-161.

333. Mishra, G., J. Kumar, and T. Bhaskar, *Kinetic studies on the pyrolysis of pinewood.* Bioresource Technology, 2015. **182**: p. 282-288.

334. Pattanayak, S., et al., *Experimental investigation on pyrolysis kinetics, reaction mechanisms and thermodynamic parameters of biomass and tar in N2 atmosphere.* Sustainable Energy Technologies and Assessments, 2021. **48**: p. 101632.

335. He, Q., et al., *Effect of torrefaction on pinewood pyrolysis kinetics and thermal behavior using thermogravimetric analysis.* Bioresource technology, 2019. **280**: p. 104-111.

336. Xu, Y. and B. Chen, *Investigation of thermodynamic parameters in the pyrolysis conversion of biomass and manure to biochars using thermogravimetric analysis.* Bioresource technology, 2013. **146**: p. 485-493.

337. Loy, A.C.M., et al., *Thermogravimetric kinetic modelling of in-situ catalytic pyrolytic conversion of rice husk to bioenergy using rice hull ash catalyst.* Bioresource technology, 2018. **261**: p. 213-222.

338. Mallick, D., et al., *Discernment of synergism in pyrolysis of biomass blends using thermogravimetric analysis.* Bioresource technology, 2018. **261**: p. 294-305.

339. Kumar, R., et al., *Lignocellulose biomass pyrolysis for bio-oil production: A review of biomass pre-treatment methods for production of drop-in fuels.* Renewable and Sustainable Energy Reviews, 2020. **123**.

340. Aboulkas, A., et al., *Valorization of algal waste via pyrolysis in a fixed-bed reactor: production and characterization of bio-oil and bio-char.* Bioresource technology, 2017. **243**: p. 400-408.

341. Zhang, W., et al., *Pb (II) and Cr (VI) sorption by biochars pyrolyzed from the municipal wastewater sludge under different heating conditions.* Bioresource technology, 2013. **147**: p. 545-552.

342. Chen, J., D. Fang, and F. Duan, *Pore characteristics and fractal properties of biochar obtained from the pyrolysis of coarse wood in a fluidized-bed reactor.* Applied Energy, 2018. **218**: p. 54-65.

343. Tala, W. and S. Chantara, *Use of spent coffee ground biochar as ambient PAHs sorbent and novel extraction method for GC-MS analysis.* Environmental Science and Pollution Research, 2019. **26**(13): p. 13025-13040.

344. Zhao, B., et al., *Effect of pyrolysis temperature, heating rate, and residence time on rapeseed stem derived biochar.* Journal of Cleaner Production, 2018. **174**: p. 977-987.

345. Peng, H., et al., *Reduction of silver ions to silver nanoparticles by biomass and biochar: Mechanisms and critical factors.* Science of The Total Environment, 2021. **779**: p. 146326.

346. Bird, M.I., et al., *Algal biochar – production and properties.* Bioresource Technology, 2011. **102**(2): p. 1886-1891.

347. Cha, J.S., et al., *Production and utilization of biochar: A review.* Journal of Industrial and Engineering Chemistry, 2016. **40**: p. 1-15.

348. Chwastowski, J., D. Bradło, and W. Żukowski, *Adsorption of Cadmium, Manganese and Lead Ions from Aqueous Solutions Using Spent Coffee Grounds and Biochar Produced by Its Pyrolysis in the Fluidized Bed Reactor.* Materials, 2020. **13**(12): p. 2782.

349. Tomczyk, A., Z. Sokołowska, and P. Boguta, *Biomass type effect on biochar surface characteristic and adsorption capacity relative to silver and copper.* Fuel (Guildford), 2020. **278**: p. 118168.

350. Murdock, J.N. and D.L. Wetzel, *FT-IR microspectroscopy enhances biological and ecological analysis of algae.* Applied Spectroscopy Reviews, 2009. **44**(4): p. 335-361.

351. Soni, B. and S.K. Karmee, *Towards a continuous pilot scale pyrolysis based biorefinery for production of biooil and biochar from sawdust.* Fuel, 2020. **271**: p. 117570.

352. Zhang, X., et al., *Characterization and sulfonamide antibiotics adsorption capacity of spent coffee grounds based biochar and hydrochar.* The Science of the total environment, 2020. **716**: p. 137015-137015.

353. Hussain, N., et al., *Cadmium (II) removal from aqueous solution using magnetic spent coffee ground biochar: Kinetics, isotherm and thermodynamic adsorption.* Materials Research Express, 2020. **7**(8): p. 085503.

354. Jagdale, P., et al., *Waste Coffee Ground Biochar: A Material for Humidity Sensors.* Sensors (Basel, Switzerland), 2019. **19**(4): p. 801.

355. Jones, E.R., et al., *Country-level and gridded estimates of wastewater production, collection, treatment and reuse.* Earth System Science Data, 2021. **13**(2): p. 237-254.

356. Kahlon, S.K., et al., *Impact of heavy metals and nanoparticles on aquatic biota.* Environmental chemistry letters, 2018. **16**(3): p. 919-946.

357. Gavhane, S., et al., *Impact of Heavy Metals in Riverine and Estuarine Environment: A review.* Research Journal of Chemistry and Environment, 2021. **25**: p. 5.

358. Hussain, A., M. Priyadarshi, and S. Dubey, *Experimental study on accumulation of heavy metals in vegetables irrigated with treated wastewater.* Applied Water Science, 2019. **9**(5): p. 1-11.

359. Agoro, M.A., et al., *Heavy metals in wastewater and sewage sludge from selected municipal treatment plants in eastern cape province, south africa.* Water, 2020. **12**(10): p. 2746.

360. Al Naggar, Y., M.S. Khalil, and M.A. Ghorab, *Environmental pollution by heavy metals in the aquatic ecosystems of Egypt.* Open Acc. J. Toxicol, 2018. **3**: p. 555603.

361. Medfu Tarekegn, M., F. Zewdu Salilih, and A.I. Ishetu, *Microbes used as a tool for bioremediation of heavy metal from the environment.* Cogent Food & Agriculture, 2020. **6**(1): p. 1783174.

362. Ratte, H.T., *Bioaccumulation and toxicity of silver compounds: a review.* Environmental Toxicology and Chemistry: An International Journal, 1999. **18**(1): p. 89-108.

363. Yan, N. and W.-X. Wang, *Novel imaging of silver nanoparticle uptake by a unicellular alga and trophic transfer to Daphnia magna.* Environmental Science & Technology, 2021. **55**(8): p. 5143-5151.

364. Drake, P.L. and K.J. Hazelwood, *Exposure-related health effects of silver and silver compounds: a review.* The Annals of occupational hygiene, 2005. **49**(7): p. 575-585.

365. Vazquez-Muñoz, R., et al., *Toxicity of silver nanoparticles in biological systems: does the complexity of biological systems matter?* Toxicology letters, 2017. **276**: p. 11-20.

366. Gottschalk, F., et al., *Engineered nanomaterials in rivers – Exposure scenarios for Switzerland at high spatial and temporal resolution.* Environmental pollution (1987), 2011. **159**(12): p. 3439-3445.

367. Yao, Y., et al., *Engineered biochar from biofuel residue: characterization and its silver removal potential.* ACS Appl Mater Interfaces, 2015. **7**(19): p. 10634-40.

368. Dong, X., L.Q. Ma, and Y. Li, *Characteristics and mechanisms of hexavalent chromium removal by biochar from sugar beet tailing.* J Hazard Mater, 2011. **190**(1-3): p. 909-15.

369. Scully, D.S., A.K. Jaiswal, and N. Abu-Ghannam, *An Investigation into Spent Coffee Waste as a Renewable Source of Bioactive Compounds and Industrially Important Sugars.* Bioengineering, 2016.

370. Armstrong, D.L., et al., *Temporal trends of perfluoroalkyl substances in limed biosolids from a large municipal water resource recovery facility.* Journal of environmental management, 2016. **165**: p. 88-95.

371. Whangchai, K., et al., *Biomass generation and biodiesel production from macroalgae grown in the irrigation canal wastewater.* Water Science and Technology, 2021. **84**(10-11): p. 2695-2702.

372. Siddique, I.J., et al., *Technical challenges in scaling up the microwave technology for biomass processing.* Renewable and Sustainable Energy Reviews, 2022. **153**: p. 111767.

373. Antunes, E., et al., *A circular economy approach for phosphorus removal using algae biochar.* Cleaner and Circular Bioeconomy, 2022: p. 100005.

374. Bok, J.P., et al., *Fast pyrolysis of coffee grounds: Characteristics of product yields and biocrude oil quality.* Energy, 2012. **47**(1): p. 17-24.

375. Fermoso, J. and O. Mašek, *Thermochemical decomposition of coffee ground residues by TG-MS: A kinetic study.* Journal of analytical and applied pyrolysis, 2018. **130**: p. 358-367.

376. He, J., et al., *Effect of temperature on heavy metal(loid) deportment during pyrolysis of Avicennia marina biomass obtained from phytoremediation.* Bioresour Technol, 2019. **278**: p. 214-222.

377. Yuan, J.-H., R.-K. Xu, and H. Zhang, *The forms of alkalis in the biochar produced from crop residues at different temperatures.* Bioresource technology, 2011. **102**(3): p. 3488-3497.

378. Lee, Y., et al., *Comparison of biochar properties from biomass residues produced by slow pyrolysis at 500 C.* Bioresource technology, 2013. **148**: p. 196-201.

379. Shin, J., et al., *Effects of physicochemical properties of biochar derived from spent coffee grounds and commercial activated carbon on adsorption behavior and mechanisms of strontium ions (Sr2+).* Environmental science and pollution research international, 2020.

380. Zhao, J., et al., *Comparison of biochars derived from different types of feedstock and their potential for heavy metal removal in multiple-metal solutions.* Scientific reports, 2019. **9**(1): p. 9869-12.

381. Taşar, Ş. and A. Özer, *A Thermodynamic and Kinetic Evaluation of the Adsorption of Pb (II) Ions Using Peanut (Arachis Hypogaea) Shell-Based Biochar from Aqueous Media.* Polish Journal of Environmental Studies, 2020. **29**(1).

382. Merck. *IR Spectrum Table & Chart*. Available from: https://www.sigmaaldrich.com/AU/en/technical-documents/technical-article/analytical-chemistry/photometry-and-reflectometry/ir-spectrum-table.

383. LibreTexts, *Infrared Spectroscopy Absorption Table*. 2020.

384. Shaikh, W.A., et al., *Biochar-based nanocomposite from waste tea leaf for toxic dye removal: From facile fabrication to functional fitness.* Chemosphere, 2022. **291**: p. 132788.

385. Zhao, T., et al., *Facile low-temperature one-step synthesis of pomelo peel biochar under air atmosphere and its adsorption behaviors for Ag (I) and Pb (II).* Science of the Total Environment, 2018. **640**: p. 73-79.

386. Naga Babu, A., et al., *Mathematical investigation into the sequential adsorption of silver ions and brilliant green dye using biochar derived from Gracilaria Rhodophyta algae.* Biomass Conversion and Biorefinery, 2021: p. 1-20.

387. El Qada, E.N., S.J. Allen, and G.M. Walker, *Adsorption of basic dyes from aqueous solution onto activated carbons.* Chemical Engineering Journal, 2008. **135**(3): p. 174-184.

388. Anandalakshmi, K., J. Venugobal, and V. Ramasamy, *Characterization of silver nanoparticles by green synthesis method using Pedalium murex leaf extract and their antibacterial activity.* Applied nanoscience, 2016. **6**(3): p. 399-408.

389. Sen, P., et al., *Preparation of Cu, Ag, Fe and Al nanoparticles by the exploding wire technique.* Journal of Chemical Sciences, 2003. **115**(5): p. 499-508.

390. Khan, N.A., et al., *Alumina supported model Pd–Ag catalysts: A combined STM, XPS, TPD and IRAS study.* Surface Science, 2006. **600**(9): p. 1849-1853.

391. Ren, M., et al., *Titanium Phosphate Nanoplates Modified With AgBr@Ag Nanoparticles: A Novel Heterostructured Photocatalyst With Significantly Enhanced Visible Light Responsive Activity.* Front Chem, 2018. **6**: p. 489.

392. Hashem, A., et al., *Non-linear adsorption characteristics of modified pine wood sawdust optimised for adsorption of Cd (II) from aqueous systems.* Journal of Environmental Chemical Engineering, 2020. **8**(4): p. 103966.

393. Islam, M.A., M.V. Jacob, and E. Antunes, *A critical review on silver nanoparticles: From synthesis and applications to its mitigation through low-cost adsorption by biochar.* Journal of Environmental Management. **281**: p. 111918.

394. Passarelli, C., et al., *Environmental context determines the impact of titanium oxide and silver nanoparticles on the functioning of intertidal microalgal biofilms.* Environmental Science: Nano, 2020. **7**(10): p. 3020-3035.

395. Makvandi, P., et al., *Advances in Functionalization of Polymers and Nanomaterials: Water Treatment, Food Packaging, Textile, and Biomedical Applications.* 2021.

396. Ho, N.A.D. and S. Babel, *Bioelectrochemical technology for recovery of silver from contaminated aqueous solution: a review.* Environmental Science and Pollution Research, 2020: p. 1-15.

397. Gagnon, C., et al., *Occurrence and size distribution of silver nanoparticles in wastewater effluents from various treatment processes in Canada.* Environmental Science and Pollution Research, 2021. **28**(46): p. 65952-65959.

398. Deycard, V.N., et al., *Inputs, dynamics and potential impacts of silver (Ag) from urban wastewater to a highly turbid estuary (SW France).* Chemosphere, 2017. **167**: p. 501-511.

399. Cervantes-Avilés, P., Y. Huang, and A.A. Keller, *Multi-technique approach to study the stability of silver nanoparticles at predicted environmental concentrations in wastewater.* Water research, 2019. **166**: p. 115072.

400. Qiu, G., et al., *Effect of silver nanoparticles on system performance and microbial community dynamics in a sequencing batch reactor.* Journal of Cleaner Production, 2016. **130**: p. 137-142.

401. Courtois, P., et al., *Transfer of sulfidized silver from silver nanoparticles, in sewage sludge, to plants and primary consumers in agricultural soil environment.* Science of The Total Environment, 2021. **777**: p. 145900.

402. Bolaños-Benítez, V., et al., *Engineered silver nanoparticle (Ag-NP) behaviour in domestic on-site wastewater treatment plants and in sewage sludge amended-soils.* Science of The Total Environment, 2020. **722**: p. 137794.

403. Zhao, J., et al., *Silver nanoparticles in aquatic sediments: Occurrence, chemical transformations, toxicity, and analytical methods.* Journal of Hazardous Materials, 2021: p. 126368.

404. Dong, B., et al., *Transformation of silver ions to silver nanoparticles mediated by humic acid under dark conditions at ambient temperature.* Journal of hazardous materials, 2020. **383**: p. 121190.

405. Fan, M., et al., *Transformation of silver nanoparticles in coagulation processes and subsequent thermal sludge treatments.* Journal of Cleaner Production, 2019. **238**: p. 117984.

406. de Souza, T.A.J., L.R.R. Souza, and L.P. Franchi, *Silver nanoparticles: An integrated view of green synthesis methods, transformation in the environment, and toxicity.* Ecotoxicology and environmental safety, 2019. **171**: p. 691-700.

407. Schlich, K., et al., *Long-term effects of three different silver sulfide nanomaterials, silver nitrate and bulk silver sulfide on soil microorganisms and plants.* Environmental Pollution, 2018. **242**: p. 1850-1859.

408. Doolette, C.L., et al., *Bioavailability of silver and silver sulfide nanoparticles to lettuce (Lactuca sativa): Effect of agricultural amendments on plant uptake.* Journal of hazardous materials, 2015. **300**: p. 788-795.

409. Levard, C., et al., *Environmental transformations of silver nanoparticles: impact on stability and toxicity.* Environmental science & technology, 2012. **46**(13): p. 6900-6914.

410. Vishwakarma, V., *Recovery and recycle of wastewater contaminated with heavy metals using adsorbents incorporated from waste resources and nanomaterials-A review.* Chemosphere, 2021: p. 129677.

411. de Sá Costa, H.P., M.G.C. da Silva, and M.G.A. Vieira, *Fixed bed biosorption and ionic exchange of aluminum by brown algae residual biomass.* Journal of Water Process Engineering, 2021. **42**: p. 102117.

412. Kumar, R., et al., *Lignocellulose biomass pyrolysis for bio-oil production: A review of biomass pre-treatment methods for production of drop-in fuels.* Renewable and Sustainable Energy Reviews, 2020. **123**: p. 109763.

413. Oladipo, A.A. and A.O. Ifebajo, *Highly efficient magnetic chicken bone biochar for removal of tetracycline and fluorescent dye from wastewater: Two-stage adsorber analysis.* Journal of environmental management, 2018. **209**: p. 9-16.

414. Krasucka, P., et al., *Engineered biochar–A sustainable solution for the removal of antibiotics from water.* Chemical Engineering Journal, 2021. **405**: p. 126926.

415. Oladipo, A.A., M.A. Abureesh, and M. Gazi, *Bifunctional composite from spent "Cyprus coffee" for tetracycline removal and phenol degradation: Solar-Fenton process and artificial neural network.* International journal of biological macromolecules, 2016. **90**: p. 89-99.

416. Lee, C.-G., et al., *Production of biochar from food waste and its application for phenol removal from aqueous solution.* Water, Air, & Soil Pollution, 2019. **230**(3): p. 1-13.

417. Oladipo, A.A., E.O. Ahaka, and M. Gazi, *Pyrochar/AgBr-derived from discarded chewing gum for decontamination of trichlorophenol via fixed-bed adsorption system.* Chemical Engineering Communications, 2021. **208**(2): p. 220-232.

418. Oladipo, A.A., E.O. Ahaka, and M. Gazi, *High adsorptive potential of calcined magnetic biochar derived from banana peels for Cu2+, Hg2+, and Zn2+ ions removal in single and ternary systems.* Environmental Science and Pollution Research, 2019.

419. Chen, W.-H., et al., *Biomass-derived biochar: From production to application in removing heavy metal-contaminated water.* Process Safety and Environmental Protection, 2022.

420. Komkiene, J. and E. Baltrenaite, *Biochar as adsorbent for removal of heavy metal ions [Cadmium(II), Copper(II), Lead(II), Zinc(II)] from aqueous phase.* International Journal of Environmental Science and Technology, 2015. **13**(2): p. 471-482.

421. Ni, B.J., et al., *Competitive adsorption of heavy metals in aqueous solution onto biochar derived from anaerobically digested sludge.* Chemosphere, 2019. **219**: p. 351-357.

422. Kovalcik, A., S. Obruca, and I. Marova, *Valorization of spent coffee grounds: A review.* Food and Bioproducts Processing, 2018. **110**: p. 104-119.

423. Zabaniotou, A. and P. Kamaterou, *Food waste valorization advocating Circular Bioeconomy-A critical review of potentialities and perspectives of spent coffee grounds biorefinery.* Journal of cleaner production, 2019. **211**: p. 1553-1566.

424. Ding, Z., et al., *Removal of lead, copper, cadmium, zinc, and nickel from aqueous solutions by alkali-modified biochar: Batch and column tests.* Journal of Industrial and Engineering Chemistry, 2016. **33**: p. 239-245.

425. Kılıç, M., et al., *Adsorption of heavy metal ions from aqueous solutions by bio-char, a by-product of pyrolysis.* Applied Surface Science, 2013. **283**: p. 856-862.

426. Pap, S., et al., *Low-cost chitosan-calcite adsorbent development for potential phosphate removal and recovery from wastewater effluent.* Water research, 2020. **173**: p. 115573.

427. Vilvanathan, S. and S. Shanthakumar, *Column adsorption studies on nickel and cobalt removal from aqueous solution using native and biochar form of Tectona grandis.* Environmental Progress & Sustainable Energy, 2017. **36**(4): p. 1030-1038.

428. Alalwan, H.A., et al., *Adsorption of thallium ion (Tl+ 3) from aqueous solutions by rice husk in a fixed-bed column: Experiment and prediction of breakthrough curves.* Environmental Technology & Innovation, 2018. **12**: p. 1-13.

429. Dawood, S., T.K. Sen, and C. Phan, *Performance and dynamic modelling of biochar and kaolin packed bed adsorption column for aqueous phase methylene blue (MB) dye removal.* Environmental technology, 2018.

430. Feizi, F., A.K. Sarmah, and R. Rangsivek, *Adsorption of pharmaceuticals in a fixed-bed column using tyre-based activated carbon: Experimental investigations and numerical modelling.* Journal of Hazardous Materials, 2021. **417**: p. 126010.

431. Hu, Y., et al., *A simple on-line detection system based on fiber-optic sensing for the realtime monitoring of fixed bed adsorption processes of molecularly imprinted polymers.* Journal of Chromatography A, 2020. **1622**: p. 461112.

432. Geankoplis, C.J., *Transport Processes and Unit Operations: PTR Prentice Hall.* City, State, Country, 1993.

433. Długosz, O. and M. Banach, *Sorption of Ag+ and Cu2+ by vermiculite in a fixed-bed column: Design, process optimization and dynamics investigations.* Applied Sciences, 2018. **8**(11): p. 2221.

434. Brion-Roby, R., et al., *Investigation of fixed bed adsorption column operation parameters using a chitosan material for treatment of arsenate contaminated water.* Journal of environmental chemical engineering, 2018. **6**(1): p. 505-511.

435. Wang, X., et al., *Mixed heavy metal removal from wastewater by using discarded mushroom-stick biochar: adsorption properties and mechanisms.* Environmental science. Processes & impacts, 2019. **21**(3): p. 584-592.

436. Wu, T., et al., *Dual-porous cellulose nanofibril aerogels via modular drying and cross-linking.* Nanoscale, 2020. **12**(13): p. 7383-7394.

437. Kaewsichan, L., et al., *Elimination of selected heavy metals from aqueous solutions using biochar and bentonite composite monolith in a fixed-bed operation.* Journal of Environmental Chemical Engineering, 2022. **10**(1): p. 106993.

438. Nishikawa, E., et al., *New perception of the continuous biosorption of cadmium on a seaweed derivative waste.* Journal of Water Process Engineering, 2020. **36**: p. 101322.

439. Verduzco-Navarro, I.P., et al., *Removal of Cu (II) by fixed-bed columns using Alg-Ch and Alg-ChS hydrogel beads: effect of operating conditions on the mass transfer zone.* Polymers, 2020. **12**(10): p. 2345.

440. Naja, G. and B. Volesky, *Behavior of the mass transfer zone in a biosorption column.* Environmental science & technology, 2006. **40**(12): p. 3996-4003.

441. El-Shorbagy, H.G., et al., *Eco-friendly chitosan condensation adduct resins for removal of toxic silver ions from aqueous medium.* Journal of Industrial and Engineering Chemistry, 2021. **100**: p. 410-421.

442. Gupta, S., et al., *Latest trends in heavy metal removal from wastewater by biochar based sorbents.* Journal of Water Process Engineering, 2020. **38**: p. 101561.

443. Yu, S.-j., et al., *Highly dynamic PVP-coated silver nanoparticles in aquatic environments: chemical and morphology change induced by oxidation of Ag0 and reduction of Ag+.* Environmental science & technology, 2014. **48**(1): p. 403-411.

444. Long, N.V., et al., *Effects of heat treatment and poly (vinylpyrrolidone)(PVP) polymer on electrocatalytic activity of polyhedral Pt nanoparticles towards their methanol oxidation.* Colloid and Polymer Science, 2011. **289**(12): p. 1373-1386.

445. Skiba, M., et al., *Plasma-chemical formation of silver nanoparticles: The silver ions concentration effect on the particle size and their antimicrobial properties.* 2019.

446. Wang, W., et al., *Developing effective separation of feldspar and quartz while recycling tailwater by HF pretreatment.* Minerals, 2018. **8**(4): p. 149.

447. Wu, F., et al., *Recycling supercapacitor activated carbons for adsorption of silver (I) and chromium (VI) ions from aqueous solutions.* Chemosphere, 2020. **238**: p. 124638.

448. Islam, M., et al., *Feasibility study for thermal treatment of solid tire wastes in Bangladesh by using pyrolysis technology.* Waste management, 2011. **31**(9-10): p. 2142-2149.

449. Yao, Z., et al., *Demonstration and multi-perspective analysis of industrial-scale co-pyrolysis of biomass, waste agricultural film, and bituminous coal.* Journal of Cleaner Production, 2021. **290**: p. 125819.

450. Bolan, N., et al., *Multifunctional applications of biochar beyond carbon storage.* International Materials Reviews, 2021: p. 1-51.

451. Sajjadi, B., W.-Y. Chen, and N.O. Egiebor, *A comprehensive review on physical activation of biochar for energy and environmental applications.* Reviews in Chemical Engineering, 2019. **35**(6): p. 735-776.

452. Mohammadi, A., *Overview of the benefits and challenges associated with pelletizing biochar.* Processes, 2021. **9**(9): p. 1591.

APPENDIX

APPENDIX 1

Table A1: Analysis of Algae Py-GCMS data

Peak No.	R.T. (min)	Quality	Compound name	Classification	Peak area %
4	2.257	59	Acetic acid	Acids	0.96
5	2.277	80	Acetic acid	Acids	0.38
7	3.094	72	2-Propenoic acid	Acids	0.96
8	3.144	68	2-Propenoic acid	Acids	0.92
10	4.118	64	Propanoic acid, 2-oxo-, methyl ester	Acids	0.56
37	19.824	99	n-Hexadecanoic acid	Acids	4.64
38	21.539	99	Oleic Acid	Acids	0.51
					8.93
23	9.304	70	2-Furanmethanol	Alcohol	**1.01**
28	12.069	95	Indole	Amines	0.42
31	13.361	87	Indole, 3-methyl-	Amines	0.54
					0.96
30	12.89	53	Glycine, ethyl ester hydrochloride	Ester	1.06
9	3.926	90	Toluene	Hydrocarbons	1.78
33	16.857	99	8-Heptadecene	Hydrocarbons	0.38
34	18.566	99	Neophytadiene	Hydrocarbons	6.22
36	19.012	91	2-Hexadecen-1-ol	Hydrocarbons	4.26
					12.64
12	4.797	95	2-Furancarbaldehyde	Ketones and aldehyde	4.41
14	6.1	91	2-Furancarboxaldehyde, 5-methyl-	Ketones and aldehyde	6.36
15	6.277	90	2-Furancarboxaldehyde, 5-methyl-	Ketones and aldehyde	2.21
22	8.901	78	2,3-Dihydro-5-hydroxy-6-methyl-4	Ketones and aldehyde	0.72
24	9.681	93	N,N-dimethylhomoserine lactone	Ketones and aldehyde	0.39

16	6.897	94	5-Methylfurfural	Ketones and aldehyde	15.58
20	8.259	50	2,4-Imidazolidinedione, 5,5-dimethyl-	Ketones and aldehyde	3.32
					32.99
26	10.89	93	1,4:3,6-Dianhydro-.alpha.-d-gluc	Monosaccharide	0.56
32	14.875	72	β-D-Glucopyranose, 1,6-anhydro-	Monosaccharide	6.09
					6.65
17	7.136	90	Phenol	Phenols	0.38
21	8.686	94	p-Cresol	Phenols	0.58
					0.96

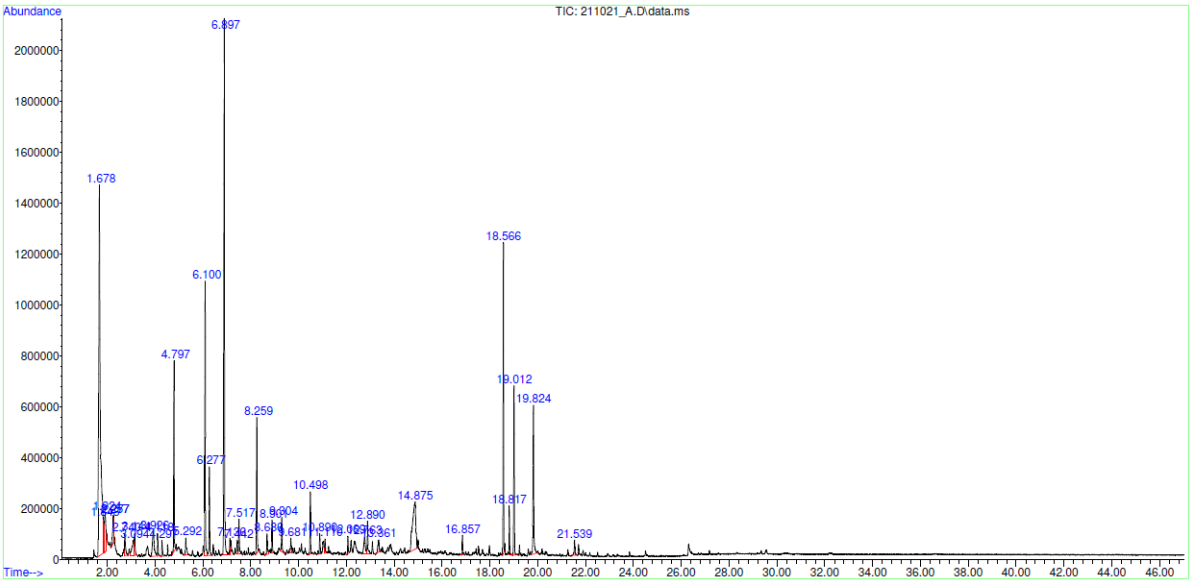

Figure A1: Py-GCMS spectra of algae

Table A2: Analysis of SCGs Py-GCMS data

R.T. (min)	**Quality**	**Compound name**	**Classification**	**Peak area %**
2.374	72	Acetic acid	Acids	1.88
9.316	62	1H-Imidazole-4-carboxylic acid	Acids	0.43
19.944	99	Hexadecanoic acid	Acids	15.95
21.553	99	9,12-Octadecadienoic acid (Z,Z)-	Acids	8.87
21.602	95	Linoleic acid	Acids	4.33
21.793	99	Octadecanoic acid	Acids	5.2
21.956	60	9-Octadecadienoic acid	Acids	0.53
23.495	99	Eicosanoic acid	Acids	1.44

15.025	52	Hexanoic acid	Acids	0.43
				39.06
5.122	95	2-Furanmethanol	Alcohol	1.43
22.47	68	2-Cyclododecylidene ethanol	Alcohol	0.41
				1.84
18.803	97	Caffeine	Alkaloid	3.88
12.075	87	Indole	Amines	0.27
13.362	91	1H-Indole, 2-methyl-	Amines	0.12
4.062	64	Ethanamine, N-ethyl-	Amines	0.42
9.109	53	2-Butanamine, 3-methyl-	Amines	1.13
13.211	72	4-acetyl-1,3-dimethylpyrazole	Amines	0.16
				5.98
28.819	53	22-Dehydro-25-epi-aplysteryl-acetate	Ester	0.22
22.742	52	Ethyl 4,4-dimethyl-3-(2,4,5-trim	Ester	0.24
8.849	74	Methyl 2-furoate	Ester	0.21
				0.67
3.046	89	1-Heptene	Hydrocarbons	0.33
3.894	90	Toluene	Hydrocarbons	0.42
3.932	76	Benzene, methyl-	Hydrocarbons	0.89
7.375	93	1-Decene	Hydrocarbons	0.28
11.965	58	Cyclotridecane	Hydrocarbons	0.37
13.334	99	1-Tetradecene	Hydrocarbons	0.19
14.625	96	1-Pentadecene	Hydrocarbons	0.1
14.721	97	Pentadecane	Hydrocarbons	0.43
16.61	55	2-Undecene, 4,5-dimethyl-	Hydrocarbons	0.65
16.758	98	6(E),8(E)-Heptadecadiene	Hydrocarbons	0.28
16.848	87	1-Pentadecene	Hydrocarbons	0.27
17.083	93	Heptadecane	Hydrocarbons	0.3
11.804	83	Benzene, 1-methoxy-4-(1-methylethyl)-	Hydrocarbons	0.35
3.598	94	Pyridine	Hydrocarbons	0.38
26.292	78	1-(3,4-Dicyanophenyl)naphthalene	Hydrocarbons	0.42
				5.66
2.699	93	Butanal, 3-methyl-	Ketones and aldehyde	0.14
4.803	76	Furfural/2-Furancarboxaldehyde	Ketones and aldehyde	0.86
5.172	59	3-Methyl-2-hexanone	Ketones and aldehyde	0.25
5.961	87	2-Methyl-2-cyclopenten-1-one	Ketones and aldehyde	0.32
6.167	53	3,6-Dihydro-2H-pyran-2-one	Ketones and aldehyde	0.25
6.293	80	2-Hydroxycyclopent-2-en-1-one	Ketones and aldehyde	1.36
6.539	93	2,5-Furandione, 3-methyl-	Ketones and aldehyde	0.18

6.881	87	5-Methylfurfural	Ketones and aldehyde	0.29
6.932	91	3-Methyl-2-cyclopenten-1-one	Ketones and aldehyde	0.19
7.231	72	3-Methyl-5-methyliden-2(5H)-furanone	Ketones and aldehyde	0.24
7.934	96	2-Cyclopenten-1-one, 2-hydroxy-3-methyl-	Ketones and aldehyde	0.8
8.277	92	Phenylacetaldehyde	Ketones and aldehyde	0.26
9.393	91	2-Cyclopenten-1-one, 3-ethyl-2-hydroxy-	Ketones and aldehyde	0.27
29.407	90	25-Epiaplysterylacetate-1	Ketones and aldehyde	0.83
3.158	92	Furan, 2,5-dimethyl-	Ketones and aldehyde	0.37
22.365	78	1H-Naphtho[2,1-b]pyran-1-one	Ketones and aldehyde	0.29
11.054	76	5-Hydroxymethylfurfural	Ketones and aldehyde	0.28
11.757	72	3-Isobutyldihydropyrazin-2-one	Ketones and aldehyde	0.63
				7.81
14.521	72	β-D-Glucopyranose, 1,6-anhydro-	Monosaccharide	3.03
7.143	95	Phenol	Phenols	0.74
8.366	95	Phenol, 3-methyl-	Phenols	0.2
8.697	95	Phenol, 4-methyl-	Phenols	0.76
8.924	93	Phenol, 2-methoxy-	Phenols	0.22
10.124	50	Phenol, 3-ethyl-	Phenols	0.36
10.577	93	1,2-Benzenediol	Phenols	1.27
10.632	87	1,2-Benzenediol	Phenols	0.37
10.913	58	4-vinylphenol $$ p-vinylphenol	Phenols	0.2
12.29	90	4-vinyl-2-methoxy-phenol	Phenols	0.4
28.72	97	β-Tocopherol	Phenols	0.24
14.127	86	trans-Isoeugenol	Phenols	0.13
				7.92
19.127	94	Hexadecanenitrile	Others	0.18
3.664	74	1H-Pyrrole	Others	0.4
9.99	53	3-Hydroxymethylquinuclidine	Others	0.26
21.981	53	Tetrahydroisoquinoline	Others	0.89
28.588	53	Bikaverin $$ 6,11-Dihydroxy-3,8-...	Others	0.24
11.347	50	(1RS,4RS,5RS,6RS)-5,6-exo-epoxy-	Others	0.23
22.83	90	Androsta-1,4,9(11)-triene-3,17-d	Others	0.15
22.516	76	7-Nitro-10,10-dimethyl-9,10-dihydr	Others	0.55
23.313	90	2-(3,4-dimethylphenyl)-3,3-(2,2'..	Others	0.57
25.136	91	7,9-Dimethoxy-8-isopropyl-4-meth..	Others	3.29
				6.76

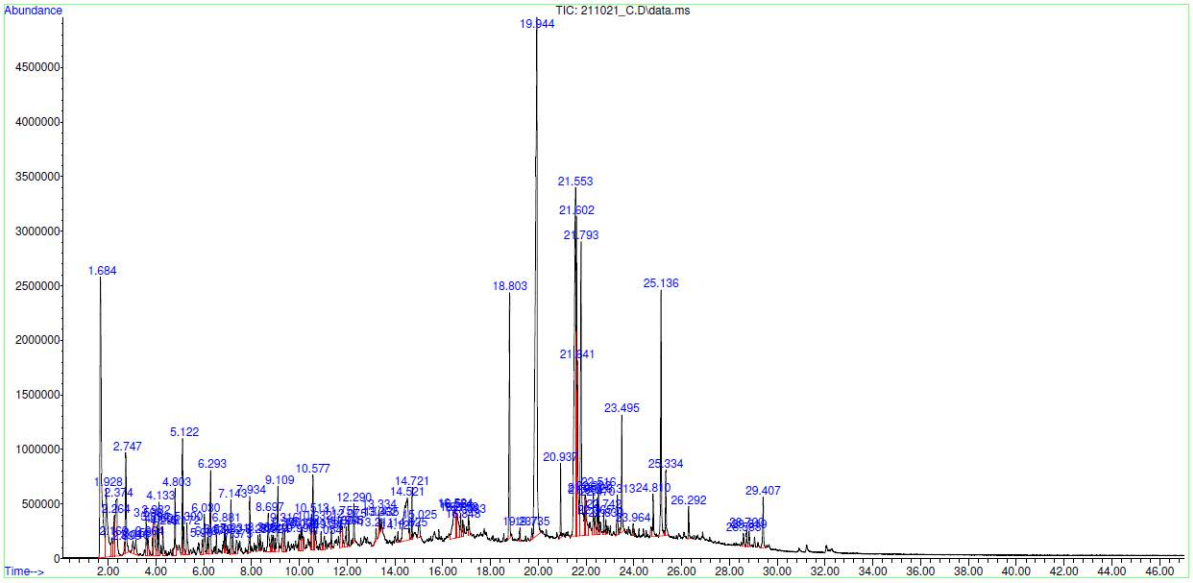

Figure A2: Py-GCMS spectra of SCGs

Table A3: Analysis of sawdust Py-GCMS data

R.T. (min)	Quality	Compound name	Classification	Peak area %
2.2	50	Butanoic acid	Acids	0.99
2.429	90	Acetic acid	Acids	4.11
14.026	72	Vanillic acid	Acids	2.98
14.99	90	2,4-Dimethyl-3-(methoxycarbonyl)...	Acids	4
15.185	65	Heptanoic acid	Acids	1.95
15.265	47	Hexadecanoic acid	Acids	3.35
				17.38
2.294	59	3-Buten-2-ol, 3-methyl-	Alcohol	1.51
5.114	95	2-Furanmethanol	Alcohol	0.52
				2.03
4.079	64	Azetidine-D1	Amines	0.91
7.39	52	1H-1,2,4-Triazol-3-amine, 1-ethyl-	Amines	0.41
9.084	59	2-Butanamine	Amines	0.85
16.984	83	3-amino-2-cyano-6-methyl-6,7-dih.	Amines	0.34
6.92	50	2-Propenamide, N-(aminocarbonyl).	Amine	0.52
				3.03
14.543	83	2-Ethyl-1,4-benzodioxin	Ester	0.18
15.518	90	2,6-Dimethyl-3-(methoxymethyl)-p	Ester	4.92
				5.1
18.353	49	Benzene, 1,1'-ethylidenebis-	Hydrocarbons	0.23

25.925	74	1,4,9,10-Tetrahydro-1,4-dimethyl...	Hydrocarbons	0.3
14.66	80	(1R)-1,6,6-Trimethyl-cis-bicyclo...	Hydrocarbons	0.26
26.286	78	1-(3,4-Dicyanophenyl)naphthalene...	Hydrocarbons	0.54
				1.33
13.475	95	Vanillin	Ketones and aldehyde	0.78
2.766	59	2-Propanone, 1-hydroxy-	Ketones and aldehyde	1.72
4.804	93	2-Furancarboxaldehyde	Ketones and aldehyde	1.97
5.171	59	3-Methyl-2-heptanone	Ketones and aldehyde	0.3
5.302	50	2-Propanone, 1-(acetyloxy)-	Ketones and aldehyde	0.1
6.02	72	2(5H)-Furanone	Ketones and aldehyde	0.65
6.164	52	5,6-Dihydro-2H-pyran-2-one	Ketones and aldehyde	0.26
6.276	78	2-Hydroxycyclopent-2-en-1-one	Ketones and aldehyde	1.33
6.883	83	5-Methylfurfural	Ketones and aldehyde	0.5
7.232	78	3-Methyl-5-methyliden-2(5H)-fura	Ketones and aldehyde	0.19
7.542	72	2,4-Imidazolidinedione, 3-methyl-	Ketones and aldehyde	1.79
7.919	97	2-Cyclopenten-1-one, 2-hydroxy-3-methyl-	Ketones and aldehyde	0.7
9.309	58	Maltol	Ketones and aldehyde	0.18
11.06	95	5-Hydroxymethylfurfural	Ketones and aldehyde	1.16
11.48	94	1,2-Benzenediol, 3-methyl-	Ketones and aldehyde	0.4
11.522	95	1,2-Benzenediol, 3-methoxy-	Ketones and aldehyde	1.58
11.907	90	1,2-Benzenediol, 4-methyl-	Ketones and aldehyde	0.97
14.068	74	Ethanone, 1-(2,3,4-trihydroxyphenyl)-	Ketones and aldehyde	0.18
14.59	93	Acetovanillone	Ketones and aldehyde	0.59
15.046	72	β-D-Glucopyranose, 1,6-anhydro-	Ketones and aldehyde	0.99
15.799	58	Propano 3-methoxy-4-hydroxyphenone	Ketones and aldehyde	0.7
16.348	58	4-Methyl-2,5-dimethoxybenzaldehyde	Ketones and aldehyde	0.42
16.639	93	Benzaldehyde, 4-hydroxy-3,5-dimethoxy-	Ketones and aldehyde	1.1
17.45	95	Ethanone, 1-(4-hydroxy-3,5-dimethoxyphenyl)-	Ketones and aldehyde	0.96

17.812	56	1-(2,4,6-Trihydroxyphenyl)-1-butanone	Ketones and aldehyde	1.09
25.866	99	3beta-Hydroxy-5-androsten-16-one	Ketones and aldehyde	0.48
10.436	81	4H-Pyran-4-one, 3,5-dihydroxy-2-methyl-	Ketones and aldehyde	0.4
17.122	64	2-Methyl-3-(methoxycarbonyl)-4,5	Ketones and aldehyde	4.63
				26.12
10.934	91	1,4:3,6-Dianhydro-.alpha.-d-gluc.	Monosaccharide	0.42
7.147	90	Phenol	Phenols	0.35
8.359	93	Phenol, 2-methyl-	Phenols	0.33
8.697	95	Phenol, 4-methyl-	Phenols	0.36
8.93	97	Phenol, 2-methoxy-	Phenols	1.72
9.847	93	Phenol, 2,4-dimethyl-	Phenols	0.26
10.525	93	Creosol	Phenols	3.52
11.763	91	Phenol, 4-ethyl-2-methoxy-	Phenols	1.48
12.295	90	4-vinyl-2-methoxy-phenol	Phenols	3.49
12.777	95	Phenol, 2,6-dimethoxy-	Phenols	3.7
12.86	97	Eugenol	Phenols	0.56
12.913	87	Phenol, 3,4-dimethoxy-	Phenols	0.69
13.192	83	1,2,3-Benzenetriol	Phenols	0.89
13.242	50	1,2,4-Benzenetriol	Phenols	0.44
14.132	97	trans-Isoeugenol	Phenols	2.08
14.208	78	Phenol, 2-methoxy-4-propyl-	Phenols	0.55
15.096	59	2-methoxy-4-propyl-phenol	Phenols	2.23
15.992	97	Phenol, 2,6-dimethoxy-4-(2-propenyl)-	Phenols	1.2
				23.85
15.664	78	1,7-Dimethyl-4,4a,5,6-tetrahydro...	Others	0.57
16.004	80	(3S)-2-chloro-1-phenyl-1-penten-	Others	0.32
16.911	78	1-isopropyl-5-methylbicyclo[3.2.1]	Others	0.46
17.537	52	(E)-1-(P-methoxyphenyl)-2-methoxy	Others	1
18.434	83	1-(1',2'-dihydroacenaphthylen-3'.	Others	0.32
20.074	94	3-(3',5'-dimethoxy-4'-hydroxyphe...	Others	1.29
				3.96

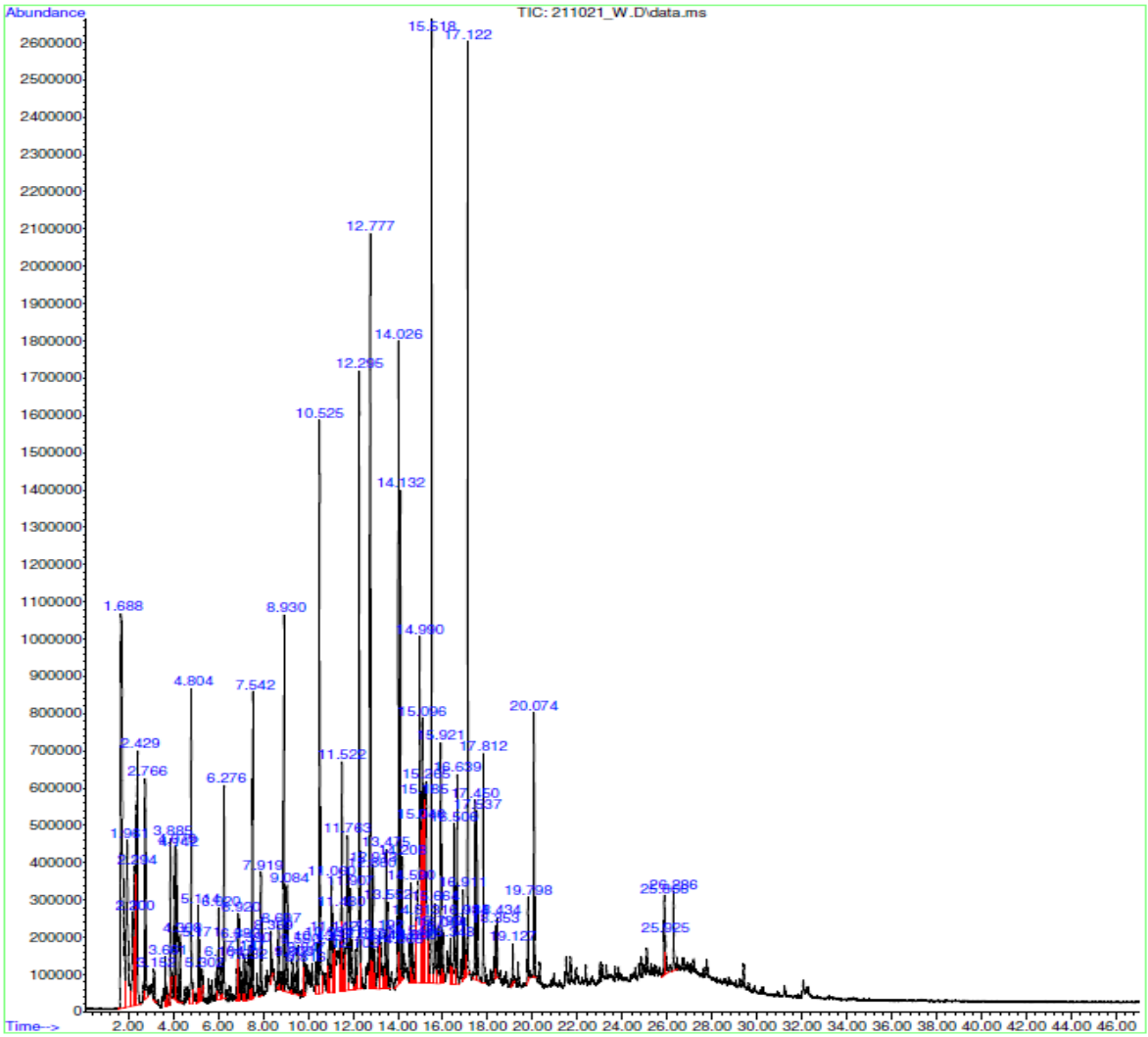

Figure A3: Py-GCMS spectra of sawdust

Table A4: Classification wise normalised total of the composition of pyrolysis vapour

Classification	**Algae**	**SCGs**	**Sawdust**
Acids	13.7	49.6	20.9
Alcohols	1.5	2.3	2.4
Amines	1.5	7.6	3.6
Esters	1.6	0.9	6.1
Hydrocarbons	19.4	7.2	1.6
Ketones and aldehydes	50.6	9.9	31.4
Monosaccharides	10.2	3.8	0.5
Phenols	1.5	10.1	28.7
Others	0.0	8.6	4.8

Table A5: Activation energy calculated by the OFW and the KAS methods along with fitted equation and correlation coefficient for both non-catalytic as well as catalytic pyrolysis.

	Conversion (α)	OFW Method			KAS Method		
		Activation Energy, E_a (kJ/mol)	Fitted linear equation	Correlation coefficient (R^2)	Activation Energy, E_a (kJ/mol)	Fitted linear equation	Correlation coefficient (R^2)
Algae	0.1	57.20	y = -7238x + 23.641	0.9871	54.57	y = -6563x + 9.998	0.9842
	0.2	68.65	y = -8685.9x + 25.12	0.9876	65.92	y = -7928.2x + 11.245	0.985
	0.3	75.40	y = -9540.6x + 22.189	0.9424	71.44	y = -8592.4x + 7.8652	0.93
	0.4	163.96	y = -20747x + 42.639	0.9454	163.99	y = -19724x + 28.164	0.94
	0.5	128.20	y = -16221x + 31.253	0.9783	125.58	y = -15104x + 16.602	0.975
	0.6	230.82	y = -29207x + 50.48	0.9693	232.79	y = -28000x + 35.675	0.9667
	0.7	276.43	y = -34978x + 53.558	0.9147	279.52	y = -33620x + 38.516	0.9084
	0.8	278.46	y = -35234x + 44.972	0.9262	279.22	y = -33584x + 29.541	0.9193
	0.9	285.33	y = -36104x + 39.273	0.9953	284.01	y = -34160x + 23.515	0.9948
		173.83			**173.00**		
SCGs	0.1	143.80	y = -18195x + 37.392	0.9989	142.69	y = -17162x + 22.898	0.9987
	0.2	165.37	y = -20925x + 40.443	1	164.88	y = -19832x + 25.837	1
	0.3	180.93	y = -22894x + 42.804	1	180.98	y = -21768x + 28.137	1
	0.4	189.17	y = -23936x + 43.62	1	189.41	y = -22782x + 28.904	1

	0.5	194.83	y = -24653x + 43.72	0.9999	195.11	y = -23468x + 28.95	0.9999
	0.6	188.76	y = -23884x + 41.181	0.9994	188.40	y = -22661x + 26.349	0.9993
	0.7	173.18	y = -21913x + 36.321	0.9947	171.53	y = -20632x + 21.396	0.994
	0.8	191.54	y = -24236x + 38.529	0.9993	190.43	y = -22905x + 23.527	0.9992
	0.9	269.74	y = -34131x + 50.297	0.9997	271.98	y = -32713x + 35.171	0.9997
		188.59			**188.38**		
Sawdust	0.1	58.41	y = -7390.6x + 23.275	0.9847	55.62	y = -6689.3x + 9.5548	0.9812
	0.2	164.64	y = -20833x + 40.817	0.9991	164.24	y = -19755x + 26.238	0.999
	0.3	175.87	y = -22253x + 41.545	0.9999	175.62	y = -21123x + 26.872	0.9999
	0.4	178.96	y = -22645x + 40.759	1	178.52	y = -21472x + 26.011	1
	0.5	175.46	y = -22202x + 39.002	1	174.58	y = -20998x + 24.201	1
	0.6	173.77	y = -21988x + 37.968	1	172.61	y = -20761x + 23.129	1
	0.7	172.93	y = -21882x + 37.255	1	171.57	y = -20636x + 22.385	1
	0.8	175.44	y = -22199x + 37.131	0.9999	174.01	y = -20930x + 22.226	0.9999
	0.9	226.45	y = -28653x + 43.42	0.9908	226.69	y = -27266x + 28.337	0.9899
		166.88			**165.94**		

Table A6: Pyrolysis thermodynamic parameters for algae, SCGs, and sawdust at 15°C/min.

α	A (min^{-1})	k	ΔH ($kJ \cdot mol^{-1}$)	ΔG ($kJ \cdot mol^{-1}$)	ΔS ($J \cdot mol^{-1} K^{-1}$)
Algae					
0.1	8.25E+09	8.24E+09	51.68	74.08	-64.64
0.2	3.47E+10	3.47E+10	62.68	83.52	-53.64
0.3	1.51E+09	1.50E+09	67.39	107.11	-81.59
0.4	2.24E+18	2.24E+18	159.68	111.23	93.48
0.5	1.39E+13	1.39E+13	120.84	124.82	-6.99
0.6	5.63E+21	5.63E+21	227.71	131.75	157.20
0.7	1.24E+23	1.24E+23	273.81	149.00	181.96
0.8	1.26E+19	1.26E+19	272.27	185.52	103.88
0.9	3.42E+16	3.42E+16	275.80	223.15	53.35
		Average	**167.98**	**132.24**	
SCGs					
0.1	8.85E+15	8.85E+15	138.32	113.46	47.35
0.2	1.95E+17	1.95E+17	160.27	119.99	72.62
0.3	2.14E+18	2.14E+18	176.23	123.52	92.29
0.4	4.83E+18	4.83E+18	184.54	126.70	98.84
0.5	5.23E+18	5.23E+18	190.11	130.42	99.28
0.6	3.78E+17	3.78E+17	183.24	135.33	77.17
0.7	2.48E+15	2.48E+15	166.12	143.32	34.99
0.8	2.28E+16	2.28E+16	184.80	148.88	53.09
0.9	3.68E+21	3.68E+21	266.01	156.76	152.32
		Average	**183.29**	**133.15**	
Sawdust					
0.1	5.39E+09	5.38E+09	52.62	77.30	-68.51
0.2	8.00E+13	8.00E+13	159.69	155.38	7.88
0.3	1.62E+14	1.62E+14	170.85	163.18	13.38
0.4	7.00E+13	7.00E+13	173.57	169.95	6.07
0.5	1.12E+13	1.12E+13	169.49	175.23	-9.39
0.6	3.80E+12	3.80E+12	167.42	178.99	-18.55
0.7	1.80E+12	1.80E+12	166.30	182.06	-24.89
0.8	1.56E+12	1.56E+12	168.65	185.56	-26.22
0.9	9.52E+14	9.52E+14	220.84	202.28	26.39
		Average	**161.05**	**165.55**	

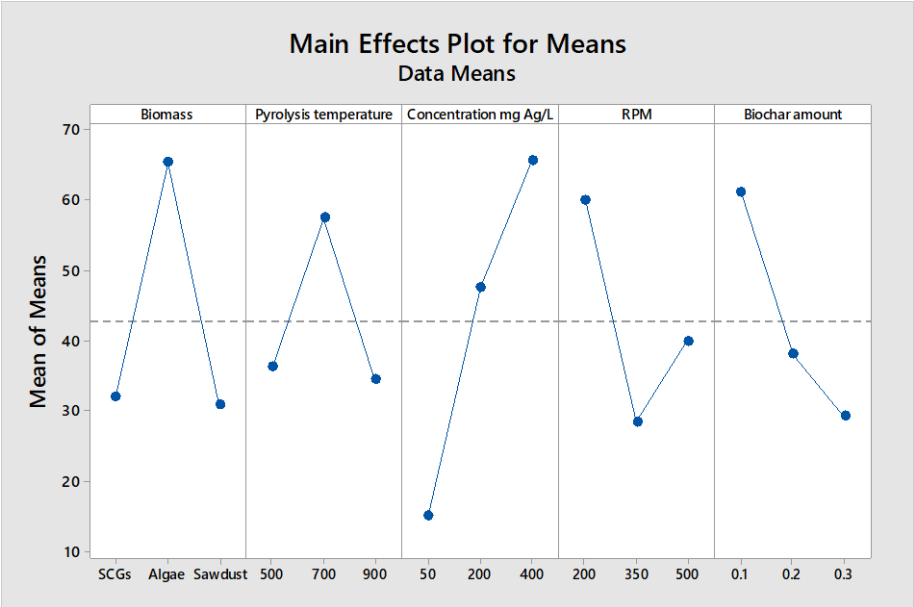

Figure A4: Taguchi analysis plot – main effects of pyrolysis and adsorption conditions on silver removal.

Table A7: Silver adsorption capacity by different biochar samples at varying operational conditions by Taguchi analysis.

Biomass	Pyrolysis temperature (°C)	Initial concentration (mg Ag/L)	Agitation speed (RPM)	Biochar quantity (g)	Adsorption capacity (mg/g)	Adsorption (%)
SCGs	500	50	200	0.1	25.13	99.90
SCGs	500	50	200	0.2	12.53	99.66
SCGs	500	50	200	0.3	8.23	98.54
SCGs	700	200	350	0.1	46.10	46.23
SCGs	700	200	350	0.2	35.48	71.11
SCGs	700	200	350	0.3	30.21	91.26
SCGs	900	400	500	0.1	43.98	22.36
SCGs	900	400	500	0.2	44.03	44.47
SCGs	900	400	500	0.3	43.42	65.33
Algae	500	200	500	0.1	99.71	99.97
Algae	500	200	500	0.2	49.92	99.97
Algae	500	200	500	0.3	33.12	99.97
Algae	700	400	200	0.1	196.20	99.98
Algae	700	400	200	0.2	98.25	99.86
Algae	700	400	200	0.3	66.22	99.99

Algae	900	50	350	0.1	24.54	99.90
Algae	900	50	350	0.2	12.59	99.90
Algae	900	50	350	0.3	8.27	99.90
Sawdust	500	400	350	0.1	35.16	17.84
Sawdust	500	400	350	0.2	31.39	33.17
Sawdust	500	400	350	0.3	32.10	48.49
Sawdust	700	50	500	0.1	24.68	99.01
Sawdust	700	50	500	0.2	12.54	99.90
Sawdust	700	50	500	0.3	8.28	99.90
Sawdust	900	200	200	0.1	55.33	55.53
Sawdust	900	200	200	0.2	45.90	91.81
Sawdust	900	200	200	0.3	33.12	99.75

APPENDIX 2

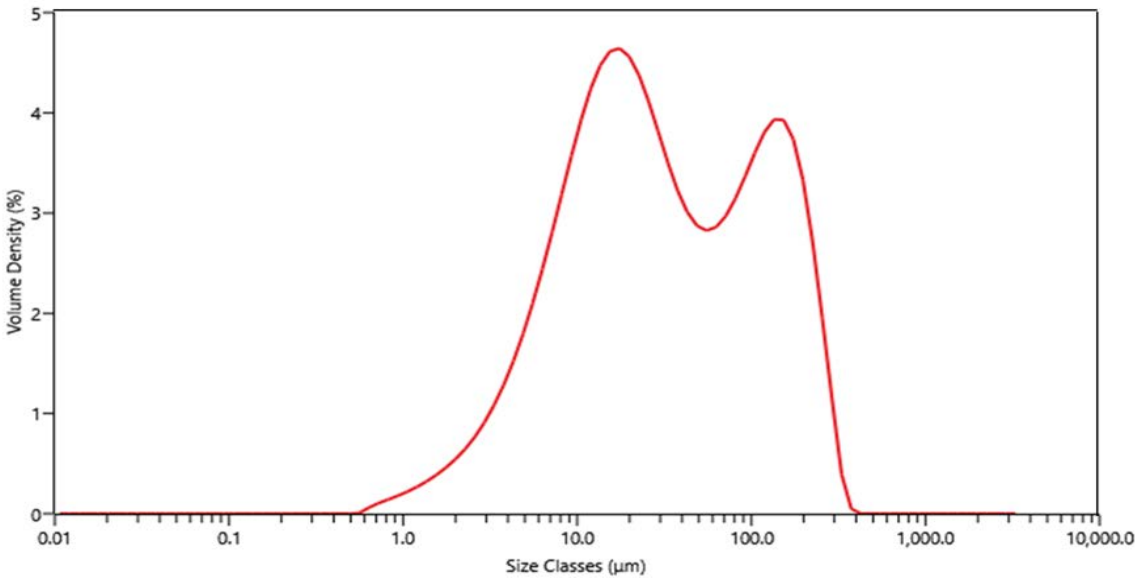

Figure A5: Particle size distribution of biochar produced at 500°C.

Table A8: XPS analysis of SCGs biochar before and after Ag^{+} adsorption

	Biochar before adsorption		**Biochar after Ag^{+} adsorption**	
	Binding energy, eV	Atomic concentration	Binding energy, eV	Atomic concentration
C-graphite	284.84	79.86	284.82	70.57
C-O-C	286.49	3.63	286.35	16.12
C=O	287.99	3.38	287.92	5.24
O-C=O	289.76	8.20	289.84	5.19
C- aliphatic	0	0	285.52	2.62
O- aromatic	531.33	44.41	533.30	93.00
O- aliphatic	532.83	55.59	535.61	7.00
Ag^{+}	0	0	368.52	52.09
Ag^{0}	0	0	374.53	34.60
Ag^{2+}	0	0	371.90	6.54

APPENDIX 3

Table A9: XPS analysis of SCGs biochar before and after Ag^+ and Ag NPs adsorption

	Biochar before adsorption		**Biochar after Ag^+ adsorption**		**Biochar after Ag NPs adsorption**	
	Binding energy, eV	Atomic concentration	Binding energy, eV	Atomic concentration	Binding energy, eV	Atomic concentration
C-graphite	284.84	79.86	284.82	70.57	284.76	73.30
C-O-C	286.49	3.63	286.35	16.12	286.53	12.61
C=O	287.99	3.38	287.92	5.24	288.33	4.83
O-C=O	289.76	8.20	289.84	5.19	290.11	2.42
C- aliphatic	0	0	285.52	2.62	293.29	0.52
O- aromatic	531.33	44.41	533.30	93.00	531.32	29.84
O- aliphatic	532.83	55.59	535.61	7.00	533.13	70.16
Ag^+	0	0	368.52	52.09	368.47	58.11
Ag^0	0	0	374.53	34.60	374.48	38.6
Ag^{2+}	0	0	371.90	6.54	371.86	0.70